# Real Time Detection of Primary Biological Aerosol Particles (PBAP) in the context of atmospheric ice formation

Zur Erlangung des akademischen Grades eines

DOKTORS DER NATURWISSENSCHAFTEN

von der Fakultät für

Bauingenieur-, Geo- und Umweltwissenschaften

des Karlsruher Instituts für Technologie (KIT)

genehmigte Dissertation

von

M.Sc. Emre Toprak

geboren in Merzifon – Türkei

Tag der mündlichen
Prüfung: 11.07.2014

Referent: PD. Dr. Stefan Norra
Korreferent: Prof. Dr. Klaus Schäfer

Karlsruhe (2014)

İlim bende kelam bende
Nice nice alem bende
Yazar levhi kalem bende
Madem ki ben bir insanım

Aşık İsmail Daimi

I comprise science and utterance
I comprise many kinds of universe
I comprise the item that writes the destiny
Since I am a human being. . .

# Acknowledgements

Believing in someone, trusting him for the work that he carried out is the greatest motivation for a young scientist regardless of the topic. Because of his boundless support and many other reasons that I will not mention here, I am grateful to Dr. Martin Schnaiter. I am also very grateful to Prof. Thomas Leisner for giving me the opportunity to write my PhD thesis in his group. I am deeply grateful to my supervisor PD. Dr. Stefan Norra for welcoming to his research group and for the constant support. He is one of the greatest scientists that someone can meet in the scientific society. I would like to take this occasion to thank Prof. Dr. A. Cemal Saydam for introducing me to Prof. Leisner and for his endless support.

I gratefully acknowledge my colleagues at IMK-AAF for their scientific and spiritual support during my work at the institute. My special thanks go to Prof. Corinna Hoose for encouraging me to work deeply on biological aerosols and their importance for understanding the whole scientific question about ice nucleation. I would like to thank my roommate and colleague Paul Vochezer for his understanding, endless support and for his friendship.

Speaking German with my colleagues in Germany was something special because by this way it was possible for me to break the ice between different cultures and to make new friendships, which guided me through my PhD journey. I am thankful to all my friends for always being there for me. I am especially grateful to Ms. Gülsen Deniz for believing in me. I know, I was not always the easiest person in the world. Thanks for your understanding and for your support. I am grateful to Muazzez Merve Yüksel and Associate Prof. Dr. Ufuk Koca for their endless support and guidance since the beginning.

My family deserves a big thank-you. Without their support, their love I could not have finished my study. I am very proud of myself not because I accomplished a PhD but I kept my word and preserved my character from deformation and built up some more

intellectual sites which will guide me through my life when I am looking for the true love. Thanks to the creator for giving me the ability to see the reality and to look beyond surface.

# Dedication

This dissertation is dedicated to my family. Especially the love and the support of my mother made it for me possible to realize my dream. So glad I have you mom…

# Contents

# Abstract

Primary Biological Aerosol Particles (PBAP) include several microorganisms either dead or alive. That the most ice nucleation active substances are the biological ones makes the PBAP important, not in global scale but maybe in regional scale. They can also act as giant cloud condensation nuclei (GCCN). There is still ongoing research about the diversity of biological aerosols. Their complex structure makes it difficult to detect and characterize with high time resolutions. Ultra violet light/laser induced fluorescence (UV-LIF) method is used lately for detection of PBAP. Although the UV-LIF method does not provide information in species level it is a great tool to gain information about biological aerosols in real time. In this study the latest prototype version of the wideband integrated bioaerosol sensor (WIBS4) has been operated during three consecutive field campaigns at different locations and different altitudes and as well as under controlled laboratory conditions. At each location spatial and temporal variability of fluorescent biological aerosols have been studied. Starting with laboratory tests including real time detection of several biological aerosols (i.e., bacterial strains, fungal spores, Snomax) and non-biological aerosols (i.e., ammonium sulfate, Saharan dust, cast soot, Arizona Test Dust) sensitivity of the WIBS has been inspected. After that three field campaigns (each for almost one year) have been performed. Sampling locations are a semi-rural site near Karlsruhe (Germany), at Zugspitze research station (near Austria border), and at Jungfraujoch (JFJ) research station (high alpine research station in Switzerland) respectively. During each field campaign single particle fluorescence data were collected. A new data analysis routine has been written and applied to all data. It has been found that in Karlsruhe the biological aerosols are strongly correlated with relative humidity. The maximum has been observed in summer and the minimum in winter season. At Zugspitze no seasonality has been seen. However similar dominating mode for biological aerosols was seen especially in summer season when the sampling site was lying within planetary boundary layer. As expected the number concentration of biological particles was the lowest at the JFJ station since the sampling site lies most of the time in free troposphere. Following the results of cloud simulations conducted at the AIDA cloud simulation chamber, Saharan dust events (SDE) at the JFJ

station were observed. Bioaerosol number concentration increased clearly during the SDE. Finally by using the new ice selective inlet and the WIBS4, during a SDE the bioaerosols have been investigated for the ice residuals. The ratio of number of fluorescent particles to total aerosol concentrations have also been calculated. This study clearly shows the first indication for the enrichment of biological particles in the ice phase, especially for particles between 1 and 5 µm.

# Zusammenfassung

Zur Gruppe der primären biologischen Aerosolpartikel (PBAP) gehören mehrere lebendige oder tote Mikroorganismen. Die Tatsache, dass die meisten eisnuklerienden Substanzen biologischen Ursprungs sind, macht die PBAP weniger auf einer globalen, vermutlich aber auf einer regionalen Skala wichtig. Außerdem können diese Partikel auch als Giant Wolkenkondensationskeime (GCCN) fungieren. Die Diversität von biologischen Aerosol Partikeln ist immer noch Gegenstand aktueller Forschung. Ihre komplexe Struktur erschwert eine zeitlich hochaufgelöste Detektion und Charakterisierung. Die Ultra violet light/laser induced fluorecence (UV_LIF)- Methode wird seit Kurzem zur Detektion von PBAP's verwendet. Obwohl die UV-LIF Methode nicht zur Unterscheidung einzelner Arten verwendet werden kann, liefert sie Informationen über biologische Partikel in Echtzeit. In der vorliegenden Arbeit wurde die aktuellste Prototypen-Version des wideband intergrated bioaersol sensor (WIBS4) in drei Feldkampagnen an unterschiedlichen Standorten und Höhen über dem Meer sowie unter kontrollierten Laborbedingungen betrieben. An jedem Standort wurde die räumliche und zeitliche Variabilität von fluoreszierenden biologischen Partikeln untersucht. Die Empfindlichkeit des WIBS wurde zuvor in Laboruntersuchungen, die die Echtzeitdetektion von mehreren biologischen Aerosolen (z.B.: Bakterienstämme, Pilzsporen, Snowmax) und nicht biologischem Aerosol (z.B.: Ammoniumsulfat, Saharastaub, Rußabgas, Arizona Test Dust) umfassten, untersucht. Im Anschluss wurden drei Feldkampagnen mit einem Gesamtumfang von fast einem Jahr durchgeführt. Die einzelnen Messorte waren: ein halb-ländlicher Standort in der Nähe von Karlsruhe, Deutschland, auf der Umwelt Forschungsstation Schneefernerhaus, Zugspitze, Deutschland, und auf der Hochalpinen Forschungsstation Jungfraujoch (JFJ), Schweiz. Bei diesen Kampagnen wurden Einzelpartikel Flurosezenz Daten aufgenommen. Außerdem wurde im Rahmen dieser Arbeit eine neue Datenauswertungsroutine entwickelt und zur Analyse aller Datensätze verwendet. Bei den Messungen in Karlsruhe wurde festgestellt, dass das Auftreten von biologischen Partikeln stark mit der relativen Feuchte korreliert. Die Konzentration von biologischen Partikeln hat ein Maximum im Sommer und ein Minimum im Winter. Auf der Zugspitze konnte kein Jahresgang festgestellt werden. Allerdings tritt

dort eine ähnliche dominierende Mode auf, besonders wenn der Messort innerhalb der planetaren Grenzschicht liegt. Wie zu erwarten war, war die Anzahlkonzentration von biologischen Partikeln auf dem Jungfraujoch an niedrigsten, da dieser Standort fast durchgängig in der freien Troposphäre liegt.

Ausgehend von Erkenntnissen die in Wolkensimulationsexperimenten an der AIDA Wolkenkammer erzielt wurden, konnten auf dem Jungfraujoch Sahra Dust Events (SDE) identifiziert werden. Während des SDE waren die Anzahlkonzentration von biologischen Aerosol Partikeln sehr deutlich erhöht. Abschließend wurde die Kombination eines neuen Eis selektiven Einlassens und des WIBS dazu verwendet die Rolle von Bioaerosolen bei der Eisnukleation zu untersuchen. Dabei wurde das Verhältnis von biologischen-zu Gesamtaerosolpartikelkonzentrationen berechnet. Im Rahmen dieser Studie wurde ein eindeutiger erster Hinweis auf eine Anreicherung von biologischen Partikeln in der Eisphase, besonders im Größenbereich zwischen 1 und 5 µm, gefunden.

# Chapter 1

# Introduction

## 1. Aerosols

Aerosols consist of fine solid or liquid particles dispersed in a gas. Atmospheric aerosols have a wide variety of sources. These sources may be either natural or anthropogenic. According to their formation and release to the atmosphere, atmospheric aerosols can be grouped into two main categories. Primary aerosols, for instance, are emitted as liquids or solids from sources such as biomass burning, incomplete combustion of fossil fuels, volcanic eruptions, and wind-driven or traffic-related suspension of road, soil, and mineral dust, sea salt and biological materials. Secondary aerosols, on the other hand, are formed following a gas-to-particle conversion process which takes place in the atmosphere (Pöschl, 2005).

Aerosols can alter the earth's radiative forcing by scattering and absorbing shortwave and longwave radiation. This process is known as the direct effect. The indirect effect on the other hand comprises all processes by which aerosols affect microphysical thus the radiative properties, the number and as well as the life time of clouds by acting as cloud condensation nuclei (CCN) and ice nuclei (IN) (Forster et al., 2007). Aerosol indirect effects have been investigated by different researchers and were summarized with following two terms; first indirect effect (also known as "cloud albedo effect") and second indirect effect (also known as "cloud lifetime effect").

The Third Assessment Report (TAR) of the Intergovernmental Panel on Climate Change (IPCC) in 2001, presented the global primary particle emissions for the year 2000 as 2150 Tg/yr for soil (mineral) dust, 3340 Tg/yr for sea salt, 56 Tg/yr for primary biological aerosol particles (PBAP) and 54 Tg/yr for biomass burning (Penner et al., 2001). Sea salt emissions were estimated later by 12 global models as 16,300 ± 200% (Textor et al., 2006). In a recent review by Despres et al. (2012) it has been suggested that PBAP concentrations

can be higher than that are estimated and important discrepancies exist. Lack of standardized methods for detecting and characterizing PBAP can also lead to those discrepancies in PBAP numbers reported by different researchers. Even though the relative contribution of PBAP to the atmospheric aerosol is low they can affect the hydrological cycle and climate on a regional scale and they can play an import role in public and agricultural health. Therefore it is crucial to know PBAP concentrations and distributions at different locations in order to come to a conclusion about the relative importance of PBAP on climate related processes.

## 1.1. Biological Aerosols

A clear definition of PBAP was given in a recent review by Despres et al. (2012). They stated that PBAP consist of solid airborne particles originated from biological organisms, including several microorganisms and as well as fragments of any biological material. The main candidates of PBAP, their number and mass concentrations in air and their typical particle diameters are summarized in Table 1.1.

Table 1.1 Main candidates of PBAP, their number and mass concentrations in air and their typical particle sizes.

| Particle type | Number concentration [$m^{-3}$] | Mass concentration [mg $m^{-3}$] | Global emissions [Tg $yr^{-1}$] | Particle size range [µm] |
|---|---|---|---|---|
| Bacteria | ~ $10^4$ – $10^5$ | ~ $10^{-1}$ | 0.7 – 28.1 | 0.5 – 30 |
| Fungal spores | ~ $10^3$ – $10^4$ | ~ $10^{-1}$ – $10^0$ | 8 – 186 | 1 – 100 |
| Pollen | ~ $10^1$ – $10^3$ | ~ $10^0$ | 47 – 84 | 10 – 100 |
| Plant debris | - | ~ $10^{-1}$ – $10^0$ | - | ≤ 10 |
| Viral particles | ~ $10^4$ | ~ $10^{-3}$ | - | ≤ 100 nm |
| Algae | ~ $10^2$ – $10^3$ | ~ $10^{-3}$ | - | 0.5 µm up to 50 m |

This chapter aims to give an overview of the recent literature about atmospherically relevant types of PBAP. Information obtained from online PBAP analyzing methods is still

not in species level. Advantages against conventional methods, limitations and basic principles of Fluorescence and Ultra-Violet Light/Laser Induced Fluorescence (UV-LIF) methods will be discussed in the following chapter.

The size of PBAP varies from tens of nanometers (e.g., viruses and cell fragments) to hundreds of micrometers (pollen, plant debris; Jaenicke 2005). Because of their small particle sizes and longer atmospheric residence times (e.g., several days, Despres et al. 2012) bacteria are one of the most abundant types of PBAP. Bacteria can interact with different other atmospheric aerosol classes and have been reported to vary in number and type for different environments. For instance, airborne viable bacteria were observed in an urban environment for two years and the number of bacteria reported changed from 0.013 to 1.88 organisms $L^{-1}$ (Mancinelli and Shulls, 1978). In the same study it has been stated that there was a significant correlation between the number of viable bacteria and the concentrations of some inorganic oxides (e.g., nitric oxide, nitrogen oxide). Most of the studies dealing with atmospheric bacterial concentrations are based on conventional culture based methods. It has been found that there is great discrepancy between the total and the culturable bacterial counts indicating that classical culture based techniques reflect only a small fraction of the whole atmospheric bacterial loading (Tong and Lighthart, 1999). In a minireview Lighthart (1997) has summarized some important aspects of bacterial aerosol research. It has been concluded that only a minor fraction (0.02-10.6%) of the total airborne bacteria is culturable and the rest is either dead or alive but not culturable.

Jaenicke and Matthias-Maser (1993) conducted different studies on PBAP and reported that the concentrations of bacteria around the cities are higher than over the country and oceans, concluding the maximum numbers were reported in September whereas the minimum occurred in March. Lighthart and Shaffer (1995) suggested that atmospheric bacterial concentrations can be divided into five time periods (i) the nighttime minimum, 23:00 to 06:00; (ii) the sunrise peak, 06:00 to 08:00; (iii) the midday accumulating concentration, 08:00 to 15:15; (iv) the late-afternoon sea breeze, 15:15 to 17:00; (v) the evening decrease to the night time minimum concentration, 17:00 to 23:00. These periods are taken into account in case of interpreting ambient bioaerosol concentrations in this study.

Fungi also known as common constituents of the airborne flora are important members of PBAP. They have aerodynamic sizes ranging from a few micrometers up to ~ 100 µm (Pady et al., 1967). Wide range of environments such as exposed rock, the sea, the North Pole, and the tropics are inhabited by fungi. To obtain the necessary nutrient for their survival they have developed different methods. For instance, some fungi exist only in symbiotic relationships (associations in which two or more organisms are in long-term interaction to be able to survive) with plant roots to form mycorrhizae (Hurst, 2007; Elbert et al., 2007). Almost 1 million fungal species are assumed to exist on Earth but only a minor fraction (~10%) has been described to date. Fungal spores can be divided into four main groups (phyla); Ascomycota (AM), Basidiomycota (BM), Chytridiomycota (CM), and Zygomycota (ZM). A large amount of fungal species belong to either AM or to BM. Basidiomycota also known as basidiomycetes comprise almost 16,000 kinds of fungal species including mushrooms, puff-balls, bracket-fungi as well as the plant pathogenic smuts and rusts. Basidiospores are known to be allergenic and are suggested to be one of the main reasons of seasonal respiratory allergy. One general argument concerning basidiospores is that the basidispore concentrations are found to show seasonal differences mainly directly correlating with relative humidity (RH) and with rainfall but only in wet season (Calderon et al., 1995). During two consecutive field studies Paulitz (1996) has found that in general higher numbers of ascospores (spores which belong to Ascomycota phyla) were released before midnight than after. Characteristic temperature (°C) and RH values were reported in the range of 11-30°C and 60-95%, respectively. In contrary to basidiospore release it has been suggested that ascospore releases were not directly associated with rainfall and continuous humid conditions.

## 2. Long range transport (LRT) of biological aerosols

Wind can carry aerosol particles, either non-biological or biological. Within the numerous biological aerosols especially certain fungal spores, pollen and some bacterial spores can be transported over long distances. Despite some minor differences, transportation mechanism of bioaerosols is suggested to be similar to the transportation of the mineral dust particles. This approach is still used for model studies in the literature (Despres et al., 2012). Pratt et al. (2009) suggested that the biological aerosols may increase the impact of desert dust

storms on the ice formation. With motivation of Pratt's work, Hallar et al. (2011) investigated several dust storms at Storm Peak Laboratory (SPL, 3210 m asl.) in northwestern Colorado. They have found some signatures for bioaerosols which may have been transported via dust storms. In another study Smith et al. (2011) reported that some bacterial cells are capable of forming 1 micrometer size spores which can serve as a microbiological fortress to protect the DNA structure inside. As it has already been mentioned in Chapter 1.1, spatial and temporal concentrations bioaerosols are not well known. It is suggested in recent literature that biological particles can be transported over long distances. However there is limited amount of data to come to a conclusion about LRT of bioaerosols. To my knowledge this is the first and the only study which investigates the spatial and the temporal variations of bioaerosols at three different altitudes in real time. The results and the conclusions of this study can be used for upcoming model simulations.

## 3. Ice nucleation and biological ice nuclei

Clouds play a very important role in human life since they contribute to atmospheric cooling and water cycles directly and indirectly. Ice formation is a process that can be classified in two groups, i.e. homogeneous and heterogeneous ice nucleation. The former indicates the formation of an ice phase from the water vapor in the absence of any solid material which does not occur in the atmosphere because it requires atmospherically irrelevant conditions such as very high supersaturations (up to a few hundred percent). However, the term homogeneous ice nucleation or homogeneous freezing is also used for the nucleation of ice in pure supercooled water droplets at temperatures below -36 °C. Heterogeneous ice nucleation on the other hand can also occur in the subzero temperature range >-36°C, albeit only in the presence of specific solid materials which are called as ice nuclei (IN). In a recent review Hoose and Möhler (2012) summarized atmospherically relevant IN as follows: mineral dust particles, soot, bioaerosols (bacteria, fungal spores, pollen and diatoms), solid ammonium sulfate, organic acids and humic-like substances. Though only a minor fraction of bioaerosols have been found to be ice nucleation active (INA) at subzero temperatures, they have the potential to initiate ice formation below -5 °C (Despres et al., 2012). Moreover, Hoose et al. (2010) investigated the role of biological aerosols on a global scale using the aerosol-climate model Cam-OSLO and concluded that

the simulated global average PBAP contribution to heterogeneous ice nucleation in mixed-phase clouds is very small. However, biological aerosols may accompany to solid insoluble materials and can be transported over large distances (Prospero et al., 2002; Uno et al., 2009). It has been found that soil dust aerosol containing biological material shows a better ice nucleation activity than the pure mineral dust does, however, noting that the soil sample with the highest bioaerosol content has been reported not to be the most ice active in the set of all soil samples (Figure 1.1., Steinke et al., 2013). It has been further suggested that biological ice nuclei are more important at warmer temperatures (~255 K) whereas at colder temperatures the stable organic matter (i.e., peptidoglycan or murein in bacterial cell wall) controls the ice nucleation process. Soil dust particles are better ice nuclei in presence of some biological aerosols and the idea that Saharan dust storms may carry some biological particles over long distances becomes more important, especially on high altitude locations where mixed-phase cloud conditions prevail. Under the light of these findings it is crucial to know the number concentration and the size distribution of the biological aerosol at the JFJ station, especially during Saharan dust events.

## 4. Scope of the study

The scope of this study is to develop a deeper understanding of how primary biological aerosol particles (PBAP) can be detected and characterized at different locations by using a WIBS instrument in real time. With the motivation from laboratory experiments that have clearly indicated the increasing ice nucleation capability of soil dust aerosol, bioaerosols have been monitored at different locations (i.e., in a semi-rural environment, at high altitude stations such as environmental research station Schneefernerhaus Zugspitze, and at Jungfraujoch research station). Starting with tests measurements that have been performed under controlled laboratory conditions, three long-term field campaigns at three different sites were accomplished, and bioaerosol concentrations as well as size distributions were discussed in the context of the meteorological conditions. A standard data analysis routine has been written in Igor Pro (WaveMetrics Inc., OR, USA). The obtained standardized approach has been applied to the extreme dust transportation events at the Jungfraujoch high alpine research station. The probability of such extreme dust transportations that occur at the Jungfraujoch station has been facilitated by optical methods and model studies (Coen

et al., 2004; Perez et al., 2006a, 2006b). Scientific questions which have been addressed in this study are:

- **Spatial and temporal variations of FBAP:**
  - ❖ What are the average integrated number concentrations and the size distributions of biological aerosol in Karlsruhe (112 m, a.s.l.), at Zugspitze (2962 m, a.s.l.), and at Jungfraujoch (3580 m, a.s.l.)?
  - ❖ Is there any correlation between the biological aerosol number concentrations and the meteorological parameters like temperature (T), relative humidity (RH), precipitation (mm), and solar radiation (W $m^{-2}$)?
  - ❖ Has any seasonality been observed for FBAP that have been investigated at Karlsruhe, Zugspitze, and Jungfraujoch sites?

- **Correlation of Saharan Dust Events (SDE) and biological aerosol concentrations at Jungfraujoch (JFJ) station:**
  - ❖ Is there a relation between the SDE and detected bioaerosol number concentrations?
  - ❖ What are the possible sources of fluorescent particles observed at JFJ?
  - ❖ Has an enrichment of the biological particles been observed in ice crystals?

# Chapter 2

# Methods

## 1. Online methods

Beginning from early eighties there has been great interest in rapid on-line biological aerosol detection methods. Most of the research has been accomplished by army research laboratories in the USA, in England and in Canada. Ultra Violet Light/Laser Induced Fluorescence (UV-LIF) method has been applied to numerous biological and non-biological materials to gain information about detection and discrimination between different materials. In the use of UV-LIF method, the idea has been constructed on a general assumption that the autofluorescent pigments are responsible for the main fluorescence emission in individual organisms or particles. However the type and the amounts of fluorophores in individual organisms are still not well known. In plants chlorophyll is the main fluorophore together with phenolic compounds (i.e., pollen wall). Cytoplasm has been suggested to be the main source for fluorescence in fungal spores concluding empty spores do not exhibit any fluorescence (Wu et al., 1984). By its nature, spores are dormant units that contain minimum amount of biomolecules required to survive harsh conditions. The fluorescence emission spectra of the spores has been reported by Arcangeli et al. (1997) and shown that spores produce three main fluorescence bands with peaks at ~ 345 nm (excitation wavelength $\lambda_{ex}$ = 280 nm), at ~ 430 nm ($\lambda_{ex}$ = 360 nm), and at ~ 510 nm ($\lambda_{ex}$ = 460 nm). It has clearly been stated that the fluorescence emission intensities of spores decrease strongly after irradiation with UV light for 1 h. In the case of bacteria, amino acids (Tryptophan, Tyrosine, and Phenylalanine; $\lambda_{ex}$ = 270-300 nm, emission wavelength $\lambda_{em}$ = 320-350 nm), NAD(P)H ($\lambda_{ex}$ = 340-366 nm, $\lambda_{em}$ = 440-470 nm), and flavin compounds (Flavin Adenine Dinucleotide (FAD), riboflavin, and flavoproteins; $\lambda_{ex}$ = 380 nm, 450-488 nm, $\lambda_{em}$ = 520-560 nm) are the primary fluorescing materials (Pinnick et al., 1995; Pöhlker et al., 2012). A more detailed list of fluorescent compounds can be found elsewhere (Pöhlker et al., 2012).

However, classification based only on intrinsic fluorescence of molecules is challenging. First of all, biological aerosols like viruses, bacteria, fungi, pollen, etc. consist of so many different molecules. Secondly, fluorescence emission spectra obtained from single particles may differ from the spectra deduced from mixtures of different compounds. Brosseau et al. (2000) have found no correlation between percent fluorescence and culturability for tested bioaerosols. However they have indicated that there could be differences between fluorescence of single cells and group of cells. Moreover, atmospheric parameters such as temperature, relative humidity and sun light as well as growth conditions may affect the spectra obtained. Therefore it may be a challenging job to discriminate same types of bioaerosols in a mixture. For instance, fluorescence emission spectra of starved and unstarved cells were reported to be different from several aspects. First, unstarved organisms fluoresce approximately five times stronger than starved ones. Second, starving increases the Nicotinamide Adenine Dinucleotide (NADH)-like fluorescence suggesting that the fluorophores responsible from the emission in this range should be different from NADH, and flavonoids which are metabolic compounds generated in living organisms. On the other hand there are differences in fluorescence spectrum of vegetative cells and cell spores which may provide a more reliable discrimination between bacterial cells and bacterial spores. *B. subtilis* vegetative cells have been suggested to fluoresce between 300 and 400 nm (Tryptophan-like fluorescence) after excitation by 266 nm light. These spectral fingerprints can be used to provide a better discrimination between different types of PBAP in field studies.

Since the relation between intrinsic fluorescence, type and amount of fluorophores that biological aerosols contain is of paramount importance, it must be known how fluorescence intensities vary with changing fluorophore concentrations. It has been found that intrinsic fluorescence intensities increase logarithmically with increasing fluorophore concentrations. However it is possible that there might be a cascade effect (i.e., energy from emission of one fluorophore is being used to excite other fluorophore) when more than one fluorophore is present in the same medium. For example, emission from pyridoxine (391-394 nm) may excite any flavins ($\lambda_{ex}$ = 380 nm) present in the same environment (Li, J. and Humphrey, E.A., 1991; Pöhlker et al., 2012).

Although several prototype instruments have been developed to detect biological aerosols in real time, only two of them are commercially available at the moment. The ultraviolet aerodynamic particle sizer (UV-APS, TSI, Shoreview, MN, USA) and the wideband integrated bioaerosol sensor (WIBS, Droplet Measurement Technologies, Boulder, CO, USA) have been deployed for several studies (Huffman et al., 2010; Huffman et al., 2012; Gabey et al., 2010, 2011, 2013; Healy et al., 2012a, 2012b; Toprak and Schnaiter 2013). Following the studies dealing mostly with biological and non-biological aerosols under controlled laboratory conditions, Huffman et al. (2010) operated the UV-APS for a long-term ambient sampling in central Europe, in Mainz, Germany. It has been assumed that coarse fluorescent particles (>1 µm) measured by UV-APS are "Fluorescent Biological Aerosol Particles" (FBAP). FBAP refers to only fluorescing biological aerosol and therefore can be regarded as a lower limit for atmospheric PBAP.

## 2. The Wideband Integrated Bioaerosol Sensor (WIBS)

A prototype multi wavelength instrument called Wideband Integrated Bioaerosol Sensor (WIBS) has been presented by Prof. Paul Kaye and his co-workers (Kaye et al., 2005). This first prototype instrument was able to measure the intrinsic fluorescence from multiple particles within a defined volume. Measuring only the total fluorescence emission following excitation of two optically filtered xenon lamps facilitated the design and operation of airflow systems. However this method was not suitable for inhomogeneous aerosol systems. Therefore a new version (WIBS2) was designed and operated under controlled laboratory conditions (Kaye et al., 2005). In contrary to UV-APS, WIBS2 was able to provide information for single particles in three different emission bands. The first detector provides fluorescence emission information for Tryptophan-like substances, whereas the second and the third detector focus more or less on NADH-like molecules and some other autofluorescent biomolecules. In 2008 Dr. Virginia Foot and her colleagues published the results from an improved version of WIBS instrument (Foot et al., 2008). Gabey et al. (2010) deployed the improved version (WIBS-3) below and above a tropical rainforest canopy in Borneo and particle events where a defined threshold level have been exceeded on both FL1 and FL3 fluorescence channels were reported as FBAP. In contrary to the term used by Huffman et al. (2010), FBAP here does not represent the viable

biological aerosol fraction since there is no published work dealing with this issue yet. Viability issue and response of WIBS (version 4, this study) instrument to different biological aerosols will be discussed in the course of the thesis in detail.

During the course of the present study the latest version of the Wideband Integrated Bioaerosol Sensor (WIBS4) has been operated to sample single particle bioaerosol data at different locations. WIBS4 is the latest prototype instrument which has been developed by the University of Hertfordshire (now licensed by Droplet Measurement Technologies, Boulder, CO, USA). Principally, WIBS4 is a single particle bioaerosol sensor that measures intrinsic fluorescence from individual particles (Kaye et al., 2005; Foot et al., 2008). Compared to the previous version (WIBS3, Gabey et al., 2010; 2011) the latest version incorporates several software improvements and provides better fluorescence detection. WIBS4 has two filtered xenon lamps which are selectively focused at 280 nm (to excite tryptophan) and at 370 nm (to excite NADH), respectively. The xenon lamps have a maximum repetition rate of 125 Hz. Thus the maximum particle concentration for which single particle fluorescence data can be acquired is limited to approximately $2x10^4$ particles $L^{-1}$. In case of higher number concentrations WIBS4 is capable of detecting and counting particles albeit no fluorescence data can be provided and those particles detected during xenon lamps are being charged are labeled as “missed particles”. Missed particles are taken into account to calculate the integrated total aerosol number concentrations and treated carefully so that the deduced ratio of fluorescent to total aerosol particles is not affected. This issue will be discussed in this chapter in detail.

Similar to the principle used in UV-APS, WIBS4 uses the UV-LIF method for the discrimination of biological aerosols from other atmospheric aerosols. Resulting intrinsic fluorescence emitted through single particles is recorded in three fluorescence channels. Characteristic excitation and detection ranges for commercially available instruments and for a few other prototype systems are summarized in Table 2.1.

Table 2.1. Comparison of the currently available UV-LIF instruments

| Name/Description | Size range | Peak excitation | Fluorescence detection band | UV light source |
|---|---|---|---|---|
| UVAPS (TSI, Inc.) | $0.5 \leq D_a \leq 20$ µm | 355 nm | 420-575 nm | Laser |
| BAWS (Lockheed Martin Inc.) | 2-10 µm | 260-280 nm | 300-400 nm | Laser |
| | | | 400-600 nm | |
| WIBS3 (Gabey et al., 2010) | $0.5 \leq D_o \leq 20$ µm | 280 nm | 300-400 nm | Xenon lamps w/ |
| | | | 400-600 nm | UV filters |
| | | 370 nm | 400-600 nm | |
| AFS (Biral, Inc.) | $0.5 \leq D_o \leq 15$ µm | 280 nm | 330-650 nm | Laser |
| | | | 420-650 nm | |
| SPFA (Eversole et al., 1999) | $Dp \geq 0.5$ µm | 266 nm | 300-400 nm | Laser |
| | | | 400-600 nm | |
| AFSA (Hill et al., 1999) | $Dp \geq 1$ µm | 266 nm | Continuous 200-700 nm | Laser |
| WIBS4 (Healy et al., 2012; this study)* | $0.5 \leq D_o \leq 13$ µm | 280 nm | 310-400 nm | Xenon lamps w/ |
| | | | 420-650 nm | UV filters |
| | | 370 nm | 420-650 nm | |
| WIBS4 (Healy et al., 2012)** | $3 \leq D_o \leq 31$ µm | 280 nm | 310-400 nm | Xenon lamps w/ |
| | | | 420-650 nm | UV filters |
| | | 370 nm | 420-650 nm | |

Da: Aerodynamic particle size (diameter of a spherical particle with unit density (1000 kg/m$^3$) having the same terminal settling velocity under gravity as the particle under consideration).

Do: Optical particle size (estimated size of particle using either the intensity of scattered light or time-of-flight of particle between two laser beams).

Dp: Particle diameter (also used to refer aerodynamic particle size).

* High gain (HG) version of WIBS4

** Low gain (LG) version of WIBS4

In a recent review Pöhlker et al. (2012) investigated possible biomarkers (fluorophores). Under the light of their findings, information that WIBS4 provides can be grouped into two main categories; first fluorescence detection channel (FL1) collects signals from common amino acids such as tryptophan ($\lambda_{ex}$=286 nm, $\lambda_{em}$= 363 nm), phenylalanine ($\lambda_{ex}$=270 nm, $\lambda_{em}$= 296 nm), and tyrosine ($\lambda_{ex}$=280 nm, $\lambda_{em}$= 307 nm), whereas second and third fluorescence channels (FL2 and FL3, respectively) gather signals mainly from coenzymes and vitamins such as NADH ($\lambda_{ex}$=341 nm, $\lambda_{em}$= 454 nm), riboflavin ($\lambda_{ex}$=380 nm, $\lambda_{em}$= 520-560 nm), vitamin $B_6$ ($\lambda_{ex}$=315-345 nm, $\lambda_{em}$= 350-425 nm). There may be some minor contribution to the FL2 signal from cell wall compounds such as cellulose ($\lambda_{ex}$=250-350 nm, $\lambda_{em}$= ~420 nm) whilst chitin ($\lambda_{ex}$=335 nm, $\lambda_{em}$= ~410 nm) may contribute to FL3 signal in case of fungi, and insects.

Owing to optical components that have been used in WIBS, there is always a finite amount of background fluorescence which can be detected in the absence of any particle by operating the instrument in forced trigger mode. In the forced trigger mode the xenon lamps are fired at a constant frequency (1 Hz) to measure solely the background fluorescence. Later on the background fluorescence in each channel will be used to estimate a background threshold which separates fluorescent biological aerosol from non-biological aerosols.

## 2.1. Calibration and operation

During the last decade, after the previous military research on the UV-LIF method had become available, several studies dealing with rapid detection/characterization of PBAP were published. One important discussion was about the exact calibration of WIBS instrument with known biological or non-biological aerosols in order to overcome interferences from fluorescing non-biological systems. However this is a challenging job since WIBS can measure only intrinsic fluorescence regardless of the source material. In this study the term fluorescence is used to designate intrinsic (or autofluorescence) which is the fluorescence of the not stained material. One important parameter is the trigger threshold which defines the smallest particle that triggers the laser to initiate sampling

procedure. One can set this trigger threshold very low to be very sensitive to smaller particles. However, a low trigger threshold results in an increase of noise triggers. Therefore it is crucial to adjust the trigger threshold correctly. Based on the personal observations during laboratory tests this trigger threshold value has been set to 3 and 4 for different experiments. It should be kept in mind that effect of use of different trigger thresholds on minimum particle size was not further investigated. Particle optical size is calculated by using a Mie scattering lookup table which is generated under controlled laboratory conditions by using polystyrene latex (PSL) spheres with known nominal diameters. Figure 2.1 shows the calibration table used for the present study.

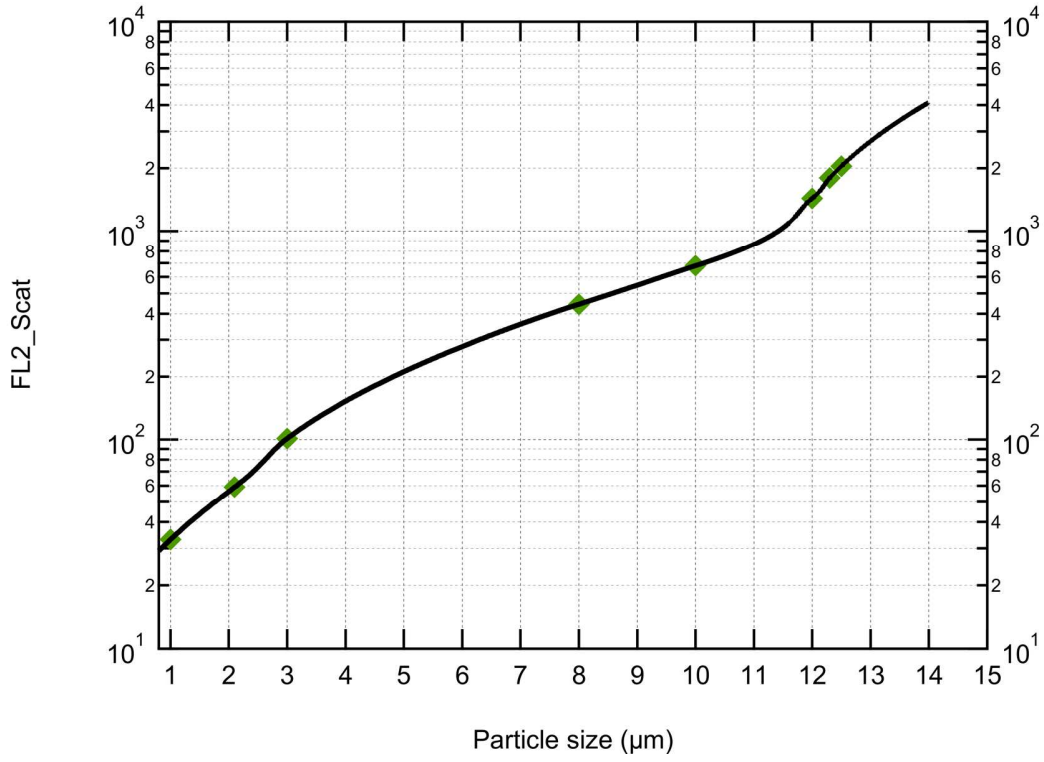


Figure 2.1: Calibration curve for WIBS4. Green squares are the experimental values deduced from calibration experiments (i.e., calibration aerosols are Polystyrene Latex particles and oleic acid droplets) that have been provided by the manufacturer. Black solid line represents the derived calibration curve that is used to estimate the optical particle sizing.

By diminishing the detector gain the particle size table can be modified. In this case the instrument will be more sensitive to the larger particles but at the same time it will not be possible to detect smaller particles. Healy et al. (2012a, 2012b) presented two WIBS instrument each has its own particle size range. The so called high-gain version is suggested to be capable of measuring particle size range of ~0.5-12 µm, whereas the low-gain version can provide particle size information in a range of ~3-31 µm. They concluded that the counting efficiency drops below unity for particles smaller than 0.7 µm. The WIBS instrument that has been used in this study is comparable to the high-gain version presented by Healy et al. (2012a).

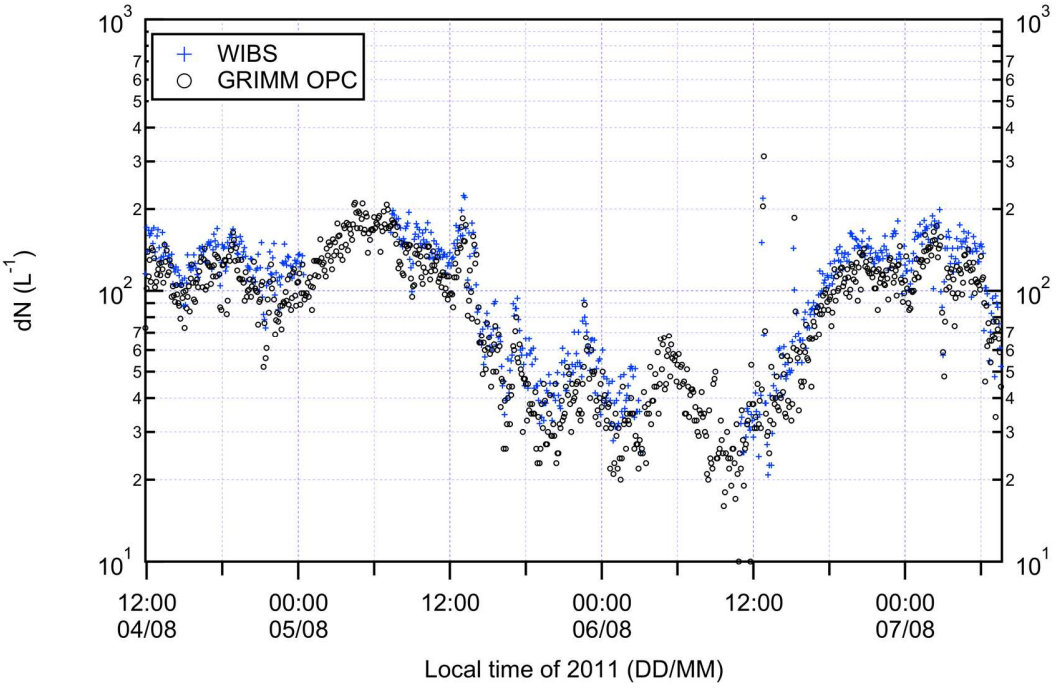


Figure 2.2: Ambient aerosol number concentration measured at Zugspitze by WIBS and Grimm OPC for comparison. Blue markers show the WIBS total aerosol number concentrations, while black open circles represent the Grimm OPC data.

As it has already been discussed the trigger threshold should be selected correctly so that the WIBS can be operated sensitive to the particles in the size range of 0.8 µm and 12 µm. During the field campaign at Zugspitze two instruments (WIBS and Grimm OPC, Model 1.0.9) sampled at the same TSP inlet. Fig. 2.2 shows a good agreement of the total aerosol

number concentration between two instruments for the size range 1.0 µm<Do<10 µm. However it should be noted that some deviations from this good agreement of the order of a few ten percent have also been observed in case of the Jungfraujoch installation where strictly isokinetic sampling was not possible.

## 2.2. Asymmetry factor (AF)

One important and unique feature of the WIBS instrument is that it can provide a rough estimate of the sphericity of single particles. Forward scattered light from single particles is collected on a quadrant photomultiplier tube (PMT). These 4 signals collected by the PMT detector are then used for calculation of AF (Eq. 1 this study; Hirst et al., 2001; Kaye et al., 2007). E-bar is the mean of E1 + E2 + E3 + E4, n is the number of discrete detectors used and k is an instrument constant to ensure the maximum value of AF is 100. According to the definition, for a perfect sphere AF will be zero, whilst for an elongated fiber AF will have a value of 100. However in practice even for perfectly spherical particles AF does not reach zero because of the fact that PMT detector has also an electrical noise which mainly affects the AF value of small particles.

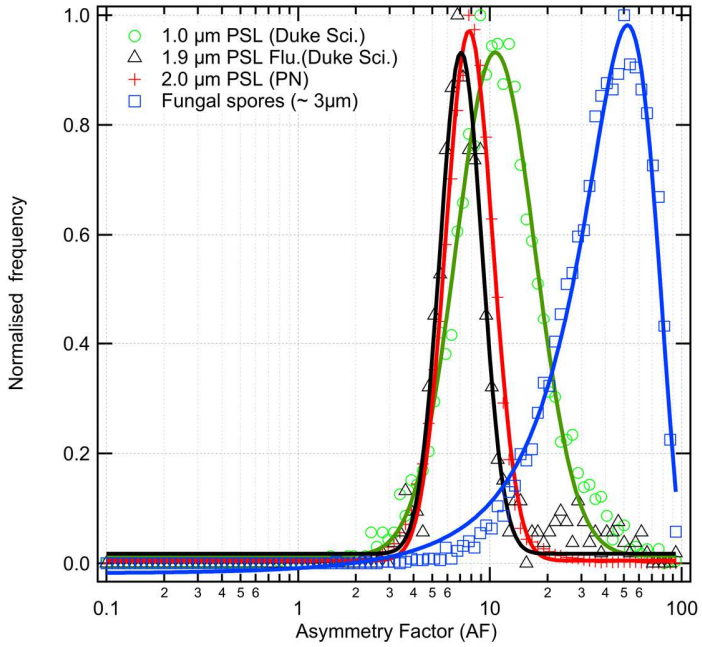

Figure 2.3: Normalized averaged asymmetry factor (AF) values for some standard PSL particles and for *Penicillium notatum* type of fungal spore. Green circles and the dark green solid line: 1.0 µm PSL particles purchased from Duke Scientific, black triangles and the solid line: 1.9 µm fluorescent PSL particles purchased from Duke Scientific, red pluses and the solid line: 2.0 µm PSL particles purchased from Postnova Analytics, blue squares and the solid line: *penicillium notatum* type of fungal spores purchased from a Swedish company (Allergon AB, Sweden).

$$AF = \frac{k\left(\sum_{i=1}^{n}(\overline{E}-E_i)^2\right)^{1/2}}{\overline{E}} \quad (1)$$

In laboratory tests with PSL particles, it has been seen that PSL particles have AF values around 8, whereas *Penicillium notatum* type of fungal spores show a brighter distribution between 25 and 70 (Figure 2.3).

## 3. WIBS Data Evaluation Procedure

WIBS is a single particle bioaerosol sensor. Therefore it records almost all parameters defined by the manufacturer for each single particle. As it has been discussed in the section 2.1, in the presence of too many particles (upper limit ≈ $4x10^4$) or when a particle is detected during the UV lamps are being recharged no fluorescence data can be provided for these particles. Such particles are marked as "missed particle" and will be taken into account when calculating total aerosol number concentration. The parameters that are recorded for each single particle are; particle arrival time, the forward and side scattering data, the power of the xenon lamps, the fluorescence intensities for the three different channels (if possible), the time of flight (TOF) values, the particle optical size in µm, the asymmetry factor values and the missed particle counts.

WIBS was operated via a laptop for data acquisition and the manufacturer's software was used to collect single particle data. Because of the amount of large dataset collected during both laboratory tests and during three consecutive field measurements, a data analysis software called "WDES" (**W**IBS **D**ata **E**valuation **S**oftware) has been written in Igor Pro (WaveMetrics Inc., OR, USA) and has been applied to all data here. WDES reads comma

separated value (csv) files and saves each in different data folders which is a very useful feature of Igor Pro. Each data folder is later on worked out one by one and the results are presented in different forms such as time series of fluorescent biological aerosols or integrated number size distribution for any type of particle according to particle selection criteria. Fluorescent particle types that are presented in this study can be found in the appendix A. For each data file (consists of maximum 30000 particle events), if available, background fluorescence intensity in each channel (F1, F2 and F3) is read, the mean ($\bar{E}$) and the standard deviation (σ) of fluorescence intensity are calculated.

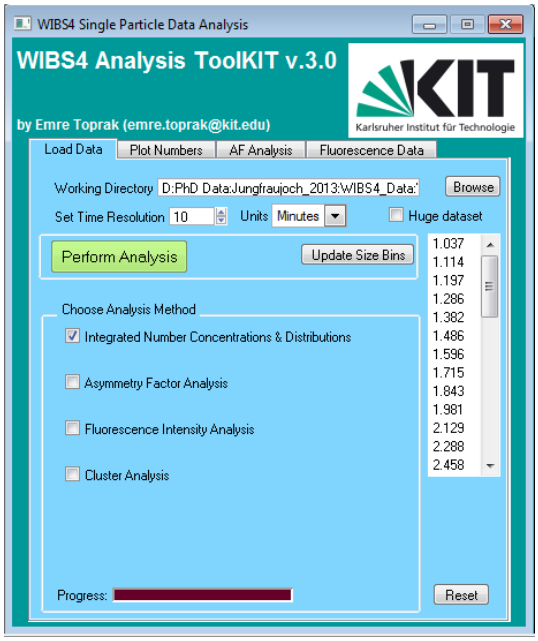


Figure 2.4: Control panel of WIBS Data Evaluation Software

Background threshold is calculated from the background forced trigger fluorescence data according to Eq. (2), and any particle for which the measured fluorescence is greater than the background threshold is accepted as a fluorescent biological particle. If data do not contain any background information, the latest background threshold value is used.

$$E_{Threshold\ (i)} = E_i + 3\sigma_i \text{ (i = corresponding fluorescence channel)} \quad (2)$$

Accordingly, WIBS can be operated in a way that the instrument collects forced trigger data automatically in every ten minutes for ten seconds (dynamic threshold) or it can also

be performed manually. In this way it has been aimed to prevent any negative or positive effects of change of background fluorescence on the analysis. During the course of this study both methods have been used. Using the dynamic threshold may be practical, especially during long-term measurement by which the background fluorescence level varies with time. Figure 2.5 shows change on the background fluorescence calculated for a one-year sampling in Karlsruhe, Germany.

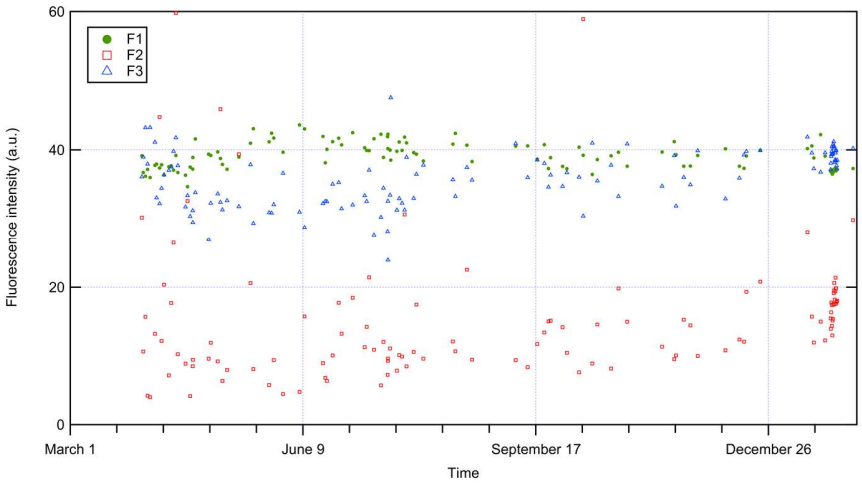


Figure 2.5: Background fluorescence threshold ($E_{\mathrm{Threshold}}$) change during a one year online sampling.

This figure shows clearly that the channel F2 and channel F3 have the greatest variability, whereas the channel-F1 was rather stable. To show to what extend the variability of the background threshold may affect the number concentration of bioaerosols, a one day sampling period at Karlsruhe site has been investigated. The sampling was conducted from 04.05.2010 to 05.05.2010. Corresponding forced trigger measurements have been collected on the sampling day as well as one day before and after the sampling. Data were worked out by using three different background threshold values. The results are shown in Figure 2.6. The background threshold values were rather stable for channel F1 and F3 on the given day. This feature was reflected on the calculated bioaerosol number concentrations on Figure 2.6.

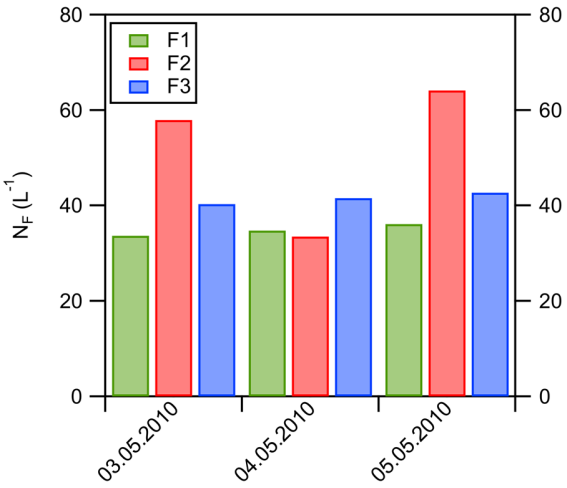


Figure 2.6: Effect of the change of background threshold on number concentrations of biological particles. Each color represents the corresponding bioaerosol number concentration for that channel on different sampling periods.

# Chapter 3

# Results and discussions: Part-1

## 1. Autofluorescence of test aerosols

In this chapter several bioaerosols (e.g., fungal spores, bacteria, snomax) and non-biological aerosols (ammonium sulfate, Arizona Test Dust, Saharan dust, soot aerosol) were discussed in details. For each experiment WIBS instrument was operated for a few minutes or sometimes longer to have a statistically good dataset. Collected data were interpreted using the WDES (data analysis tool, written in Igor Pro) to find the time series for fluorescing particles. For each experiment presented in this chapter the same midpoint size bins were used. Background thresholds were calculated for each experiment separately.

## 2. AIDA/NAUA cloud simulation and preparation chambers

The Aerosol Interactions and Dynamics in the Atmosphere (AIDA) cloud simulation chamber of the Institute of Meteorology and Climate Research, Atmospheric Aerosol Research (IMK-AAF) at Karlsruhe Institute of Technology (KIT) is unique from several aspects. The AIDA chamber is a cylindrical vessel made of aluminum and has a diameter of four meters and a height of 7.5 meters, accounting a volume of about 84 m3. This special cloud chamber allows simulating mixed-phase clouds, cirrus clouds, as well as polar stratospheric and noctilucent clouds (Skrotzki et al., 2012 and references therein). In this study only a small number of experiments have been performed in AIDA chamber, whereas the NAUA chamber was preferred for aerosol characterization because of its ideal volume (~ 3.7 m3), ease of cleaning and the amount of test sample required to fill the chamber up. The NAUA chamber is a stainless steel aerosol chamber. The AIDA and the NAUA chambers have been equipped with set of aerosol instruments including the WIBS, an Aerodynamic Particle Sizer (APS, mod. 3321, TSI Inc., USA), a Condensation Particle Counter (CPC mod. 3022, 3375, TSI Inc., USA), as well as a rotating brush generator (RGB-1000, Palas GmbH, Karlsruhe, Germany). CPC 3022 had a maximum detectable

particle size of around 3 µm, whilst the minimum detectible particle size is given to be around 0.007 µm (with 50 % counting efficiency) and around 0.015 µm (with 90 % counting efficiency).

## 3. Preparation of the dust samples (pre-activation)

Except the Saharan dust sample, which had been collected from Sahara desert (33°58'53.9'' N; 8°0'6.7'' E, Tunisia) somewhere near Tozeur, all other desert dust or soil samples were dispersed either via the rotating brush generator (RBG-1000, Palas GmbH, Karlsruhe, Germany) or by using small scale powder disperser (SSPD, TSI Inc., USA). Saydam et al. (2002) has previously investigated the Saharan dust samples that were used in this study. They found that the $Fe^{2+}$ amount increases steadily after irradiating the dust-water mixture with visible light. They further hypothesized that this ferrous iron production is related to the presence of bacterial and fungal species in the medium. With help of enough energy (i.e., sun light) this process can be initiated and the resulting biological species may affect the cloud formation and precipitation. Following the procedure described by Saydam et al. (2002) Saharan dust sample that had been collected from Sahara desert was first sieved to remove the very large particles and the fraction up to 70 µm was used for cloud experiments. First of all, 3 g dust was weighed and placed in a cylindrical bottle. Almost 100 mL nano pure water was poured on it and the resulting heterogeneous solution was mixed by using a magnetic stirrer for approximately five minutes. Then the bottle was placed in a reservoir which is covered from all sides with aluminum folio. The top of the reservoir was left intentionally open and a visible light source was placed to the top of this reservoir. The solution was illuminated with 500W visible light for almost two hours. This process was applied to Saharan dust samples that were investigated in AIDA chamber and called as pre-activation of dust samples during the course of this study. Before each cloud expansion nucleopore filters were collected for approximately 20 minutes. Later on Polymerase Chain Reaction (PCR) method has been applied to each filter samples and it has been found that both pre-activated and not activated samples contain bacterial and fungal species. However the size of these organisms was not large enough to be detected by the WIBS instrument.

# 4. Test aerosols

## 4.1. Ammonium sulfate and fungal spores

Ammonium sulfate pellets were dissolved in water by using ultrasonic atomizer. Resulting 10% (w/w) homogeneous solution was dispersed into the NAUA chamber for several seconds. Ammonium sulfate aerosol was added to the NAUA chamber until the number concentration measured by the CPC reached an initial value around $5x10^4$ $L^{-1}$. Because of the gravitational settling of large aerosol particles and the sampling trough several instruments such as APS, CPC, WIBS, etc. the total aerosol number concentration dropped to about $2.5x10^4$ $L^{-1}$ in approximately 80 minutes. After that about $2x10^4$ $L^{-1}$ of *penicillium notatum* type of fungal spores were added. After addition of fungal spores, WIBS total aerosol number concentration was calculated to be around $1.0x10^4$ $L^{-1}$. Towards the end of the sampling period (i.e. in 40 minutes) the total aerosol number was calculated as approximately $0.6x10^4$ $L^{-1}$. Time evolution and the responses deduced from single fluorescence channels and as well as from combination of different channels are shown in Fig. 3.1.

WIBS fluorescence data can be interpreted in several different ways. In this study I used not only data from single channels (F1, F2, and F3) but I also applied different selection criteria such as combination of individual channels in a way that a particle is supposed to be fluorescent only when signal on two fluorescence detectors exceeds the defined background thresholds respectively. For instance, when a particle fluoresces both on F1 and F3 at the same time, this particle is counted for $N_{F1F3}$. These combinations may provide in some cases a better discrimination between biological and non-biological aerosols. Figure 3.1 (left panel) shows that WIBS counted approximately 12 particles $L^{-1}$ on channel F1, 25 particles $L^{-1}$ on channel F2, and 36 particles $L^{-1}$ on channel F3 as fluorescent. When total aerosol number concentration detected by WIBS for pure ammonium sulfate aerosol is considered, these numbers correspond to only a very small fraction (0.16 % for $N_{F1}/N_T$, 0.32 % for $N_{F2}/N_T$, and 0.47 % for $N_{F3}/N_T$, respectively).

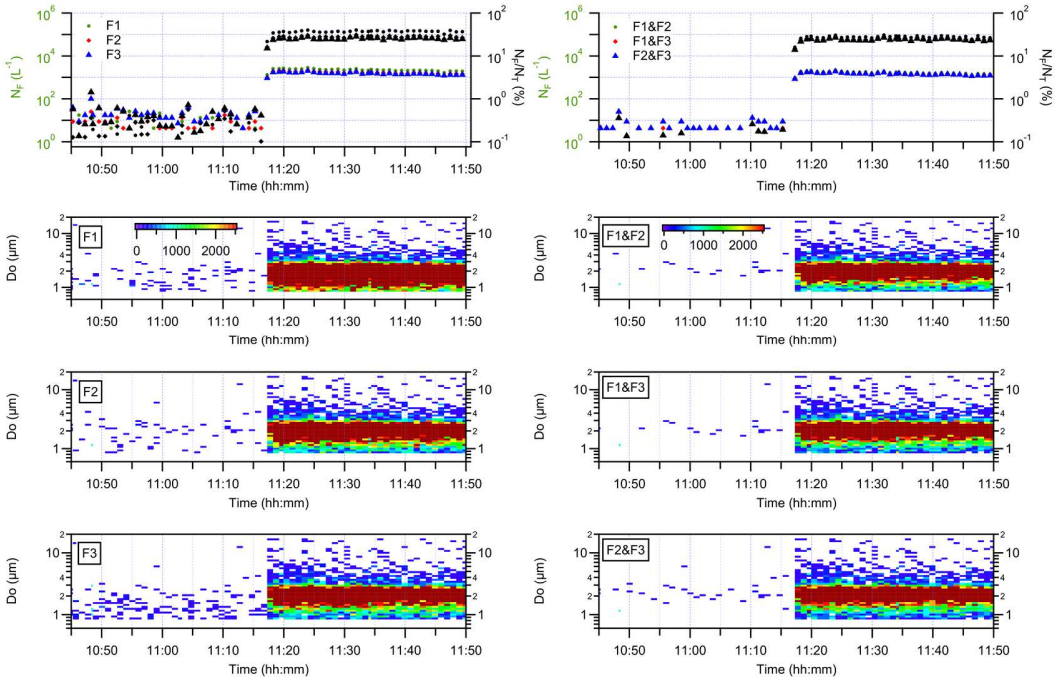


Figure 3.1: Fluorescence data deduced from WIBS measurement for ammonium sulfate aerosol and *penicillium notatum* type of fungal spores. Top panel for each graph, left axis: number concentration of fluorescent particles in the size range of 0.8-16 µm. Top panel, right axis: ratio of number of fluorescent particles to the total aerosol number concentration (without missed particles). Lower panels: size distribution (*dN/dlogDo*) of fluorescent particles.

When I further investigated the Fig. 3.1 (right panel) I have seen that using combinations of different fluorescence channels (see Table 2.2) decreased the cross-sensitivity of the instrument to a very low degree for ammonium sulfate aerosol. $N_{F1F2}$, $N_{F1F3}$, and $N_{F2F3}$, can be given as approximately 6.7 $L^{-1}$, 6.9 $L^{-1}$, and 7.4 $L^{-1}$ respectively. Again the ratios of number of fluorescent particles to the total aerosol number were very low, namely approximately 0.09% for $N_{F1F2}/N_T$, and for $N_{F1F3}/N_T$, and 0.1% for $N_{F2F3}/N_T$. After addition of fungal spores WIBS total count and the counts on individual fluorescence channels increased steeply. Average fluorescent particle numbers can be given as follows: $N_{F1}$ = 2192 $L^{-1}$, $N_{F2}$ = 1644 $L^{-1}$, $N_{F3}$ = 1487 $L^{-1}$. Corresponding number ratios are approximately 28% for $N_{F1}/N_T$, 21% for $N_{F2}/N_T$, and 19% for $N_{F3}/N_T$ respectively. Since the larger particles that have been added to the aerosol chamber settled quickly calculation of a stable

average aerosol number concentration during the course of the experiment was difficult. WIBS nevertheless classified a major portion of the fungal spores as non-fluorescent. This feature was then seen on characterization experiments which have been conducted using only fungal spores (data not shown). One reason for that could be the low sensitivity of individual fluorescence channels which may not be able to detect very low autofluorescence from small particles. For instance, Huffman et al. (2012) suggested that, in some cases, some fraction of bioaerosols (e.g. particles of small size), may be below the detection limit of the UV-APS. In case of detection of fungal spores there have been slight differences between single detection wavebands and combination of two wavebands. However the ammonium sulfate aerosol was detected mostly on single channels (i.e., F1, F2 and F3) but less on the two fluorescence channels at the same time. This feature may provide an advantage for ambient aerosol measurements. Since the channel F1 (indication for Tryptophan-like particles) is also used as a marker for the pollution, it is also good to combine the F1 with F2 or F3 to overcome the cross-sensitivity of the WIBS. On the other hand using the combination of two channels may also be a disadvantage for detecting Try-like species which fluoresce only on channel F1 but not on other channels. It is almost always the question of interest whether the single channels or combinations of two or three channels will be preferred.

## 4.2. Soot and ammonium sulfate

Soot aerosol that had been emitted through a propane diffusion flame (mini-CAST, Jing Ltd, Switzerland) was added to ammonium sulfate aerosol to investigate the autofluorescence of fossil fuel combustion aerosol in NAUA chamber. Fuel-to-oxygen (C/O) ratios can be altered in order to obtain soot aerosol emissions with different organic carbon contents. Details concerning the combustion aerosol generator and soot composition can be found elsewhere (Schnaiter et al., 2006). From previous section (Sc. 4.1.) it is known that the fluorescent particles deduced from WIBS measurements for ammonium sulfate aerosol were approximately between 12-36 particles $L^{-1}$ for individual fluorescence channels F1, F2 and F3, respectively. Therefore the counts that are given for this experiment should be considered as a mixture of contribution from ammonium sulfate and

soot aerosol. The mixing ratio of the ammonium sulfate and soot was around 1:7. After cleaning the NSUA chamber, aerosol number concentration was controlled via CPC measurements. Then the ammonium sulfate aerosol was dispersed by following the same procedure that has been described in subsection 4.1. After addition of ammonium sulfate aerosol the initial concentration that has been measured by WIBS was around $0.2x10^5$ $L^{-1}$. Soot aerosol was added for almost seven minutes and the $N_T$ was approximately $1.6x10^5$ $L^{-1}$. Total aerosol number concentration decreased quickly owing to the sedimentation during the experiment and also because of the instruments that were connected to the chamber. Time evolution of the experiment was illustrated in Fig. 3.2.

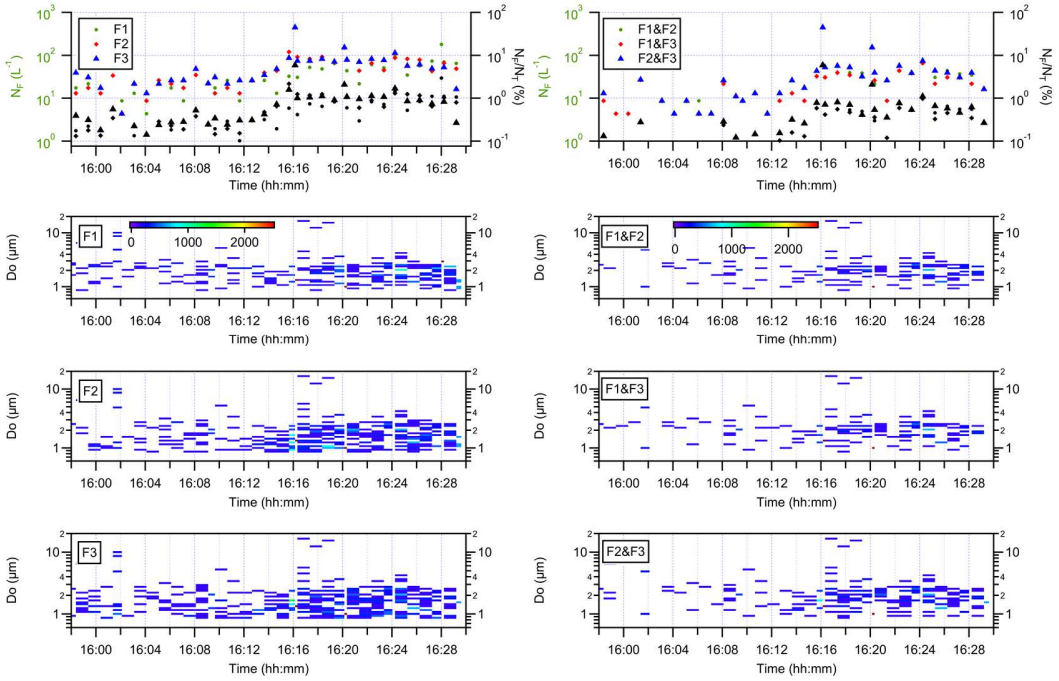


Figure 3.2: WIBS fluorescence data for ammonium sulfate – soot aerosol mixture. The data were plotted in the same way as in Fig. 3.1.

Measured average fluorescent particle number counts were 61 $L^{-1}$ on channel F1 and 75 $L^{-1}$ on channel F2 and on channel F3. Absolute numbers of fluorescent particles are not directly comparable with the previous experiment (see 4.2.) because each experiment was performed with different amounts of material and therefore the total aerosol number concentrations varied. In this case it may be a better idea to look at the number ratios

instead of investigating number of fluorescent particles directly. Figure 3.2 shows clearly that ammonium sulfate – cast soot mixture fluoresces weakly on both single and combined fluorescence channels. For single channels ratios of fluorescent particles to the total aerosol number were calculated as 0.88 % for channel F1, 1.1 % for channel F2 and 1 % for channel F3. For combinations of channels the calculated ratios were 0.53 % for F1&F2, 0.47 % for F1&F3 and 0.64 % for F2&F3, respectively. It should be noted that ammonium sulfate fluoresces weakly, contributing approximately 0.2 % to the total aerosol count. Using a combination of two fluorescence channels provided again a better discrimination between biological and non-biological particles. However, a weak cross-sensitivity (less than 1%) of the WIBS to the soot combustion aerosol has been found.

## 4.3. Dust aerosol

Mineral dust aerosol is of major importance in this study because of the fact that it is one of the most abundant aerosols in the atmosphere (Rosenfeld et al., 2008; Monks et al., 2009). My motivation for this thesis was developing a standard procedure to investigate the pre-activation of Saharan dust aerosol and its autofluorescence behavior in a cloud chamber by using the WIBS. Autofluorescence of different mineral particles including kaolin and Arizona Test dust (ATD) has been studied by Pöhlker et al. (2012). They have suggested that ATD fluoresces weakly between 300-420 nm after excitation with UV light.

The Arizona Test Dust (ATD) was dispersed into the NAUA chamber by using a small-scale powder disperser (SSPD 3433, TSI). Figure 3.3 represents the contribution from ATD to the fluorescent particle number measured by WIBS. $N_T$ was measured around $1.0 \times 10^6$ $L^{-1}$ (solid black line on Figure 3.3), however, due to the instrumental limitations only a minor fraction of the total aerosol (dashed black line on Figure 3.3) could be analyzed for fluorescence. This means that WIBS was able to detect around $1.0 \times 10^6$ particles $L^{-1}$, but due to the dead times of the UV-lamps in the instrument the autofluorescence was measured only for a small fraction of the total aerosol. The particles that are detected during the dead time of the UV-lamps are called as “missed particle count”.

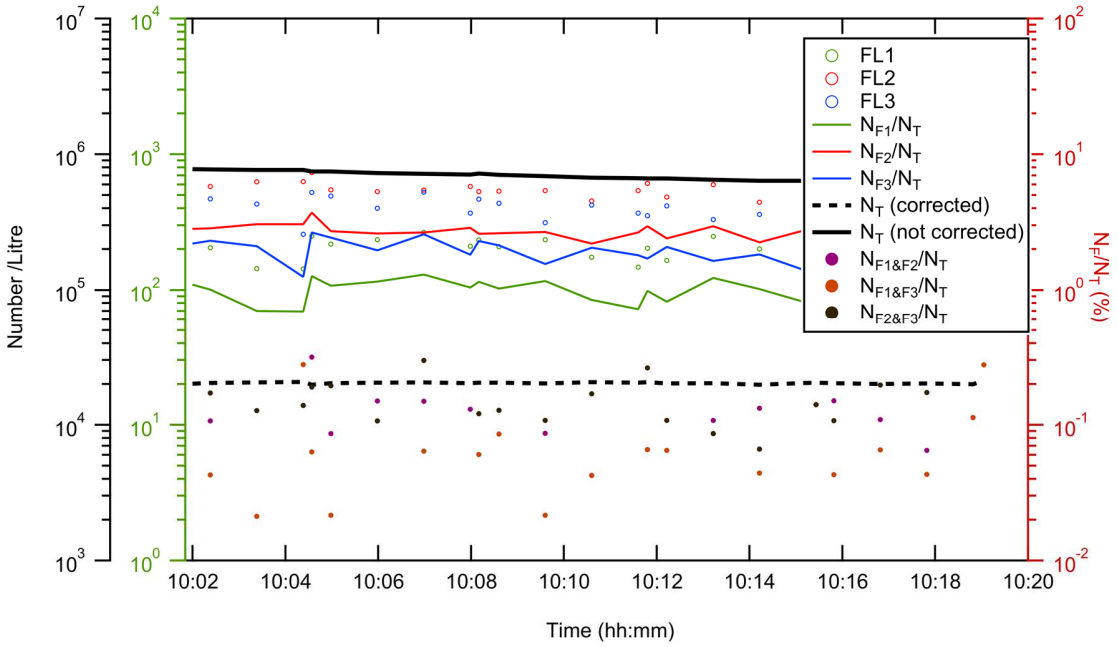


Figure 3.3: WIBS fluorescent particle number concentration data obtained during an experiment at IMK-AAF. Far left axis: WIBS total counts (including missed particle count). Inner left axis: WIBS fluorescent particles represented with open circles. Right axis: Ratio of fluorescent particles to the WIBS total counts (excluding missed particle count).

For calculation of the ratio of fluorescent particles to the total aerosol only those the particle events were taken into account where it was possible to measure the autofluorescence. Nevertheless, ATD fluoresced significantly after both short-wave (280 nm) and long-wave (370 nm) illuminations, suggesting that it should be taken into account when operating WIBS for investigation of, i.e. biological aerosol content of a soil dust sample. $N_{F1}/N_T$, $N_{F2}/N_T$, and $N_{F1}/N_T$ were found as 1%, 3% and 2%, respectively. Using the combination of fluorescence channels on the other hand eliminated this cross-sensitivity to a degree. $N_{F1\&F2}/N_T$ and $N_{F2\&F3}/N_T$ were found to be around 0.2% while $N_{F2\&F3}/N_T$ was calculated as 0.1%. Under the light of these findings a new approach has been suggested and used for the first time to investigate the soil dust samples in AIDA cloud simulation chamber. Figure 3.4 illustrates the response of WIBS to the soil sample (collected from the surface, somewhere in Mongolian and contains significant amount of biological substance). Details concerning the collection and preparation of the sample can be found elsewhere

(Steinke et al., 2013). It has been found that Mongolian dust contains significant amount biological aerosol. The fluorescence data are in good agreement with the conventional methods which are based on culturability of substances. A more detailed investigation on different soil samples will be published in a separate study (Steinke et al., in preparation).

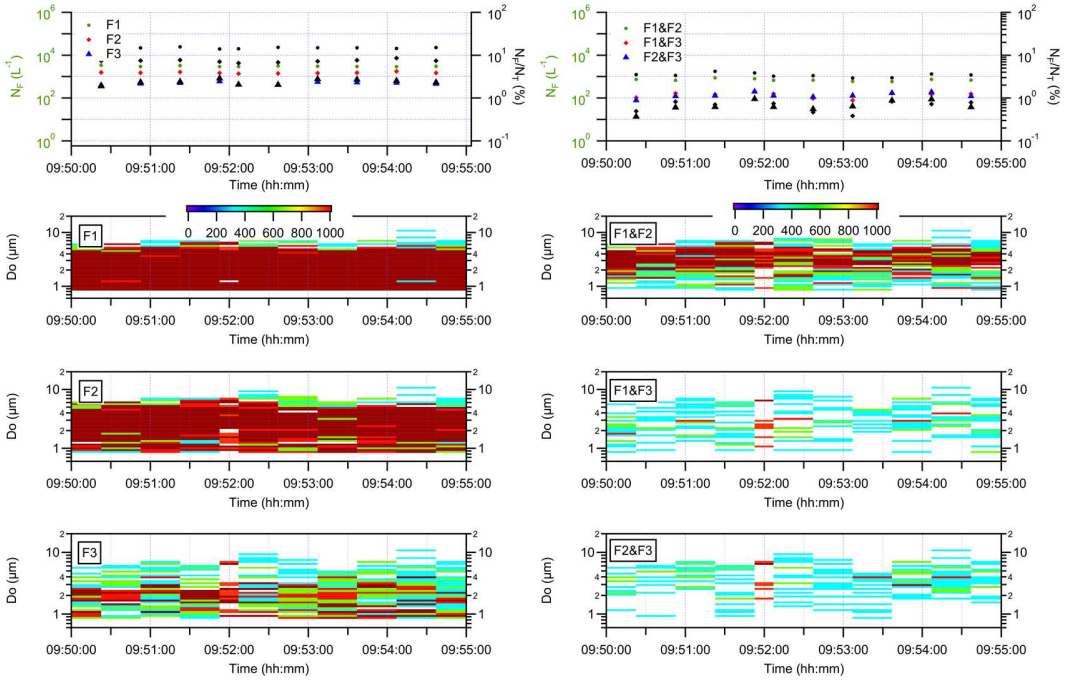


Figure 3.4: WIBS fluorescence data for Mongolian dust that has been investigated during IN19 campaign in July 2012. Left panel: dashed line represents the $N_{F1\&}/N_T$. Lower panels show the integrated fluorescence data. Top panels (both on left and right): show the number concentration of fluorescent particles.

During the course of the BIO-05 campaign (25 March 2010 at IMK-AAF, KIT) a Saharan dust sample (SD2) was investigated. The SD2 was a surface sample that has been collected about 50 km north of Cairo, Egypt. Details concerning the collecting, treatment, and the elemental composition can be found elsewhere (Möhler et al., 2006). The small-scale powder disperser was used to disperse the aerosol into the NAUA chamber. Figure 3.5 illustrates the WIBS fluorescence data for Saharan dust aerosol. Following the same approach that has been suggested for ammonium sulfate and fungal spores mixture it can be seen that WIBS was not able to suppress the autofluorescence comes from Saharan dust

particles even if the combination of two fluorescence channels were used for discrimination criterion.

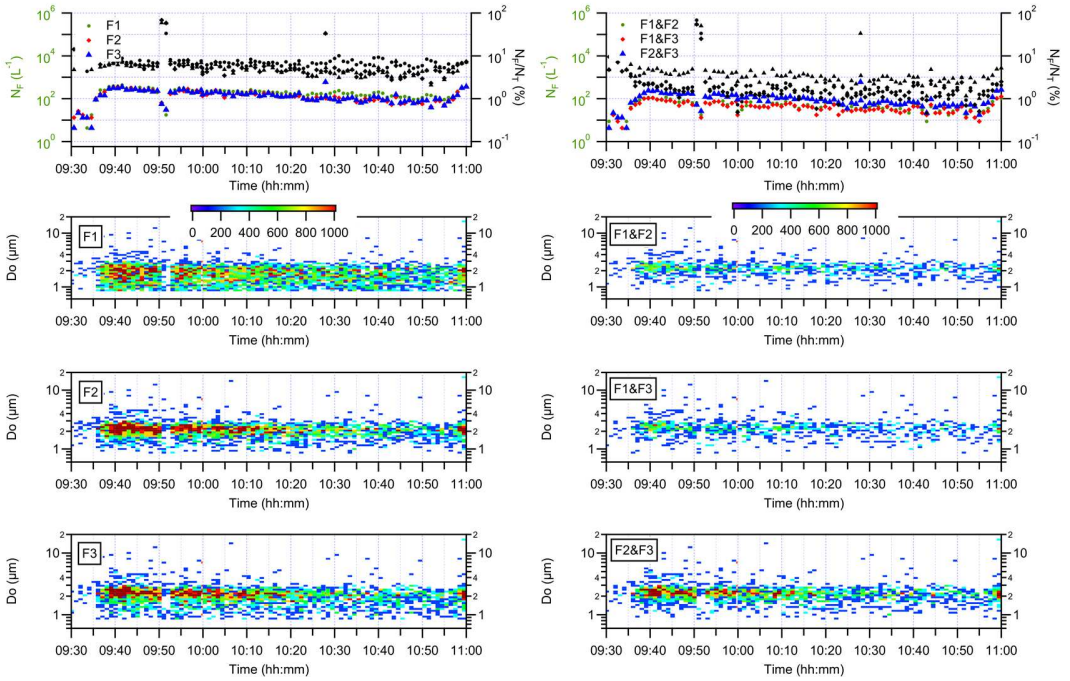


Figure 3.5: WIBS fluorescence data for Saharan dust investigated during BIO-05 campaign in March 2010. The data were plotted in the same way as in Fig. 3.1.

Nevertheless, the nature of the observed autofluorescence of Saharan dust is quite interesting. Recent studies have shown that biological substances residing on dust aerosols can travel over long distances and, therefore, strong sand storms might disperse viable and nonviable microorganisms over wide continental regions (Hallar et al., 2011) or even globally (Smith et al., 2011). Toprak and Schnaiter (2013) suggested that this behavior of Saharan dust aerosol might be attributed to the misclassification in which mineral dust particles produce false positives, or could be the first indication of microorganisms on the dust particles, which can fluoresce on different fluorescence channels. However, the Arizona Test Dust that has been investigated in this study fluoresces surprisingly only on single channels (e.g., channel F1, F2, and F3), albeit not on two of these channels at the same time. This feature is reflected on the significantly lower FBAP numbers for combinations of fluorescence channels such as F1&F2, F1&F3, and F2&F3 of WIBS

(Figure 3.3). One important motivation of this study was investigating the nature of the autofluorescence measured from Saharan dust aerosol that has been collected during heavy dust transportations at Jungfraujoch station. A more detailed discussion about this topic will be given in Chapter 5.

## 4.4. Bacteria and Snomax

Bacteria are one of the most abundant candidates of PBAP in the atmosphere. Unfortunately many of the conventional methods are based on the cultivation of bacteria which is challenging. Therefore the rapid detection of bacteria in the presence of other biological and/or non-biological aerosols is of major importance. In this context, I had the opportunity to perform some test measurements by using bacterial strains from *Psydomona syringe* (PS) that has been isolated from cloud water and investigated in AIDA cloud simulation chamber during BIO-05 campaign. During several cloud simulations, filter samples have been collected and analyzed by a research group in France. It has been found that the viability of bacteria decreases steeply, noting that the method used has not been proven. It should be kept in mind that this is only a preliminary result and may mislead. I will present here only one example for PS to investigate the detection capability of WIBS. Figure 3.6 illustrates the WIBS fluorescence data for PS aerosol which was injected into the AIDA chamber by using a two-stage nozzle. By looking at Figure 3.6 (left panel) it can clearly be seen that WIBS was able to detect almost all bacteria on channel F1. Assuming that channel F1 measures only the intrinsic fluorescence (hereafter fluorescence) from tryptophan (which is a common amino acid) and that channel F3 measures fluorescence from coenzymes and vitamins such as NADH, riboflavin, and vitamin $B_6$, one can speculate that the combination of channel F1 and channel F3 may provide the number of viable species. One commercially available instrument (UV-APS) is suggested to provide the viable FBAP (Huffman et al., 2010, and references therein). Basically UV-APS fluorescence data correspond to the third fluorescence detection band of WIBS (channel F3) with small differences between excitation and detection wavelengths of two instruments.

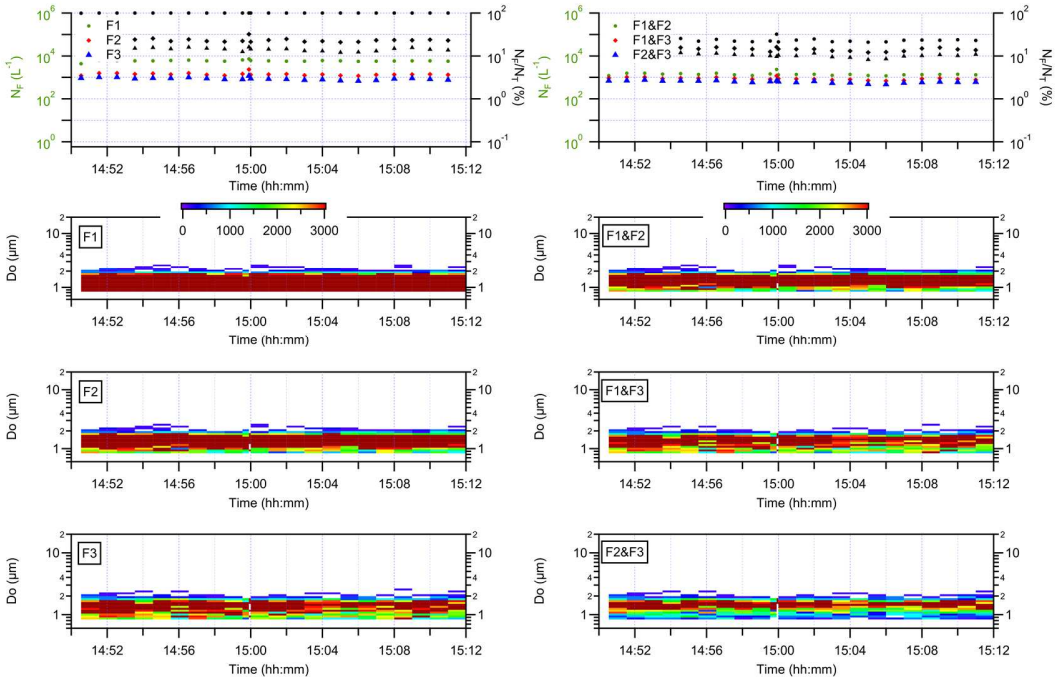


Figure 3.6: WIBS fluorescence data for strain *P. syringae* sampled during BIO-05 campaign. The data are plotted in the same way as in Fig. 3.1.

To overcome one uncertainty about what exactly the first fluorescence detection band (F1) measures, I have investigated a special aerosol called Snomax™ (York Snow Inc.). Snomax™ is an industrial product of strain P. syringae 31R1 grown under conditions (proprietary information) to maximize the ice nucleation activity (Möhler at al., 2008). Figure 3.7 illustrates the fluorescence data recorded by WIBS for a polydisperse Snomax™ solution which has been injected into the AIDA by using a laboratory developed atomizer. As anticipated almost all Snomax™ particles were successfully detected on channel F1 (tryptophan-like signal) while only a minor fraction fluoresces on channel F2 or on channel F3. There is limited literature information dealing with the signal recorded on channel F2. It can be suggested that the cellulose which is the structural component of primary cell wall in bacteria (Pöhlker et al., 2012) is responsible for the fluorescence on channel F2. Since the Snomax™ aerosol does not represent the bacteria itself but only the protein extracted from the bacteria, the sample that has been investigated in this study may not contain all components of a bacteria. This can explain the lower counts on channel F2 and F3.

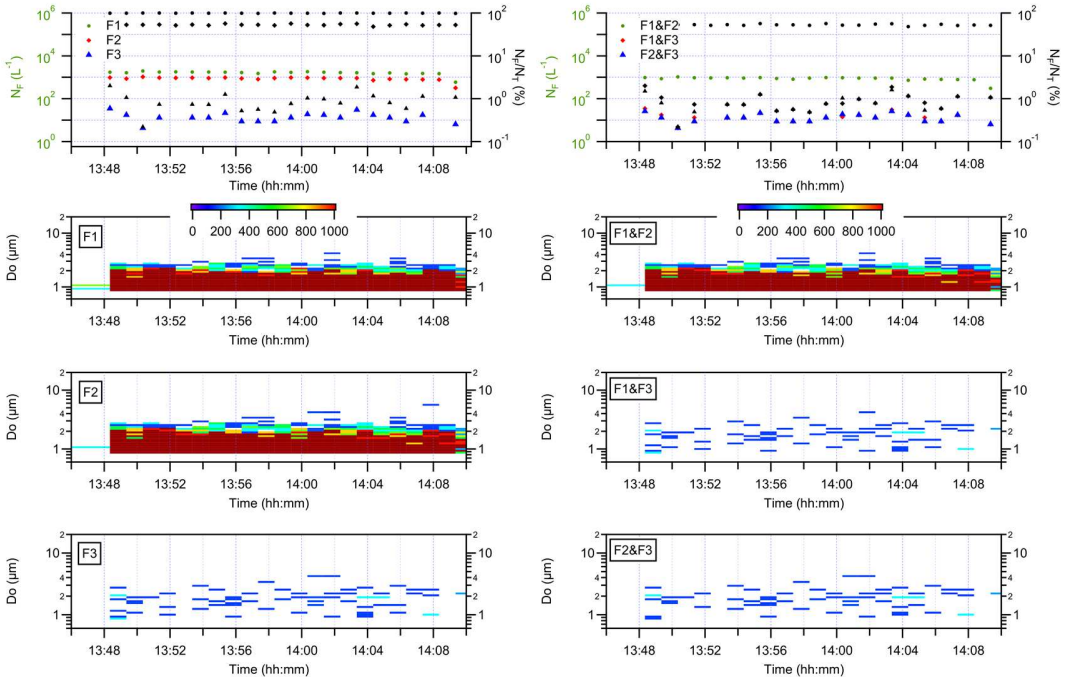


Figure 3.7: WIBS fluorescence data for Snomax$^{TM}$ aerosol sampled during INUIT-03 campaign in 2012.

## 4.5. Analysis of pre-activated dust samples

The Saharan dust samples that have been described in section 2.4 were investigated for their ice nucleation (IN) activity at two different temperatures (at -18°C and at -25°C). Pre-activated dust samples were injected into the AIDA cloud simulation chamber and characterized by aerosol instruments such as APS and SMPS (TSI Inc.). The bioaerosol content of wetly and also dry dispersed Saharan dust sample was measured by WIBS. To interpret the IN ability of the dust samples the ice-active surface site density (INAS) approach (Niemand et al., 2012) was followed. According to the INAS approach, the ice nucleation process is dominated by the number of available ice-active nucleation sites. The higher the active surface sites the more active the related material is supposed to be. Number of ice-active surface sites per unit area are given by a term called $n_s$. For dry and wet dispersed aerosol samples $n_s$ values were calculated and presented in Figure 3.8 to compare those findings with other studies in the literature.

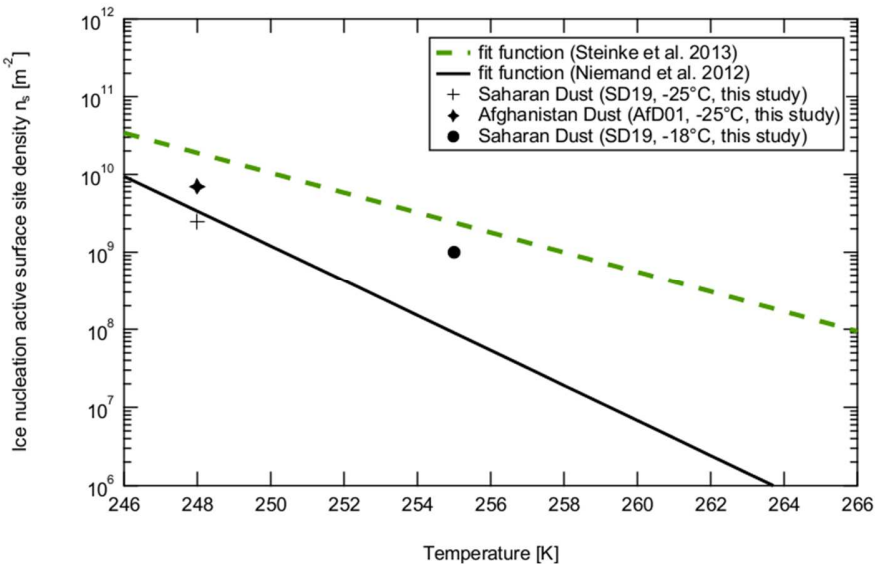


Figure 3.8: Ice nucleation capabilities of different soil dusts and desert dusts that have been investigated at IMK-AAF. Black solid line: Desert dusts investigated by Niemand et al. (2012). Green dashed line: Fitting curve that was observed from soil dust experiments by Steinke et al. (2013).

The main output of this investigation was that the WIBS instrument is capable of detecting bioaerosols in presence of non-biological aerosols (i.e., mineral or soil dust aerosol). Table 3.1 summaries the analysis of different soil dust samples from the point of view of optical and conventional methods.

Table 3.1: Comparison between UV-LIF method and conventional method in case of analyzing three soil dust samples. $N_F/N_T$, represents the WIBS data, while bacteria, actinobacteria, pseudonomads, and fungi show the results from conventional analysis. Data for the conventional analysis method were adopted from Steinke et al. (2013).

| Sample | $N_{F1}/N_T$ | $N_{F2}/N_T$ | $N_{F3}/N_T$ | Bacteria | Actinobacteria | Pseudonomads | Fungi |
|---|---|---|---|---|---|---|---|
| Ms01 | 9 % | 3 % | 1 % | $2.0x10^9$ | $1.4x10^9$ | $2.1x10^5$ | $1.3x10^6$ |
| Gs01 | 3 % | 1 % | nd | $9.5x10^8$ | $5.2x10^8$ | $2.9x10^6$ | $4.7x10^7$ |
| As01 | 5 % | 2 % | nd | $1.2x10^9$ | $5.8x10^8$ | $1.5x10^5$ | $1.8x10^6$ |

The second important result is that the wet dispersed Saharan dust samples, which were pre-activated before dispersing into the AIDA chamber, were not better ice nuclei than the dry dispersed samples. However this result may be due to either ineffective dispersion method which prevented the dispersion of larger particles into the chamber or this result shows us that the pre-activated had no influence on ice nucleation of Saharan dust under given conditions (i.e., activation temperature). Corresponding $n_s$ values are higher for dry samples but lie on the curve that was presented by Niemand et al. (2012). The higher IN activity of biologically richer surface samples that were investigated by Steinke et al. (2013) points out that the bioaerosols may impact the nucleation of ice in mixed-phase clouds. Therefore the ambient aerosol at high altitude research stations was monitored continuously for one year and the idea of nucleation of ice in presence of Saharan dust and bioaerosols was investigated. Saharan dust event and related bioaerosol measurements will be discussed in Chapter 5.

## 4.6. Conclusions and summary

To summarize the laboratory tests that have been performed under controlled conditions by using known atmospherically relevant biological and non-biological aerosols, I can say that WIBS is able to distinguish *penicillium notatum* type of fungal spores from ammonium sulfate aerosol by taking one of the three fluorescence emission bands into account. The fluorescent particles that are eventually misclassified by the WIBS are strongly dependent on the background threshold that we used. This means, one can set a relatively higher threshold to provide a better discrimination of biological aerosols from non-biological fluorescent particles (interferences), however, this will suppress the contribution from some biological particles with small sizes which fluoresce weakly. In the case of using a single fluorescence detection channel such as channel F1, the misclassification was less than 1%. Combustion soot aerosol fluoresced significantly which may be misclassified by WIBS in case of ambient monitoring. The ratio of fluorescent particles to the total concentration was found around 1% on channels F1, F2 and F3 respectively. However the use of combination of any two channels decreased the misclassification to less than 1%. Still, if one plans to measure bacteria in an environment where the air is polluted with soot, possible

contribution from non-biological fluorescent aerosols should be taken into account. As it has already been mentioned in previous sections (Sc. 1.4., and Sc. 4.3.) the fluorescence of mineral dust aerosol is important to be able to make an assumption for further investigation of strong dust events from the point of view of biological content. Thus I have analyzed the mineral dust aerosol and found that mineral dust fluoresces significantly on channels F1, F2 and F3. $N_{F1}/N_T$ was found to be about 7%, while $N_{F2}/N_T$ and $N_{F3}/N_T$ were approximately 5.4%. It is known that artificial mineral dust sample (ATD) contributes around 1% on channel F1, whereas the signal counted on channel F2 and channel F3 were approximately 3% and 2%, respectively. However, ATD fluoresces significantly less than that was observed for single channels when only combinations of any two channels (i.e., channel F1&F2, F1&F3 or F2&F3) are considered. In that case the $N_F/N_T$ was calculated around 0.1%. Although it is rather speculative, the remaining fluorescence measured from Saharan dust aerosol (Sc. 4.3 of chapter 3) may be attributed to some biological material which fluoresces on each fluorescence channels. Different bacterial strains have been investigated and it has been found that bacteria fluoresce mostly on channel F1. This result is in a good agreement with previously published studies (Hill et al., 1999; Pan et al., 2007; Hill et al., 2009). Saharan dust samples were collected from the surface of Sahara desert and pre-activated providing sunlight and water for approximately two hours. Those pre-activated samples were investigated from the point of view of biological activity and ice nucleation capability at mixed-phase cloud temperatures. It has been found that the wet dispersed (always pre-activated) samples are worse ice nuclei than the dry dispersed samples. However there has been found a significant difference between the size distributions of aerosol samples, especially for the wet dispersed samples. This major difference may explain the lower IN capability of these samples which apparently consisted of mostly soluble salt material rather than Saharan dust particles.

# Chapter 4

# Results and discussions: Part-2

## 1. Field campaigns

In this chapter mainly the results from three consecutive long term field campaigns were presented. Main focus will be on the comparison of the number concentrations of fluorescent and total aerosol particles during different seasons. The three sampling sites represent features which are characteristic to those environments. Karlsruhe site for instance was suggested to be representative for a sampling site where vegetation is substantially active. Zugspitze site on the other hand lies most of the time isolated from its environment in free troposphere, albeit in some cases planetary boundary layer may reach the sampling site and convection may influence the aerosol composition by moving aerosol from the local environment. Jungfraujoch station is assumed to be representative of the free troposphere and therefore the aerosol is most of the time not affected by the local changes. If so, it is of major importance to quantify the amount of biological aerosol and also its temporal variation over the course of a year. At these levels the formation of ice clouds may be triggered by minor amount of bioaerosol and this may increase the formation of new ice particles by collision with supercooled cloud droplets.

### 1.1. Eggenstein-Lepoldshafen in Karlsruhe

WIBS has been operated almost continuously for approximately one year in order to characterize the ambient aerosol in the vicinity of the IMK-AAF building in Eggenstein-Leopoldshafen, Karlsruhe, Germany (49°5´43.58´´N, 8°25´45.048´´E; 112 m a.s.l.). WIBS was operated from 31 March 2010 to 30 March 2011 (365 days, 30474 total 15 min samples). A total suspended particles inlet (TSP, Digitel, Model DTSP01/00/16) was placed on the roof of aerosol laboratory, i.e. approximately 5 m above the ground. The TSP inlet is an omnidirectional inlet, which is widely used for general particulate pollution

monitoring. In this study the low-volume TSP inlet has been used, which requires a sample flow rate of 1 $m^3h^{-1}$ (~16.7 $Lmin^{-1}$). This sample flow rate allowed me to collect particles up to 30-40 µm. The TSP inlet has been connected to a stainless steel sampling line (i.e. inner diameter of 13 mm) which penetrates the roof of the laboratory and has been fitted to a 40 mm inner diameter flow tube, which was kept at flow rate of 16.7 $Lmin^{-1}$. Another 13 mm inner diameter stainless steel tube (i.e. approximately 40 cm length) has been connected to the far end of the wide flow tube mentioned above to accomplish an isokinetic sampling. The whole sampling is said to be isokinetic when is isoaxial and the mean sample flow velocity through the face of the inlet is equal to the gas flow velocity (Kulkarni et al., 2011). The WIBS has a sample flow rate of 2.5 $Lmin^{-1}$. The final connection between the isokinetic sampling system and the WIBS has been done by using an electrically conductive silicon rubber tube (length 35 cm, inner diameter ~13 mm). The overall sampling line was approximately 3 m, noting that the whole sampling was strictly vertical, i.e. there were no horizontal connections in order to avoid any sedimentation losses. The measurement site is surrounded by a forest from the north-east to south-west where the average wind direction was dominant and the closest highway is almost 550 m away from the sampling unit. Ambient temperature (T), relative humidity (RH) and pressure were measured simultaneously using a chilled mirror hygrometer. Wind speed and direction were measured using a 3-D sonic anemometer (USA-1, ACH+T, one second time resolution). Additional meteorological data including ambient temperature and relative humidity at two different altitudes, precipitation (mm) and global solar radiation ($Wm^{-2}$) have also been supplied by the meteorological tower of KIT located about 500 m to the south-west of the sampling site. In this chapter, integrated number concentrations and size distributions of fluorescent biological aerosol particles and their correlation with meteorological parameters, diurnal and seasonal changes are presented and discussed in details.

## 1.2. High altitude research station Schneefernerhaus (UFS)

Following the consecutive field campaign in Karlsruhe, WIBS was located at the environmental research station in the Schneefernerhaus (UFS) on the southern side of the Zugspitze mountain (47°24’59.91’’N, 10°58’46.56’’E, 2962 m a.s.l.). Owing to the climate

conditions prevailing at the Zugspitze, the environmental weather station is surrounded by clouds which then enable in-cloud sampling without aircrafts. The research station is located on the highest floor of the Schneefernerhaus and is located on a steep slope facing south on the edge of the Zugspitze, namely approximately 350 m above the Zupspitzplatt, the 'Zugspitze plateau'. The plateau is surrounded by mountain peaks and is open to the east. In the west there is an aeolian hole, leading to the prevailing wind direction being east to west or west to east. Riehl (graduate study) has shown that the yearly averaged temperature, relative humidity and pressure values are -2 °C, 80% and 735 hPa, respectively. Annual precipitation accounts for approximately 5700 mm. The temperature changes around -9°C in January and 8°C in August. The lowest values for relative humidity are found in January (around 75%) and the maximum values were reported for July (around 85%). Rain fall is at minimum in July accounting for 300 mm, while the highest rain fall is observed in December and January accounting for 800 mm and 900 mm, respectively. At high altitude research station Schneefernerhaus the sampling was started in August 2011 and lasted for approximately ten months to evaluate the respective diurnal and seasonal behavior of total and fluorescent biological particles.

### 1.3. High altitude research station Jungfraujoch

The Jungfraujoch (JFJ) Sphinx research station (46°33'N, 7°59'E) is located at 3580 m (a.s.l.). Owing to its high elevation, it can be assumed that the measurements at the JFJ weather station reflect the free troposphere (FT). However a minor effect of the Planetary Boundary Layer should be kept in mind (Coen et al., 2011). As a final step for this PhD study WIBS has been operated at JFJ station for almost one year starting in June 2013. During the entire monitoring WIBS has sampled on a TSP inlet.

## 2. Aerosol number concentrations

The WIBS was operated almost continuously (i.e. measurement stopped sometimes due to undefined problems with data acquisition program). In Karlsruhe, sampling was initiated in April 2010 and the ambient aerosol was sampled for one year. Owing to the time schedule of this study the data collected at JFJ station reflect three complete seasons. WIBS single

particle data were integrated for every 15 minutes time intervals and median aerosol number concentrations together with 5$^{th}$, 25$^{th}$, 75$^{th}$, and 95$^{th}$ percentiles were illustrated in Fig. 4.1 and Fig. 4.2. Details can be found in the appendix B.

First and foremost each location exhibit similar patterns of higher FBAP concentrations in summer than in winter though in completely different sampling climates and at different sampling altitudes (Fig. 4.1, and Fig. 4.2).

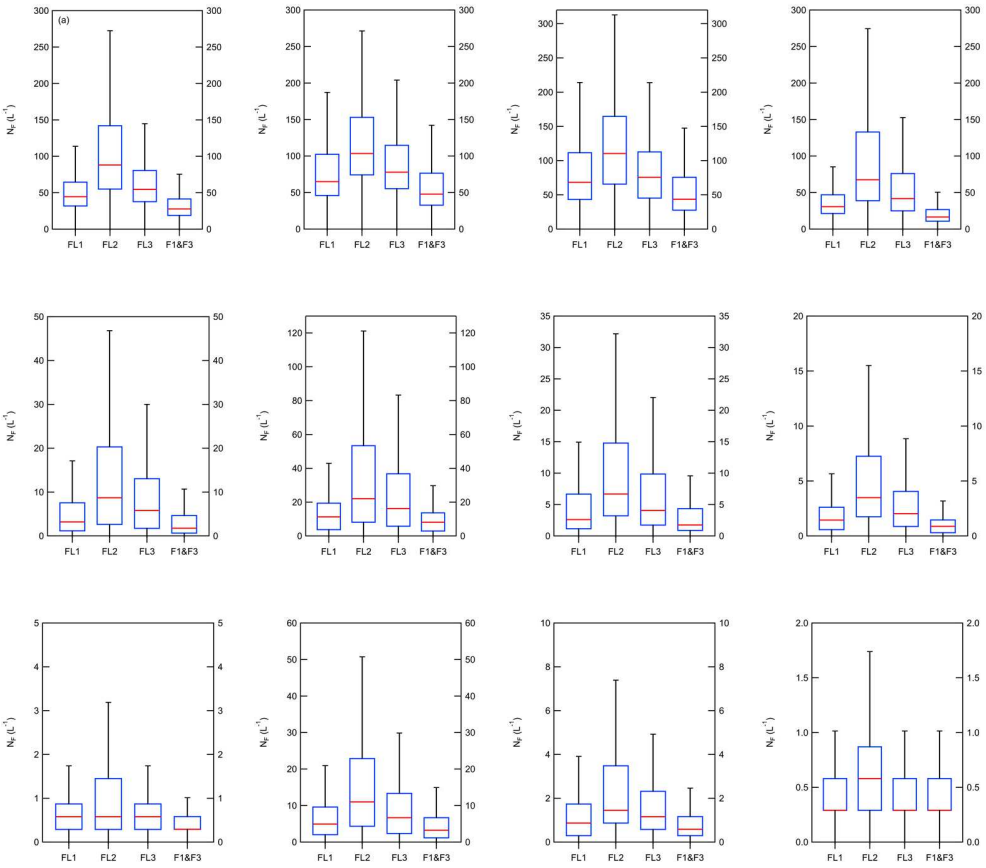


Figure 4.1: Seasonal change of fluorescent biological aerosols at three different locations. Upper panel: Leopoldshafen, Germany (112 m a.s.l.); central panel: Zugspitze, Germany (2650 m a.s.l.); lower panel: Jungfraujoch research station, Switzerland (3580 m a.s.l.). (a) spring, (b) summer, (c) autumn, (d) winter.

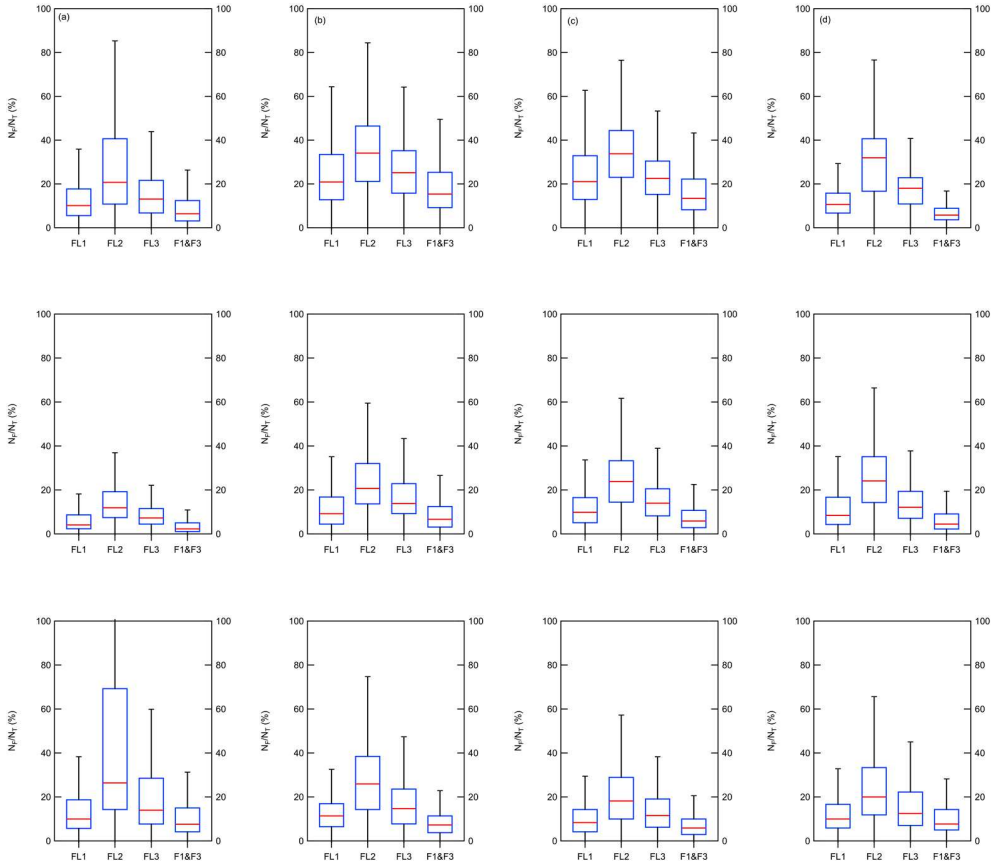


Figure 4.2: Seasonally averaged number ratios ($N_F/N_T$ (%)) for fluorescent particles at Karlsruhe, Zugspitze and Jungfraujoch sites.

The relative increase of the bioaerosols between winter and summer was found to be approx. factor 2 for channel F1 and for channel F3, less than factor 2 for channel F2 and factor 3 for F1&F3 at Karlsruhe site. Same increase of FBAP was observed at Zugspitze site, albeit with different magnitudes pointing out similar sources for fluorescent particles at two sites. The relative increase at Zugspitze site was found to be approx. factor 8 for channel F1 and for channel F3 (same trend observed at Karlsruhe site), factor 6 for channel F2 and factor 9 for F1&F3. The largest difference between two locations were observed for $N_{F2}$, which did not change much at Karlsruhe site, while at Zugspitze site the relative increase was found to be about factor 6, suggesting the contribution from a different aerosol at high altitude station. To our knowledge, this is the first study in the literature that provides single particle fluorescence data of a full seasonal cycle at a high altitude station.

Therefore it is difficult to perform a direct comparison between other studies at similar environments. Again or the first time complete seasonal behavior of bioaerosols at a semi-rural environment was published by Toprak and Schnaiter (2013).

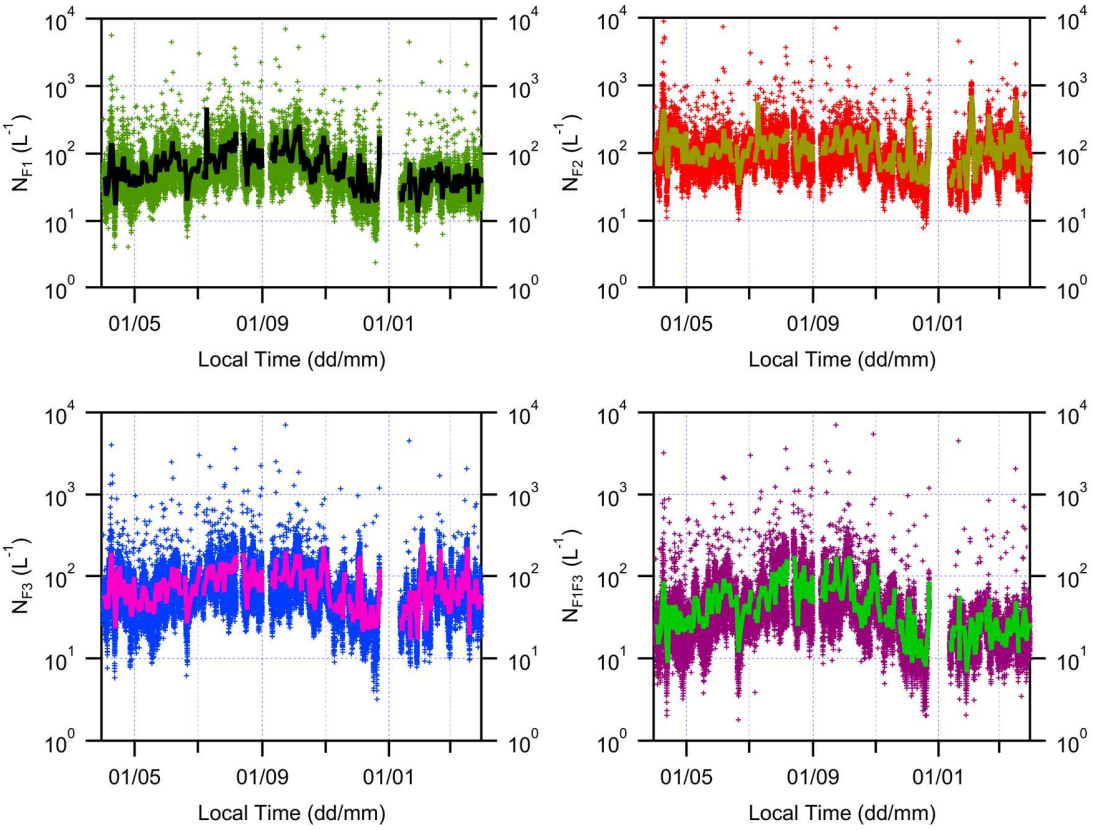


Figure 4.3: Overview of FBAP number concentrations at Karlsruhe site for one year period. Small markers represent the 15 min data points from WIBS. Solid lines show 24 h averaged FBAP number concentrations for the same data.

The results from Karlsruhe site are comparable with the study from Huffman et al. (2010) which reported four months online measurement performed with a UV-APS (TSI Inc., USA) in Mainz, Germany, only in case of considering the combinations of fluorescence detection channels F1 and F3 of the WIBS, but not the single detection channels. Schumacher et al. (2013) reported the seasonal cycle of fluorescent particles in Finland and in Colorado which were measured with the UV-APS. They have found also similar trends for relative change on fluorescent particle number concentration at each location. The

fluorescence channel F3 of WIBS can be compared theoretically with UV-APS since they both detect NADH-like molecules in particles. If it is assumed that the average fluorescent particle number in Mainz was around 20 $L^{-1}$ for summer (Huffman et al., 2010 – Table 1), channel F3 of WIBS reported for the same period ~83 particles $L^{-1}$. This large difference was observed in a very recent study by Healy et al. (2014) where the WIBS and the UV-APS were operated behind the same inlet, in south western Ireland. It has been stated that the fluorescent particle concentration ($N_F$) measured by the UV-APS was by a factor of 2.4 lower than that was measured by the WIBS. That the WIBS and UV-APS have slightly different detection bands, different background levels especially for fluorescent particles and completely different excitation sources can explain this difference in fluorescent particle concentrations. Results are indeed in same order of magnitude which is a good result for the beginning. The low concentration of FBAP in winter can be attributed to the cold temperatures and snow cover which decreases the vegetative production (Schumacher et al., 2013). Another parameter that explains the low winter time FBAP concentrations is the increasing fluorescent particle counts on sunny days, suggesting an increasing biological activity in the environment.

One distinct difference between Karlsruhe and Zugspitze sites is the change on $N_T$ over the course of sampling periods. At Karlsruhe site the $N_T$ did not change significantly and kept constant from summer until the beginning of spring. However the $N_T$ was found to be higher in spring than in summer in contrast to $N_{FBAP}$. A similar observation was reported by Schumacher et al. (2013) in Colorado where a UV-APS was operated for complete four seasons. In Karlsruhe, spring median $N_T$ was approx. 797 $L^{-1}$ which dropped to approx. 400 $L^{-1}$ towards the end of sampling period. On the other hand, at Zugspitze site $N_T$ increased from winter to summer and decreased again at the end of summer period. FBAP increased also with increasing total aerosol. Since the Karlsruhe site lies most of the time in planetary boundary layer (PBL) $N_T$ is strongly affected by convective mixing and local changes (i.e., Figure 4.13, panel “a”). Zugspitze site, however, lies in free troposphere (FT) and the PBL effect is of minor importance. Moreover TAP number concentration at Zugspitze summit starts increasing when the PBL effect and vertical transport process become more prevalent.

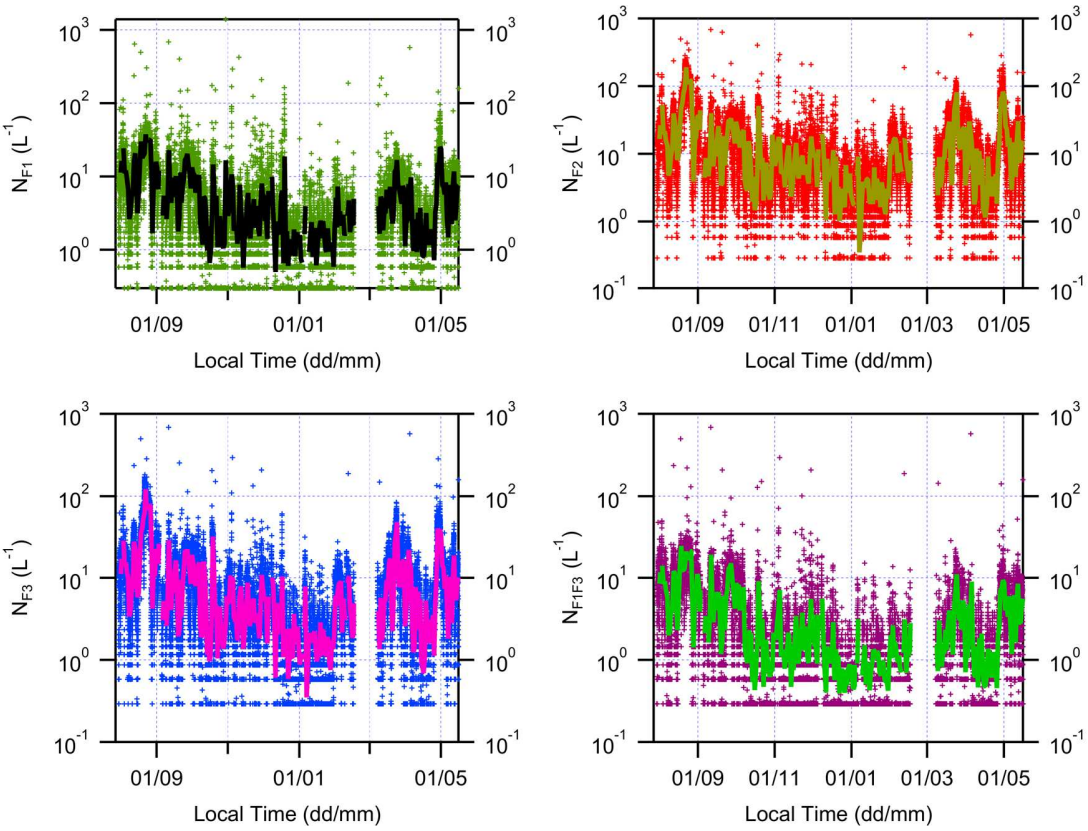


Figure 4.4: Overview of FBAP number concentrations at Zugspitze site for 10 months between 31/07/2011 and 16/05/2012. Small markers represent the 15 min data points from WIBS. Solid lines show 24 h mean FBAP number concentrations.

It is of major importance to investigate the aerosol number concentrations at different locations. Coen et al. (2011) for instance reported aerosol climatology at the Jungfraujoch station and discussed the planetary boundary layer effects. They found that the JFJ is not influenced by any synoptic weather types, albeit a considerably high influence of the planetary boundary layer (PBL) has been seen in the rest of the time. Any change on PBL may influence the composition, number, and size distribution of the aerosol especially biological aerosol at sampling sites. Therefore one has to keep in mind that the aerosol sampled at a certain time at a certain place may have been influenced by some local sources. During the course of this study it has been found that coarse mode aerosol number concentrations at the JFJ station are only slightly influenced by the PBL change in summer.

To illustrate the effect of PBL on aerosol number concentrations $N_{F1}$ has been stacked in Figure 4.5. It can clearly be seen that the PBL effect is the greatest in Karlsruhe which is reflected on clear diurnal cycles of fluorescent particles. At Zugspitze site this feature is not as clear as at the Karlsruhe site. However for some days a clear diurnal change of fluorescent particles can be seen. In contrary to Karlsruhe and Zugspitze sites, at JFJ no diurnal cycle of fluorescent particles has been seen.

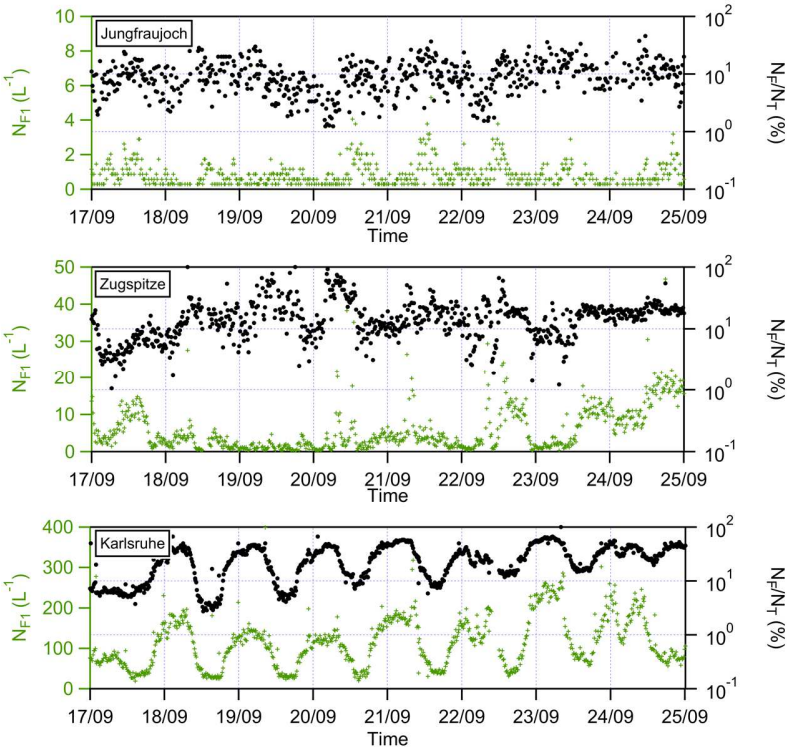


Figure 4.5: Time series of FBAP at three different locations. For each panel, left: number of fluorescent particles, right: ratio of fluorescent particles to the total aerosol count (without missed particle count correction). Top panel: Jungfraujoch station, sampling year: 2013. Centered panel: Zugspitze station, sampling year: 2011. Lower panel: Karlsruhe site, sampling year: 2010.

# 3. Aerosol number size distributions

For detection of optical particle size, a continuous-wave 635 nm diode laser has been used. Resulting elastic scattering data were sampled in the forward direction and at a 90° offset. Based on Mie theory a calibration approach was developed and in this calibration approach particles are assumed to be spherical and have a specific refractive index. Over the course of two consecutive field campaigns in Karlsruhe and at Zugspitze, and as well as for some of the laboratory investigations WIBS has been operated in a mode where the particle detection was performed by integrating the area under the pulse of forward scatter signal. This method has the advantage on detecting smaller particles (i.e. Do< 5 µm approximately). On the other hand any problem that arises on the PMT detector may influence the integration of the forward scatter signal. In this the larger particles (approx. Do > 5 µm) are misclassified, while the smaller particles are less affected. Toprak and Schniater (2013) used this method and the main fluorescent particle mode seems correct and was not affected by sizing issue. In May 2012 the sizing principle has been changed to peak detection mode where the maximum value of the scattered signal is measured rather than the area under the pulse. After the sizing principle was changed a one-month dataset was collected at Karlsruhe site, under identical sampling conditions that have been preferred for the Karlsruhe sampling. Both measurements at the same place and in same season, albeit on different dates were plotted in Fig. 4.6 and Fig. 4.7, respectively.

Figures represent the aerosol number size distributions. In Fig. 4.6 it can clearly be seen that there is a peak between 2 – 3 µm on each panel (i.e. each panel represents a different particle selection criteria which is defined on Table 2.2), suggesting that the fluorescent particles in this size range dominated the whole population at the sampling site. To be able to see the difference between two different particle sizing methods the number size distribution for particles sampled from 17 October 2012 to 5 November 2012 was plotted in Fig. 4.7. Note that all sampling conditions are identical with the previous sampling at Karlsruhe site and the only difference is the modified particle sizing method of WIBS from pulse integration to peak height detection.

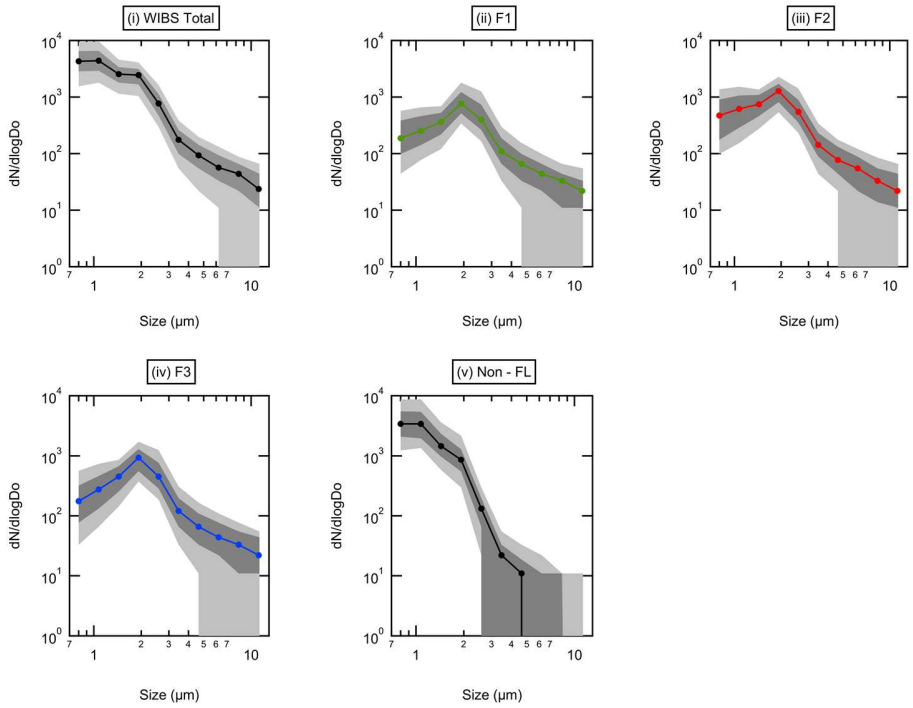


Figure 4.6: Number size distributions (old principle) for Karlsruhe site (logarithmic mid-size bins; from 17 October 2010 to 5 November 2010) for different particle types including fluorescent and non-fluorescent particles. Solid line: median values. Dark shading: inter-quartile range (25$^{th}$ and 75$^{th}$ percentiles). Light shading: 10$^{th}$ and 90$^{th}$ percentiles. Note that percentiles or median values intersecting the x-axis represent a zero concentration which cannot be shown in logarithmic scale.

The most distinct difference between Fig. 4.6 and Fig. 4.7 is for larger particles. In Fig. 4.6 there is a steep decrease on the distribution curve for particles larger than a few micrometers, while in Fig. 4.7 the same curve follows a plateau and the decrease is slower than it is in Fig. 4.6. The submicron size particles seem to be better reflected in Fig. 4.6 than in Fig. 4.7 which can be seen from the narrower 10$^{th}$ and 90$^{th}$ percentiles. As a conclusion of this direct comparison one can say that size distributions of fluorescent particles between 0.8 and 3 µm are only slightly affected in all cases reported in this study, i.e. for some of the laboratory tests, for the Karlsruhe site and for the Zugspitze site. However, for particle sizes larger than 5 µm there is a great uncertainty for the aerosol number size distribution reported for Karlsruhe site (Fig. 4.6).

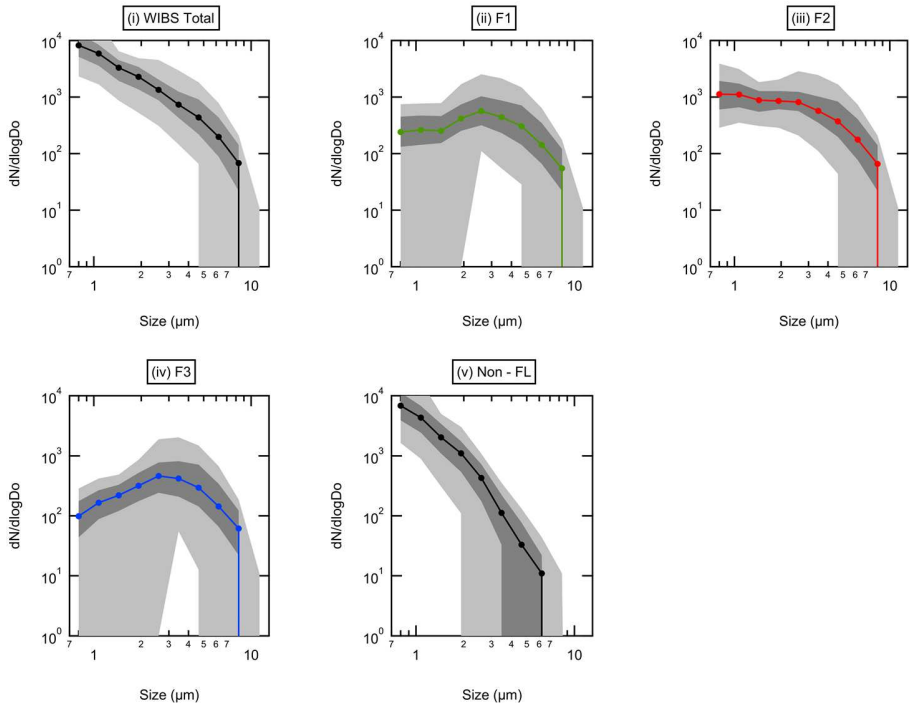


Figure 4.7: Number size distributions (new principle) for Karlsruhe site (logarithmic mid-size bins; from 17 October 2012 to 5 November 2012) for different particle types including fluorescent and non-fluorescent particles. The data are plotted in the same way as in Fig. 4.6.

Keeping in the mind that the FBAP number concentration found at Zugspitze site was comparably lower than it has been observed at Karlsruhe site, main features of aerosol number size distributions for summer term have been discussed in Fig. 4.8 and Fig. 4.9. If number size distribution plot is divided into fine mode and coarse mode, I can state that throughout the measurement periods non-fluorescent particles dominated the total aerosol in fine mode while the coarse mode consisted of fluorescent particles. Number distribution for each fluorescent type (i.e. F1, F2 and F3) contained one distinct mode at ~ 2.5 µm and a shoulder at approximately 1.8 µm at Karlsruhe site. At Zugspitze site there was only one distinct mode at ~ 2.5 µm, suggesting that the fluorescent particles can be transported to very high altitudes and may impact cloud formation and precipitation. However to what extend the bioaerosols may impact the ice and/or droplet formation at Zugspitze site is beyond the scope of this thesis. It was one of the major objectives of this study to find

indications about long range transportation of biological aerosols. The main mode between 1.8 – 3 µm was attributed to fungal spore release at Karlsruhe site (Toprak and Schnaiter, 2013) and there are also other studies at different locations giving similar indications of release of actively wet discharged fungal spores (Huffman et al., 2010; Gabey et al., 2010; 2011). Schumacher et al. (2013) found similar trends for FBAP in Hyytiälä and in Colorado, concluding that the mode at ~ 3µm was the most common individual mode and it has been attributed to mainly fungal spores and agglomerated bacteria. In WIBS bacteria fluoresce mostly on channel F1. However, it has been found that bacteria fluoresce less but significantly on channels F2 and F3 either (chapter 3 sect. 4.4.).

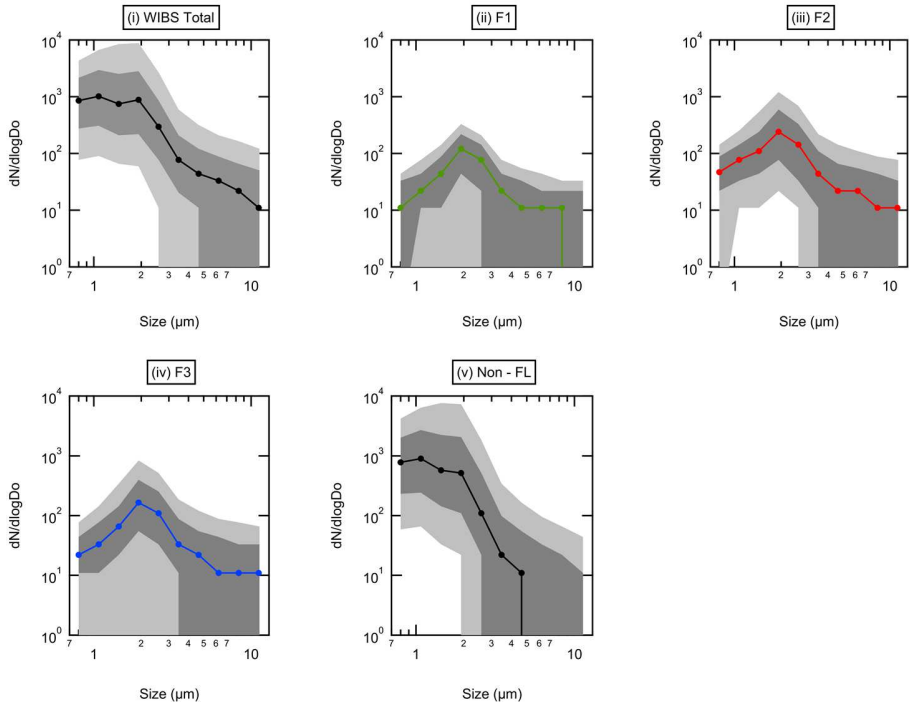


Figure 4.8: Number size distributions of Zugspitze (logarithmic mid-size bins; for August 2011) for different particle types including fluorescent and non-fluorescent particles. The data are plotted in the same way as in Fig. 4.6.

One other important feature that has been observed only at Zugspitze site is that the particles fluoresce on channel F1 are smaller than 5 µm, while channels F2 and F3 show better statistics for particles larger than 5 µm. That the channels F2 and F3 are not correlated with non-fluorescent particles in coarse mode suggests that the coarse mode

aerosol consists of mostly fluorescent biological aerosol. This feature is slightly different at Karlsruhe site where all three fluorescence channels have identical number size distributions, suggesting one type of source is responsible for the fluorescence measured at this site. In contrary to Zugspitze site, at Karlsruhe site the main total aerosol particles (TAP) mode (1.8 – 3 µm) consisted mostly of fluorescent particles.

In contrary to the fluorescent particles, non-fluorescent particles did not contribute to the coarse mode part of the size distribution. Both at Karlsruhe and at Zugspitze site number of non-fluorescent particles decreased with increasing particle size. This behavior was shown in Figures 4.8 and 4.9 (panel Non-FL) where the $10^{th}$ and $90^{th}$ percentiles are broadened and also the median values drop below unity.

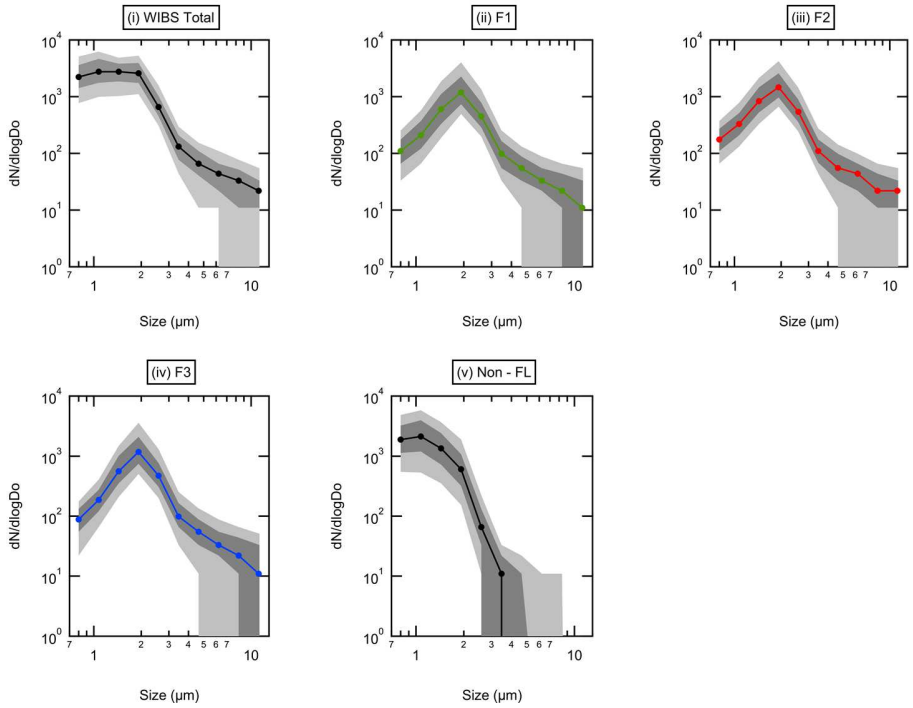


Figure 4.9: Number size distributions of Karlsruhe (logarithmic mid-size bins; for August 2010) for different particle types including fluorescent and non-fluorescent particles. The data are plotted in the same way as in Fig. 4.6.

# 4. Diurnal patterns

Another advantage of the online bioaerosol monitoring is that the high time resolution of the collected data allows for the representation of daily (diurnal or 24h) averages of number size distributions and number concentrations for individual channels. However in some cases because of lack of statistically good dataset available it may not be possible to generate a 3D plot to present the averaged fluorescent aerosol number distributions (i.e., data collected at Zugspitze site). Therefore I will only present seasonally averaged diurnal patters belong to Karlsruhe site in this chapter. Seasonally averaged number size distributions and number concentrations have been plotted together with corresponding meteorological parameters such as ambient temperature (T) and relative humidity (RH) for fluorescence channel F1, F2, and F3 (Fig. 4.10, Fig. 4.11, and Fig. 4.12), accordingly. Diurnal change of TAP for individual seasons was shown in Figure 4.13.

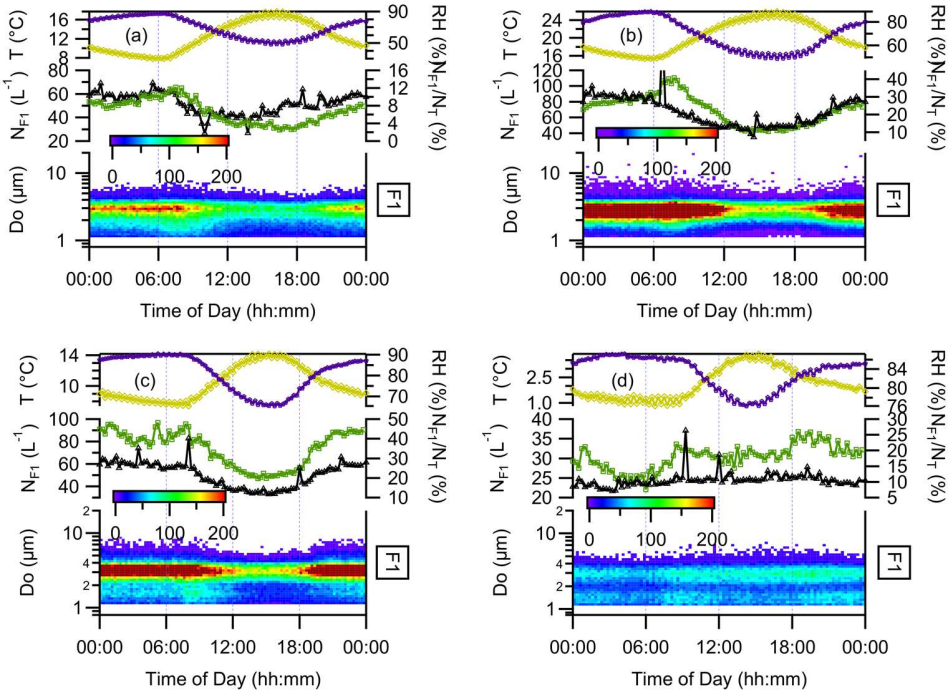


Figure 4.10: Seasonally averaged diurnal fluorescent particle number distributions and number concentrations at Karlsruhe site. Fluorescence data represent the channel F1 of WIBS. Top panel, left axis (yellow markers): temperature (T), right axis (purple markers): relative humidity (RH). Central panel, left axis (green markers): fluorescent aerosol number

concentrations ($L^{-1}$), right axis (black markers): ratio of fluorescent particles to the total aerosol number (%). Lower panel: size distribution (d*N*/dlogDo) of fluorescent aerosol particles for individual fluorescence channels. Transparent or light bluish areas represent zero or very low numbers. (a) spring, (b) summer, (c) autumn, (d) winter.

The most important and the most distinct feature of all three figures is that the fluorescent particle number concentrations were higher in the evening hours than they were during day time. In some cases an early morning peak has also been observed.

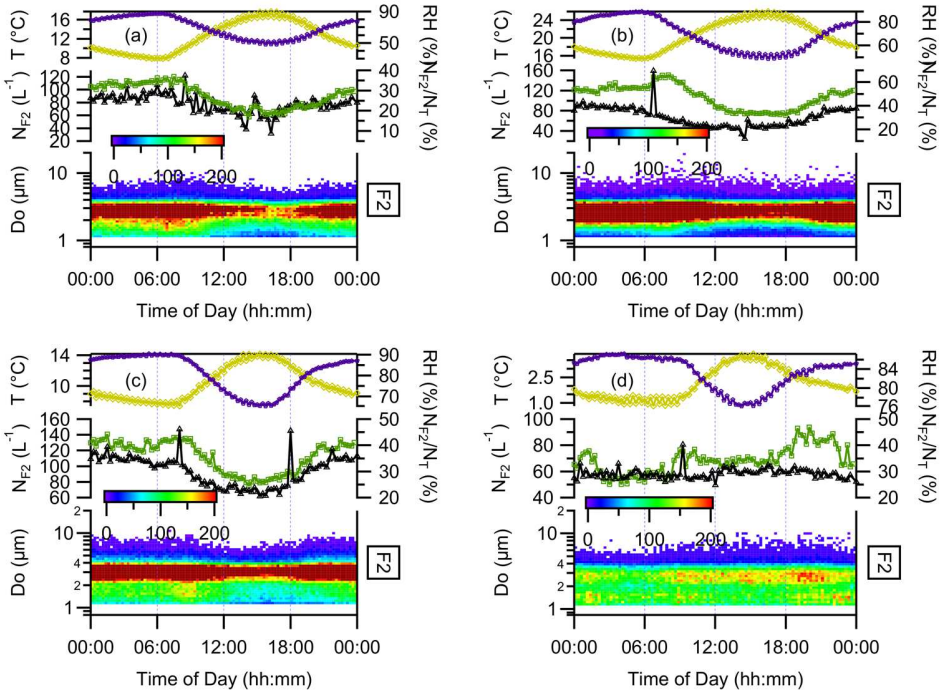


Figure 4.11: Seasonally averaged diurnal fluorescent particle number distributions and number concentrations at Karlsruhe site. Fluorescence data represent the channel F2 of WIBS. The data are plotted in the same way as in Fig. 4.10.

This behavior of fluorescent biological aerosol was reported by several studies in literature (Huffman et al., 2010; Gabey et al., 2010, 2011; Toprak and Schnaiter, 2013; Schumacher et al., 2013) and it has been suggested that there should be a positive correlation between FBAP and relative humidity and/or temperature as well.

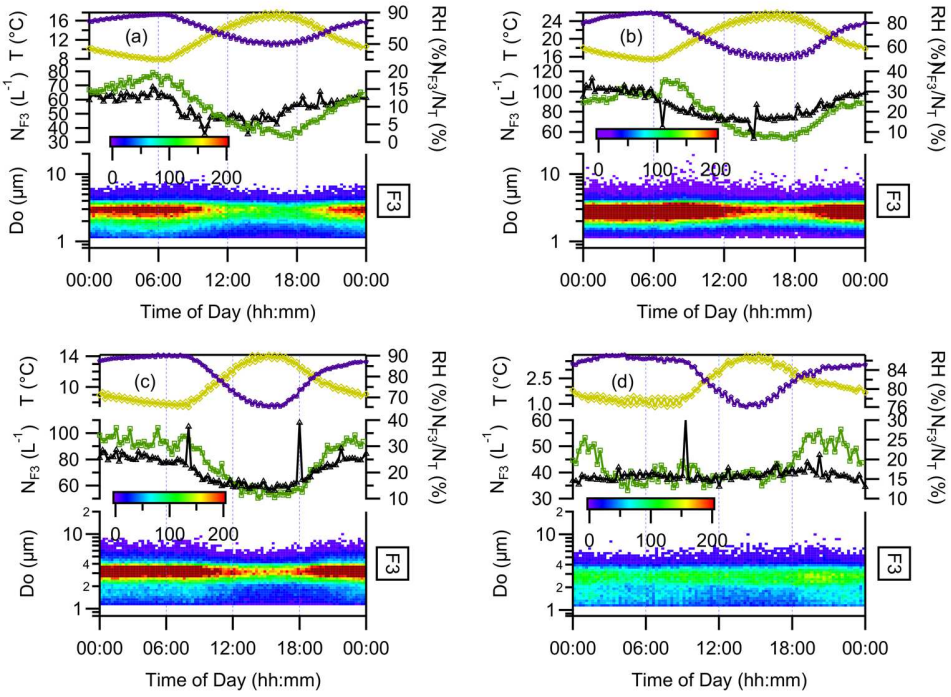


Figure 4.12: Seasonally averaged diurnal fluorescent particle number distributions and number concentrations at Karlsruhe site. Fluorescence data represent the channel F3 of WIBS. This channel is similar to the commercially available UV-APS instrument. The data are plotted in the same way as in Fig. 4.10.

In the spring term, $N_{F1}$ started to increase in the evening hours (in most of the time after sunset) and reached a fairly large number in the midnight. During the night time $N_{F1}$ kept almost constant and in some cases a maximum value has been observed in the morning hours, after the sunrise. The lowest $N_{F1}$ values have been found during day time (between 12:00 – 15:00) when the temperature was higher and the relative humidity was lower. $N_T$ started to increase after sunrise and kept relatively constant during day time. TAP number concentration started to decrease after 15:00 until sunset. After sunset, $N_T$ slightly increased and stayed constant until the next sunrise. In summer, similar diurnal trends have been observed in all fluorescence channels and as well as for TAP. FBAP were again higher between 18:00 and 09:00 (local time), albeit in general average $N_{FBAP}$ has been found to be higher than it has been in spring. In addition, observed decrease in the $N_{F1}$, $N_{F2}$, and as well as in the $N_{F3}$ shifted to early noon hours. In contrary to spring term a clear morning peak

has been observed in summer. Similar to the spring term, $N_T$ was high during daytime and lower but almost constant between 17:00 and 06:00. The diurnal change of $N_{FBAP}$ was observed also in autumn term but the average number concentration of fluorescent particles have been found to be lower compared to the summer period. The same diurnal mode between 2 – 3 µm has again been seen, suggesting that the release of the same type of particles continue all the year round. A higher number concentration of larger particles, which has been observed in this term, was attributed to the release of another type of aerosol (Toprak and Schnaiter, 2013). However, the new particle detection principle has shown that this feature was most probably because of the timing issue, which was more effective for particles larger than 5 µm. It should be still noted that the pollen release in autumn could be the reason for the clear increase in the latest size bin. Major difference between autumn and spring – summer samplings is that a new particle mode between 1 – 2 µm was observed. This new mode can be attributed to a different aerosol source because both in spring and summer terms, there is no distinct mode in this size range.

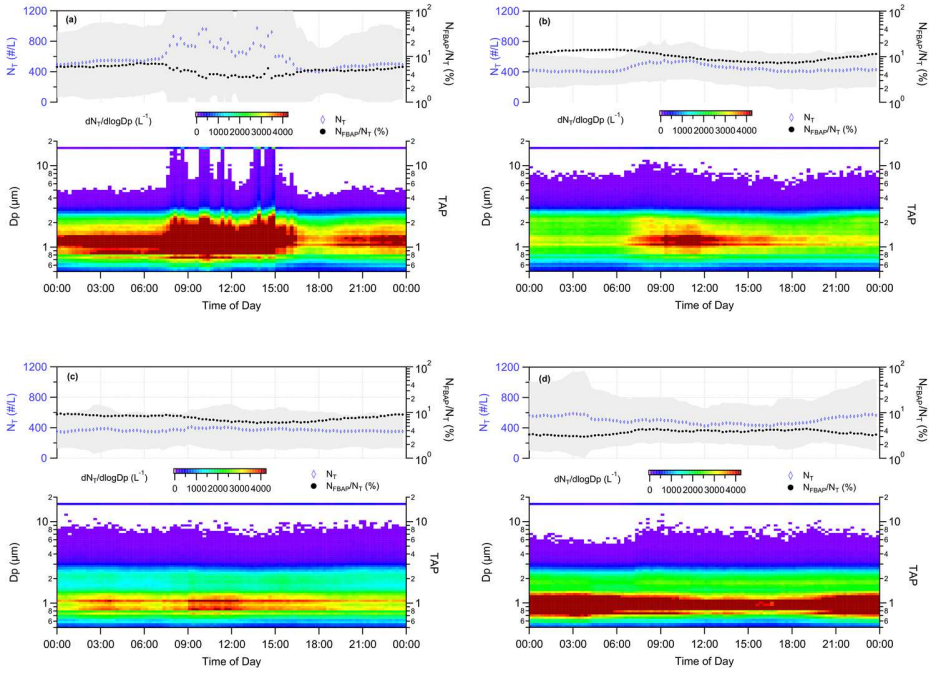


Figure 4.13: Diurnal change of TAP number concentrations at Karlsruhe site (upper panels) and integrated number size distributions (lower panels) for individual seasons.

Interestingly, this mode has become clear towards the beginning of winter term where the average ambient temperatures are at their minimum values and the RH lies between 76% and 88%. Buller at al. (1910) has already reported in the first decay of twentieth century that the bacterial concentrations have the maximum in September and also the minimum in March. Thus, the second mode that was observed in the late autumn and in winter can be attributed to bacterial releases (panels “c” and “d” of Figures 4.10, 4.11, and 4.12). Similar to the summer term, in autumn TAP was nearly constant during day- and nighttime. Unlike the other three seasons, $N_F$ and $N_T$ were almost constant during entire season. However, nighttime $N_T$ was for the first time higher than it was in daytime. In winter the land surfaces were covered by snow and the release of biological aerosol was prohibited. Because of the fact that the atmospheric boundary layer is narrower in the night, $N_T$ was also higher in nighttime than it was in daytime. Another reason for this behavior is that the $N_T$ was dominated mostly by non-fluorescent particles in winter. The general particle mode between 2 and 3 µm was again observed but for the first time another distinct mode between 1 and 2 µm was observed, especially in channel F1 (Fig. 4.10d). The reason for this particle mode that appears towards the end of autumn is though not clear, products of the combustion gases. The reader should keep in mind that the ratios of number of fluorescent particles for soot aerosol (i.e., for each fluorescence detection channel) were calculated for Karlsruhe site and were less than 1%.

## 5. Correlation of bioaerosols with meteorological parameters

In several studies published over the last decade a clear correlation of number concentration of FBAP has been found between relative humidity, temperature, and as well as rain events (Gabey et al., 2010, 2011; Huffman et al., 2010, 2012, 2013; Toprak and Schnaiter, 2013; Schumacher et al., 2013). Here, I will show the correlation of FBAP with RH at the Karlsruhe site. Figures 4.14 and 4.15 illustrate the dependency of FBAP on different meteorological parameters such as RH, temperature (T), global solar radiation ($Wm^2$), wind speed ($ms^{-1}$), rain fall (mm) for four seasons between April 2010 and April 2011. To get a first overview of the effect of each meteorological parameter all data have been plotted in the same figure. In Fig. 14a and Fig. 4.14b, the strong correlation between $N_{FBAP}$ and the RH is notable, especially during clear sky periods (indicated by distinct diurnal trends of

global solar radiation) with warm and dry days and cool and humid nights (i.e. between 22 May – 25 May). A continuous release of biological aerosol has been observed in this time of the year, which was apparently triggered by highly humid conditions. Relative humidity related release of biological aerosols has been investigated in several studies. Hirst (1953) found a direct relationship between release of *Basidiomycota* (BMC) type of fungal spores and RH. This type of fungus ejects its spores according to a specific mechanism, which has been investigated and reported by Pringle et al. (2005). They have successfully visualized the mechanism of *ballistospore* discharge by using conventional still photomicroscopy. To be able to quantify the correlation between the number of fluorescent biological particles and the ambient relative humidity I have performed a statistical analysis on the data for individual seasons. The number of particles that simultaneously fluoresce in channels F1 and F3 were correlated with RH values, which were measured with the same time resolution. $N_{F1,F3}$ were averaged into 100 RH bins and the corresponding mean and median values were plotted in Fig. 4.16.

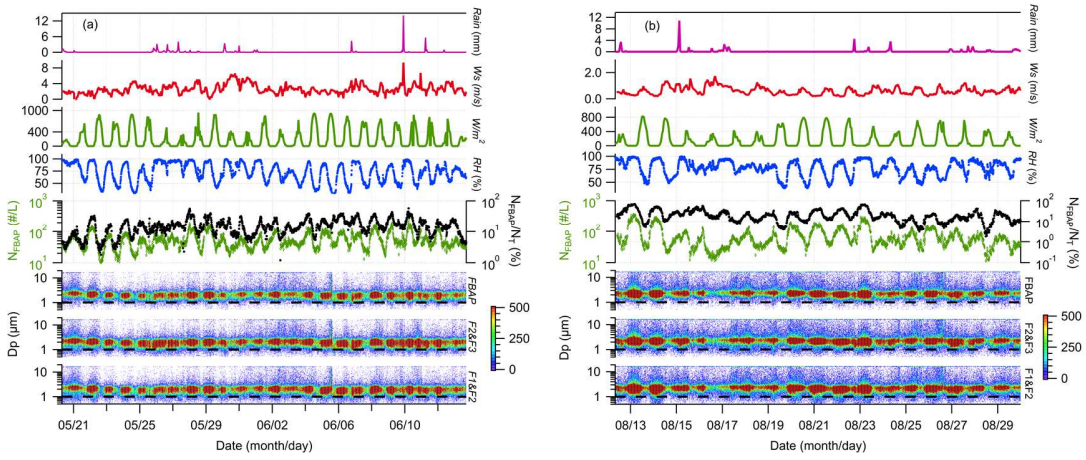


Figure 4.14a: (left) and 4.14b (right) WIBS fluorescence data for a selected period in spring correlated with meteorological data collected at the same time. The lower panels: different combinations of fluorescence channels F1, F2 and F3 (e.g. F1andF2 represents the particles that simultaneously fluoresce in both channels F1 and F2). The upper panels: from bottom to top, number concentration of FBAP (left) and ratio of FBAP to all particles (right) measured by WIBS, relative humidity (%), global solar radiation ($Wm^{-2}$), wind speed ($ms^{-1}$), and precipitation (mm). (a) spring, (b) summer.

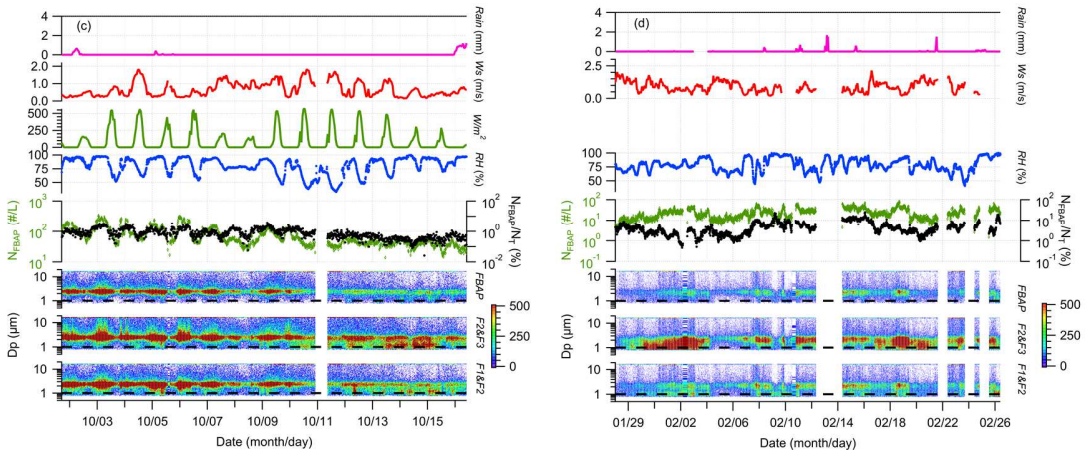


Figure 4.15a: (left) and 4.15b (right) WIBS fluorescence data for selected periods in autumn and winter correlated with meteorological data collected simultaneously. The data were plotted in the same way as in Fig. 4.13. (c) autumn, (d) winter.

The resulting curves were fitted according to a power law function and the coefficients of determination ($R^2$) for the non-linear regressions were also calculated (see Fig. 4.16). Figure 4.16 clearly shows that the biological aerosol number concentration increases exponentially with increasing RH, especially between ~70% RH and 95% RH in spring and in summer, as well as in autumn albeit to a lower degree. Although a certain RH is required to initiate the release of fungal spores it seems that the dew formation is the limiting factor for bioaerosol release. Schumacher et al. (2013) suggested that after some point (e.g., ~82% during summer) formation of dew on plant and terrestrial surfaces prevented release of biological particles. At Karlsruhe site however this limit RH was found a bit higher (Figure 4.16).

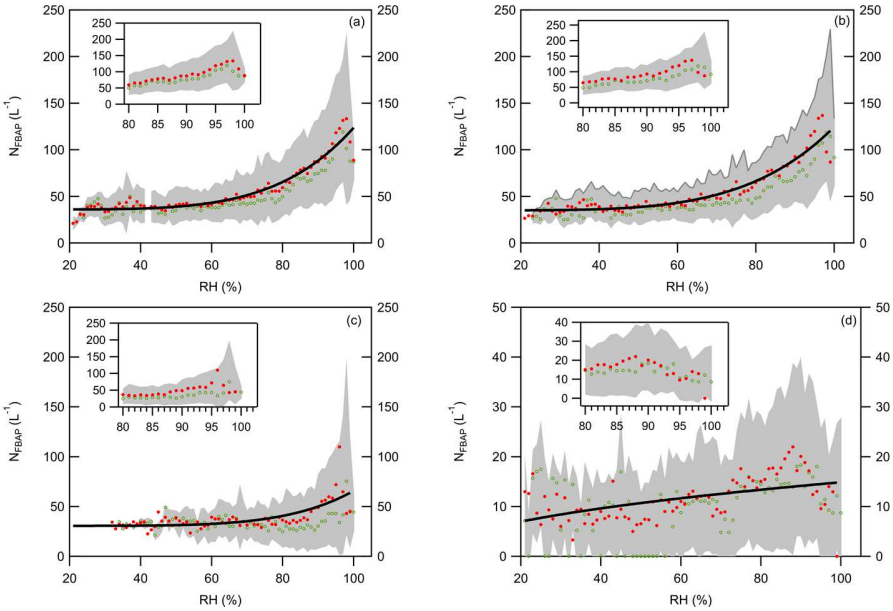


Figure 4.16: Correlation of the fluorescent aerosol number concentration with the relative humidity; mean $N_{F1,F3}$ (red markers), median $N_{F1,F3}$ (green markers), fitted curve according to the mean values (solid black lines), variability of $N_{F1,F3}$ represented with plus-minus standard deviations (grey shaded areas). Fit function: $f(x) = a.x^b+c$; (a) spring ($R^2 = 0.924$), (b) summer ($R^2 = 0.911$), (c) autumn ($R^2 = 0.541$), (d) winter ($R^2 = 0.652$).

My findings are in good agreement with the recent study from Gabey et al. (2010). As a conclusion it can be speculated that the fungal spores which are seen most of the time at Karlsruhe site are most probably *Basidiomycota* (BMC) type of fungal spores, which are released mostly during nighttime and under very humid conditions. Fröhlich-Nowoisky et al. (2012) performed the DNA-based analysis of airborne fungi in continental, coastal and marine air. They found that the BMC dominate continental air, while Ascomycota (AMC) prevails mostly in marine and coastal air. On the other hand, I did not find any evidence of passive release of fungal spores which is generally related to the wind speed or wind direction. However, in some cases FBAP release increased after rain events. This feature was also reported in the recent literature by Huffman et al. (2013) and Schumacher et al. (2013).

# 6. Size segregated asymmetry factor (Af) data

The asymmetry factor (Af) and its definition has been discussed in chapter 2 (sec. 2.2) in details. The particle sphericity has been investigated for individual seasons at Karlsruhe site and as well as at the Zugspitze site. Data were sorted in a way that the dependency of each single particle on both particle size and asymmetry factor can be shown in one figure. The data were categorized into a multidimensional array. Dimensions are Af, particle optical size, frequency of occurrence of single particle detections, accordingly. Each particle event was split into pre-defined arbitrary size- and asymmetry bands. Frequency distributions, each was normalized to its own maximum to provide a better visual interpretation, were plotted respectively in Figures 4.17, 4.18, and 4.19. With other words, each single particle has been selected first according to the optical size and then categorized further taking into account the corresponding asymmetry factor value. The resulting four dimensional array was averaged for the entire sampling period (here individual seasons) and plotted in corresponding figures. It should be kept in mind that these figures reflect all particle events but not only the biological particles.

In the following paragraph AF features of the Karlsruhe site will be discussed in detail. Particles that were smaller than 1 µm had a modal AF between 7 and 18. In summer and in autumn a bimodal distribution was observed. This suggests that there were two different types of aerosol in this size range.. Particles having sizes between 1 and 2 µm had modal AF between 10 and 15, and this feature was stable during complete four seasons. In autumn and in winter a second AF mode below 10 has also been seen. Apparently non-biological aerosols dominate this size range and small increase in bacteria concentrations was not reflected on normalized AF distributions. Due to their high asphericity one would expect to see the bacterial mode close to right hand side of the AF distribution. Previously Gabey et al. (2010) deployed a WIBS instrument in the tropical forest and found that mostly fungal spores dominating the size range between 2 and 4 µm. This dominating mode was reflected on normalized AF distributions with an AF mode of 20. This dominating mode between 2 and 4 µm was attributed to fungal spores. The same dominating mode was seen also at Karlsruhe site. The modal AF had a monomodal distribution in spring and in summer. Later

on a bimodal distribution was observed, suggesting that a second type of aerosol contributed to this size range.

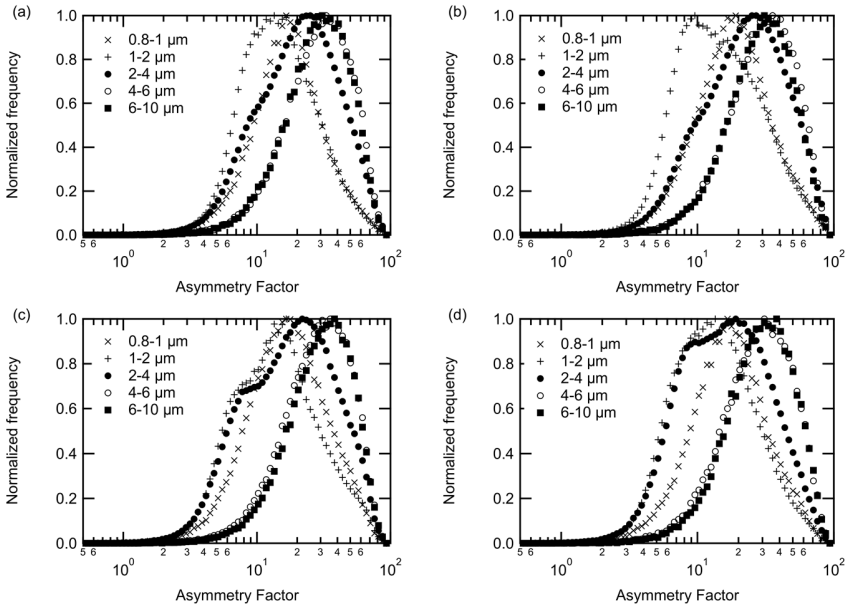


Figure 4.17: Asymmetry factor distributions at Karlsruhe site for: (a) spring (b) summer (c) autumn (d) winter

In contrary to particles that are smaller than 4µm, larger particles had a modal AF between 15 and 60. This feature was almost constant during the course of the one year online sampling. It has been shown that in this range the ratio of number of fluorescent particles to the total aerosol number is greater than for smaller particles (Toprak and Schnaiter, 2013 and next section). Thus the larger particles are more likely of biological origin. However, the larger the AF values the less spherical the particles are can be explained with the fact that in the atmosphere there is a continuous mixing of different aerosol species. Thus the larger AF values may represent biological aerosols mixed with several biological and non-biological aerosols which most probably have irregular shapes.

At Zugspitze site the AF distributions were almost identical, pointing out the lack of constant release of biological aerosol at this site (Fig. 4.18). Minor differences between individual plots can be explained with the local effects. It can clearly be seen that there was no seasonality at Zugspitze site.

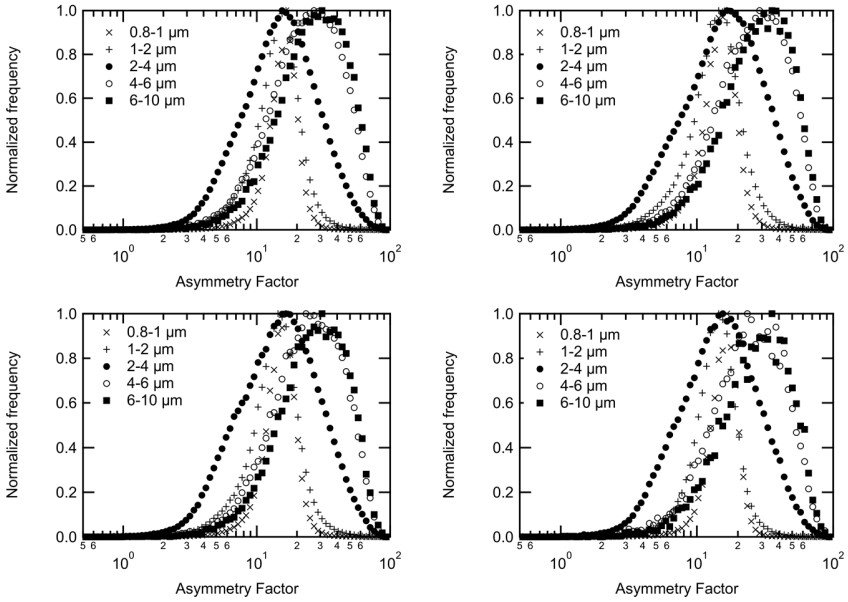


Figure 4.18: Asymmetry factor distributions at Zugspitze site for: (a) spring (b) summer (c) autumn (d) winter

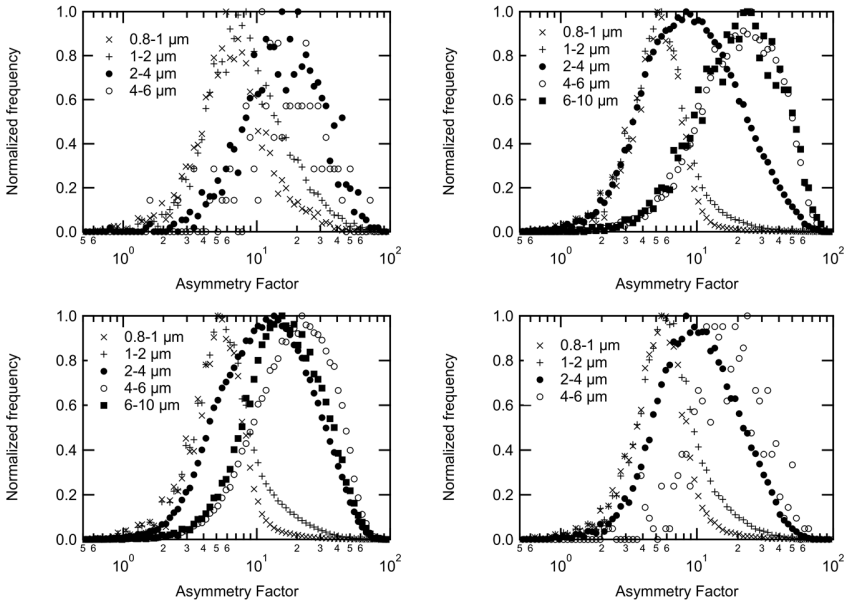


Figure 4.19: Asymmetry factor distributions at Jungfraujoch site for: (a) spring (b) summer (c) autumn (d) winter

## 7. Size dependence of FBAP/TAP ratio

Though there is no direct evidence that particle size is directly proportional to detected autofluorescence, it has been shown that the amount of fluorophore in any particle is correlated with fluorescence intensity (Hill et al., 2001). Thus it is likely that larger aerosol particles contain more fluorophore which should ease the detection of those particles in compared to smaller particles. Another valuable result of this study is quantifying the size dependence of the relative contribution of FBAP to TAP. Size segregated ratios of number of fluorescent particles to the total aerosol were illustrated in Fig. 4.19 and in Fig. 4.20.

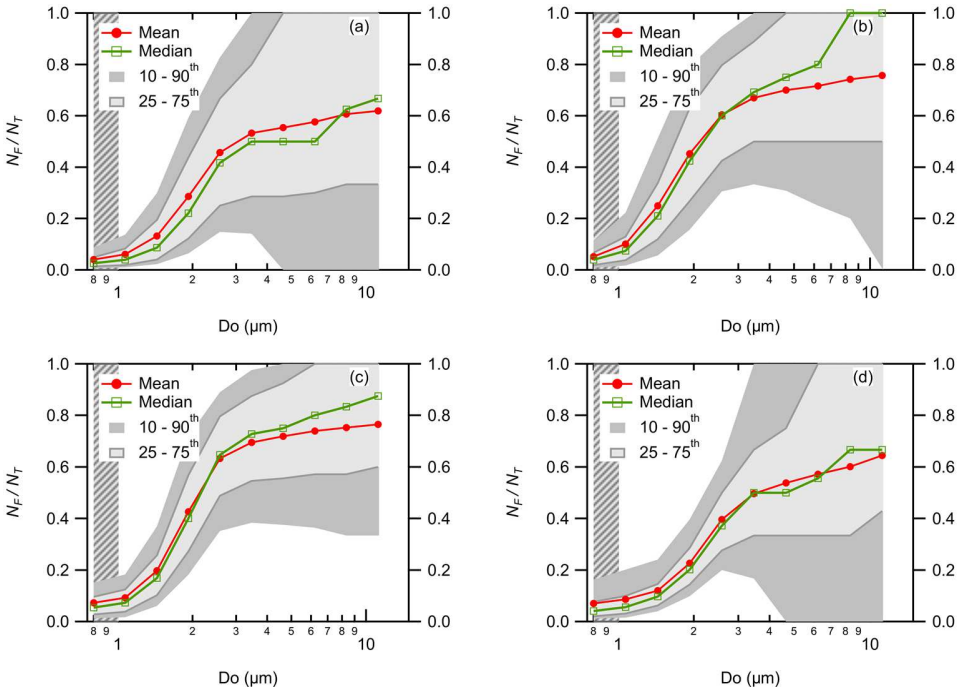


Figure 4.20: Average number size distribution of the FBAP to TAP number concentration ratio ($dN_{F1}/dN_T$) for individual seasons. Measurement site: Karlsruhe. (a) spring, (b) summer, (c) autumn, (d) winter

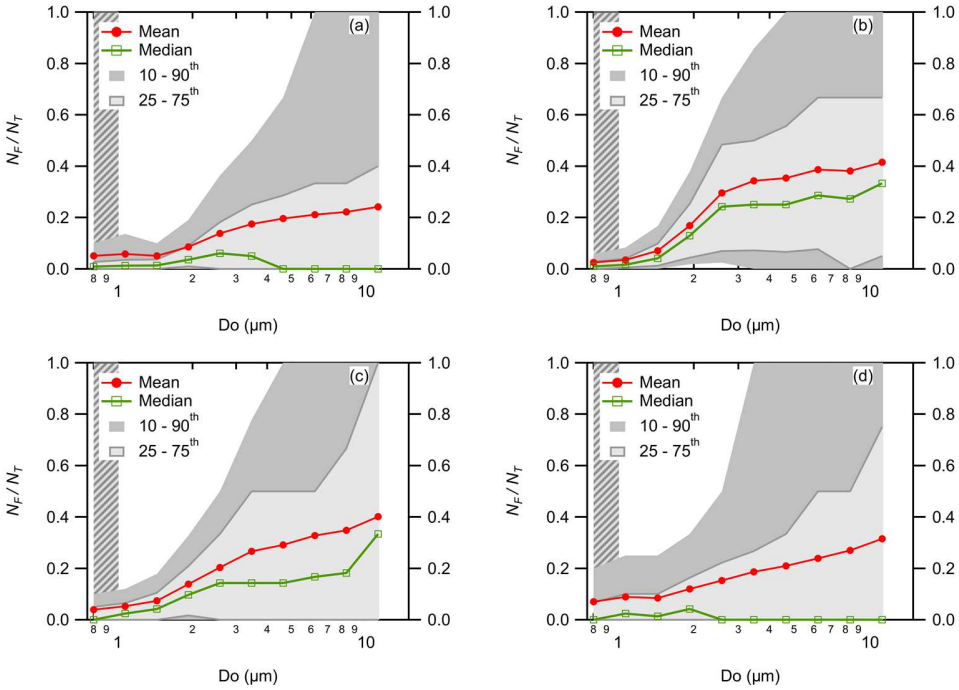


Figure 4.21: Average number size distribution of the FBAP to TAP number concentration ratio ($dN_{F1}/dN_T$) for individual seasons. Measurement site: Zugspitze. (a) spring, (b) summer, (c) autumn, (d) winter

## 8. Conclusions and summary

The number concentrations and distributions of fluorescent biological aerosol have been studied at three different locations in three different altitudes. Aerosol number concentrations are different by several orders of magnitude, albeit the number size distributions are similar to a certain extent. For the first time the seasonal variation of FBAP has been reported at a semirural environment and at two high altitude observation stations, one at the Zugspitze in Germany and the one at Jungfraujoch research station in Switzerland. At both sampling sites, the FBAP increased from beginning of the early spring and reached a maximum towards the end of summer term and decreased again to its minimum in winter term. This seasonality has been observed also at Zugspitze site, albeit to a less extent. The Karlsruhe site showed clear seasonal and diurnal cycles, with concentrations highest during the summer ($N_{F1}$= 93 $L^{-1}$, $N_{F2}$= 150 $L^{-1}$, $N_{F3}$= 93 $L^{-1}$, $N_{F1F3}$= 66 $L^{-1}$). These results are in good agreement with the recent study by Schumacher et al.

(2013). They reported the maximum bioaerosol number concentrations in summer ($N_{F,C}$ = 51 $L^{-1}$) for a boreal site in Hyytiälä and ($N_{F,C}$ = 30 $L^{-1}$) for a semi-arid environment in Colorado. UV-APS and WIBS were operated side by side to sample the ambient aerosol for several months at Karlsruhe site. It has been found that the integrated coarse mode FBAP concentrations are in a good agreement if the channel F3 of WIBS is compared to UV-APS counts (data not shown). However, this agreement is not valid for entire size range of UV-APS or WIBS. Counting efficiency of WIBS decreases steeply below 1 µm. For particles that are larger than 10 µm there could be some sedimentation loses in the sampling tube. Therefore, we applied the comparison only for particles between 1.0 µm and 10 µm. At the Zugspitze site the maximum concentrations were observed on sunny and warm summer days ($N_{F1}$= 11 $L^{-1}$, $N_{F2}$= 22 $L^{-1}$, $N_{F3}$= 16 $L^{-1}$, $N_{F1F3}$= 8 $L^{-1}$). In contrary to Karlsruhe site no diurnal change of FBAP was observed at Zugspitze site.

Number size distributions of fluorescent particles were similar for both Karlsruhe and Zugspitze sites. Because of the worse statistics at Zugspitze site there was a large uncertainty for particles larger than approximately 3 µm. This behavior was reflected on the $10^{th}$ and $90^{th}$ percentiles where $10^{th}$ percentile crosses the x-axis for larger particles. On the other hand at Karlsruhe site a better statistics has been observed which was reflected on a broader number size distribution until 10 µm. As it has been previously reported, the mode between 1.5 and 3.0 µm was especially distinct at Karlsruhe site but was observed also at Zugspitze site. A recent study by Gabey et al. (2013) showed that the bacterial release is an important source of FBAP at the high-altitude site in central France. They further concluded that there is no correlation between channel F1 and channel F3 during the entire sampling period. At Zugspitze site channel F1 and channel F3 showed lower counts but they correlated together when both of the channels measures fluorescence signals above a certain threshold, suggesting that the source of bioaerosol at Karlsruhe site and at Zugspitze site may be similar in nature. One of the most important objectives of this study was to find out whether biological aerosols can be transported over long distances. It is very well known that biological aerosols are mostly better cloud condensation and ice nuclei than mineral dust or soot. Under the light of my findings it can be stated that biological aerosols can be transported over very large distances and are ubiquitous even at high-altitude

mountain regions (above 2500 m a.s.l.). Thus they can act as giant cloud condensation nuclei (GCCN) and as well as ice nuclei and may influence the precipitation, especially the mixed-phase clouds prevail. However it should be kept in mind that there is a significant effect of planetary boundary level (PBL) at Zugspitze for most of the time. This PBL effect was more significant in summer time. At JFJ station (~ 3500 m a.s.l.) effect of PBL has been shown to be negligible between November and January. In summer time the PBL effect is significant and should be considered to come to conclusion about the impact of biological aerosols at these altitudes.

# Chapter 5

# Monitoring and characterization of extreme dust events at JFJ

## 1. Scientific motivation

The main motivation to study the fraction of biological particles in the ambient aerosol was the potential elevated ice nucleation activity of mineral dust or soil dust aerosol in presence of some biological organisms. For instance, Steinke et al. (2013) investigated the IN ability of different soil dust samples that had been collected from all over the world and found that the soil dust samples that contain biological material initiate ice formation at warmer temperatures in comparison with ATD or other classical mineral dusts under similar conditions. My laboratory studies have shown that WIBS is able to detect the biological aerosol from the ambient atmosphere to a certain extent and is also able to distinguish bioaerosol from non-biological particles within some uncertainties that arise from fluorescence of non-biological compounds (see Chapter 3). Table 5.1 gives an overview of the laboratory characterization of some soil dusts. As a final step of this PhD study, ambient aerosol has been monitored online at JFJ for several months with the intent of finding a correlation between extreme dust transportations and the biological aerosol activity. Ambient aerosol that has been analyzed during several Saharan dust events (SDE) at the high alpine research station Jungfraujoch (JFJ) are also given in Table 5.1. In this study four SDE were investigated and the number concentrations and size distributions of FBAP within or without SDE were provided. It has been previously suggested that the number of ice nuclei (IN) increases during SDE (Chou et al., 2011). However, the reason for this increase has not been explained yet. Authors suggested that new instrumentation and also more studies are necessary to be able explain this increase in IN numbers. A possible increase in IN numbers during SDE by co-transport was the motivation for online

monitoring of coarse mode aerosol at the JFJ. By using the latest version of the WIBS, ambient bioaeorosol was monitored from 25th of May 2013 until 1st of February 2014. An increase on FBAP number concentration was found during several SDE. In order to predict a SDE, both the BSC-DREAM8b dust model (Nickovic et al., 2001; Perez et al., 2006a,b) and the wavelength dependence of the single scattering albedo (SSA) and the Ångström exponent (Coen et al., 2004) were used. These exponents were provided by Paul Scherer Institute (PSI). Satellite pictures supported the presence of mineral dust and some biological aerosol during the observed SDE. A direct comparison between the commercially available dust monitor (Grimm 1.109) and WIBS was also provided. This chapter shows mainly the first dataset of online fluorescent particle measurements over several months and discusses variation of FBAP number concentrations and number size distributions with respect to several SDE at the JFJ. Investigation of ice nucleation properties of Saharan dust aerosol together with WIBS online sampling during SDE at JFJ would be an interesting contribution to the field and may provide a possible explanation to the findings of Chou et al. (2011). However this will be the subject of forthcoming studies and is beyond the scope of this PhD thesis.

## 2. Data analysis method

That the single scattering albedo exponent is negative for at least 4 hours, it was assumed that a SDE occurred and an email notification was sent to users. WIBS was established at the JFJ station on 25th of May 2013. Number of fluorescent particles and the ratio of number of fluorescent particles to total aerosol count were summarized in Table 5.1. It has been assumed that Arizona Test Dust (ATD) contains no biological material. However ATD produces significant amount of false positives on all of the fluorescence detecting units of WIBS. Therefore the counts were corrected in a way that the median fluorescent aerosol particle ratio calculated from ATD aerosol was taken out from each dust sample. The main difference between the soil samples that Steinke et al. (2013) investigated and the Saharan dust that WIBS detected at JFJ is that the soil dust fluoresces mostly only in channel F1, while Saharan dust at JFJ fluoresces in all channels. This feature of Saharan dust will be discussed together with chemical composition of the collected aerosol at JFJ in this chapter. The beginning time and the duration of SDE events were tabulated in Table

5.2. Events lasting longer than 24h refer to strong dust events, while events lasting between 4h and 10h refer to weak dust events. It has been previously reported that the strong dust events occur mostly in March – June and August – November periods (Coen et al., 2004). Figure 5.1 shows an example of how dust is transported across Europe.

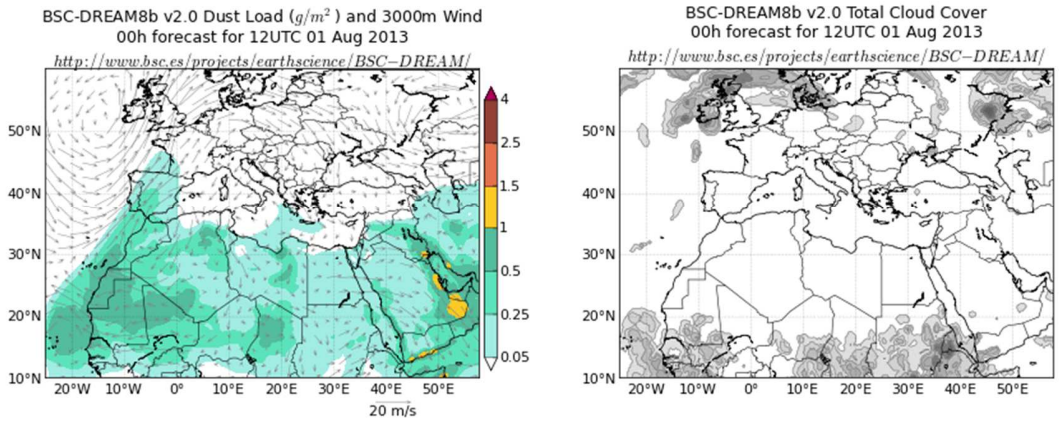


Figure 5.1: Dust load from Sahara desert over Spain and the cloud cover for the same region.

Table 5.1 Mean fluorescent aerosol number concentrations and number ratios in several dust samples and during some SDE events. Number ratios were corrected by subtracting the contribution from autofluorescence of Arizona test dust (ATD).

| | $N_{F1}$ | $N_{F2}$ | $N_{F3}$ | $N_{F1}/N_T$ (%) | $N_{F2}/N_T$ (%) | $N_{F3}/N_T$ (%) |
|---|---|---|---|---|---|---|
| ATD | 204 ± 43 | 526 ± 72 | 396 ± 82 | 1 ± 0.2 | 3 ± 0.4 | 2 ± 0.4 |
| Ms01 | 678 ± 80 | 185 ± 39 | 39 ± 13 | 9 ± 1 | 3 ± 1 | 1 ± 0.1 |
| Gs01 | 222 ± 39 | 70 ± 16 | 26 ± 12 | 3 ± 1 | 1 ± 1 | nd |
| As01 | 213 ± 71 | 100 ± 107 | 9 ± 5 | 5 ± 1 | 2 ± 2 | nd |
| SD19 | nd | nd | nd | nd | nd | nd |
| AfD | nd | nd | nd | nd | nd | nd |
| Non-SDE-Day | 3 | 5 | 3 | 10 | 22 | 13 |
| SDE01 | 22 ± 6 | 81 ± 25 | 43 ± 14 | 2 | 8 | 4 |
| SDE02 | 46 ± 12 | 133 ± 33 | 74 ± 19 | 4 | 11 | 6 |
| SDE03 | 8 ± 5 | 18 ± 263 | 12 ± 7 | 2 | 5 | 3 |
| SDE04 | 8 ± 8 | 34 ± 24 | 32 ± 20 | 2 | 10 | 6 |
| SDE05 | 14 ± 9 | 42 ± 18 | 27 ± 12 | 2 | 5 | 3 |

nd: not detectable

AfD: Afghanistan dust; SD19: Saharan dust; Ms01: Mongolian dust; Gs01: German dust; As01: Argentinian dust

Table 5.2 Details of SDE events at JFJ station

| Short name of the event | Start date of the event | Duration | Remarks |
|---|---|---|---|
| SDE01 | 17.06.2013 | ~ 2 days | Low $N_{F1}$<br>High $N_{F2}$, High $N_{F3}$<br>1 µm ≤ Do ≤ 10 µm |
| SDE02 | 03.08.2013 | ~ 5 days | Low $N_{F1}$<br>High $N_{F2}$, $N_{F3}$<br>1 µm ≤ Do ≤ 6 µm |
| SDE03 | 23.08.2013 | ~ 10h | Low $N_{F1}$<br>Higher $N_{F2}$ and $N_{F3}$<br>1 µm ≤ Do ≤ 8 µm |
| SDE04 | 28.09.2013 | ~ 11h | Low $N_{F1}$<br>Higher $N_{F2}$ and $N_{F3}$<br>1 µm ≤ Do ≤ 4 µm |
| SDE05 | 18.02.2014 | ~ 2 days | Low $N_{F1}$<br>Low $N_{F2}$ and $N_{F3}$<br>1 µm ≤ Do ≤ 6 µm |

## 3. Bioaerosols during SDE periods

WIBS was operated in parallel to a Grimm 1.109 dust monitor to investigate the responses of two different optical particle counters to the change on coarse mode aerosol number concentrations and size distributions. Figure 5.2 illustrates the direct comparison of WIBS and Grimm OPC for the size range of 1.0 µm ≤ Do ≤ 10 µm during SDE01. It can clearly be seen that WIBS underestimates the total aerosol number concentrations during SDE events. This can be explained with the fact that the WIBS and the Grimm OPC have different sampling flows and the sampling system is not isokinetic. The largest uncertainty between two instruments was for particles smaller than 2 µm. This feature is reflected on the lower panel of Fig. 5.2 (e.g., black and red solid lines). $N_{WIBS}/N_{Grimm}$ ratio falls below unity for this size range and increases with increasing particle size, suggesting that WIBS counting efficiency is better than the Grimm OPC in this size range

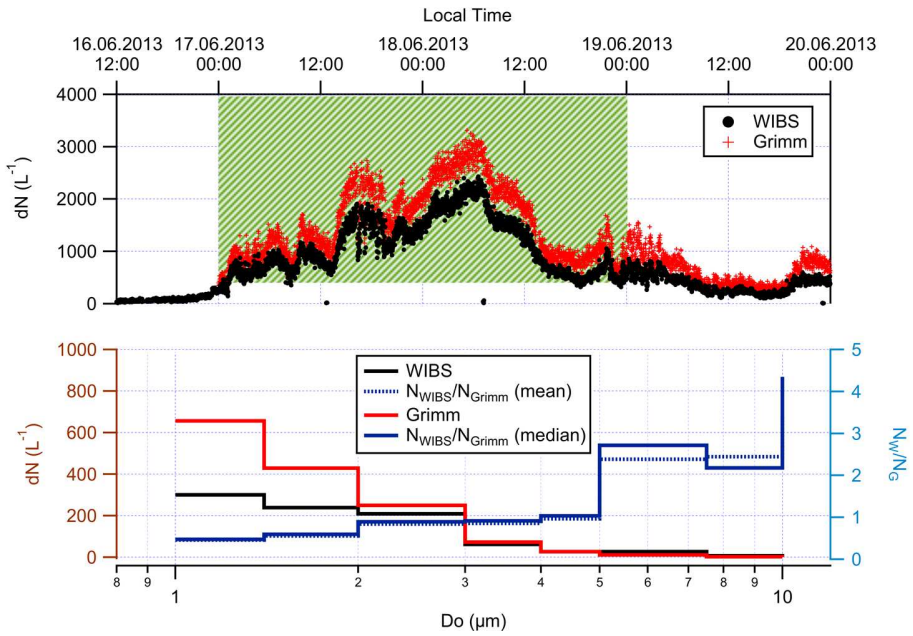


Figure 5.2: Integrated coarse mode aerosol number concentrations, number size distributions and size segregated ratio of number concentrations of WIBS and Grimm. Upper panel: aerosol number concentrations measured by WIBS (black markers) and Grimm (red markers). Lower panel: left, aerosol number size distributions for WIBS (black solid line) and for Grimm (red solid line); right, $N_{WIBS}/N_{Grimm}$ (mean, blue dashed line; median, blue solid line).

## 3.1. Saharan dust event 01

The first SDE was observed on June 17 and lasted for approximately two days. Corresponding Dream8b simulation shows the arrival of dust at Jungfraujoch on June 17 (Figure 5.3). The same figure illustrates the increase on fluorescent particles after dust load. A 96-hour back trajectory for this event (Figure 5.5, upper panel left) was created using HYSPLIT. Back trajectory ensemble indicates that the air reaches JFJ station on June 17 originates mostly from Sahara region and from North Atlantic Ocean. The fluorescence data show that the aerosol number size distribution covers a large particle size between 1 µm and 10 µm. However two distinct modes were identified for channel F2 and channel F3 type of particles. The first mode was between 2 and 3 µm, whereas the second mode lied

between 6 µm and 9 µm. Surprisingly, this feature of the aerosol number size distribution was different for different dust events. When I compared the data with laboratory tests that have been conducted using different soil and mineral dust aerosols, I have seen that there were some major differences between fluorescence channels.

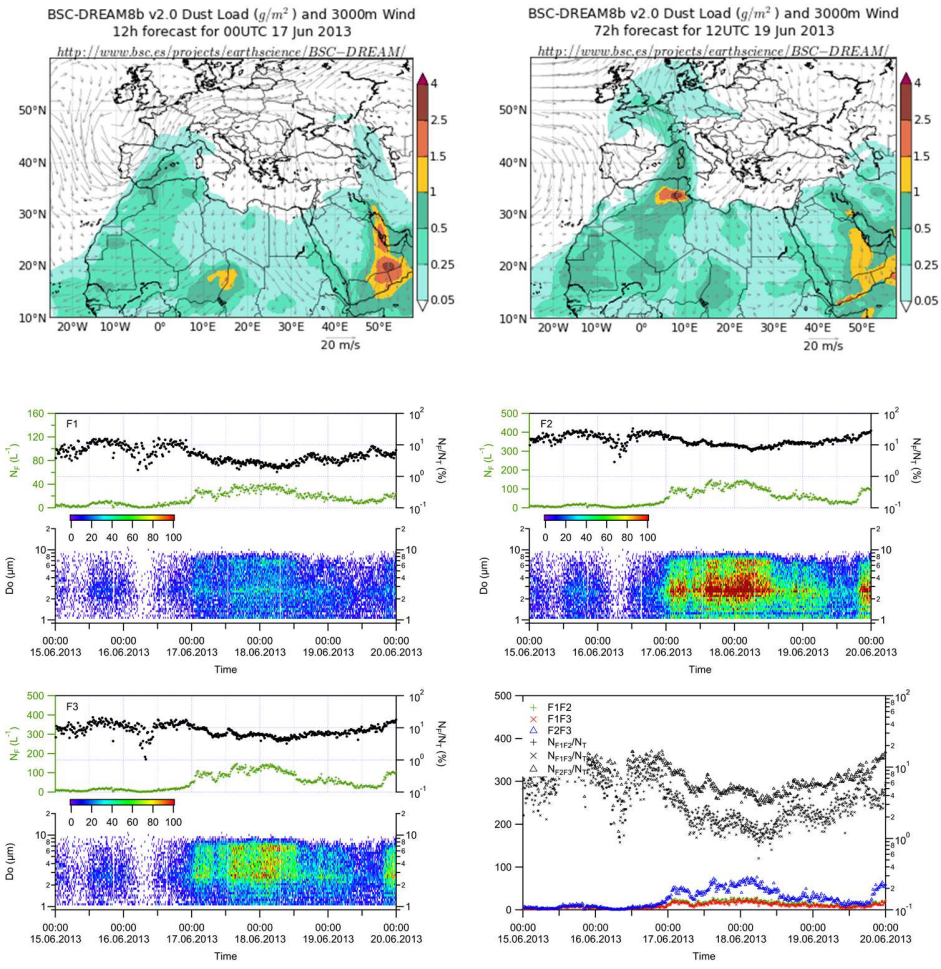


Figure 5.3: Time series of fluorescent biological aerosol particles for SDE01 and the corresponding Dream8b model data.

ATD for instance fluoresces on each of the channels, albeit the fluorescence on combination of any two channels is significantly low. The lowest panel on the right hand side of the Figure 5.3 shows the number of fluorescent particles for combination of fluorescence channels. It can clearly be seen that the aerosol detected during the SDE01

consists of biological particles. One can argue that the dust aerosol produces false positives. Therefore the fluorescent particle numbers was corrected for each SDE by subtracting the possible contribution from the fluorescence of mineral dust itself (see Table 5.1). That the NADH-like particles dominate the aerosol collected during SDE it can be suggested that the aerosol was polluted with fungal species and some viable bacteria.

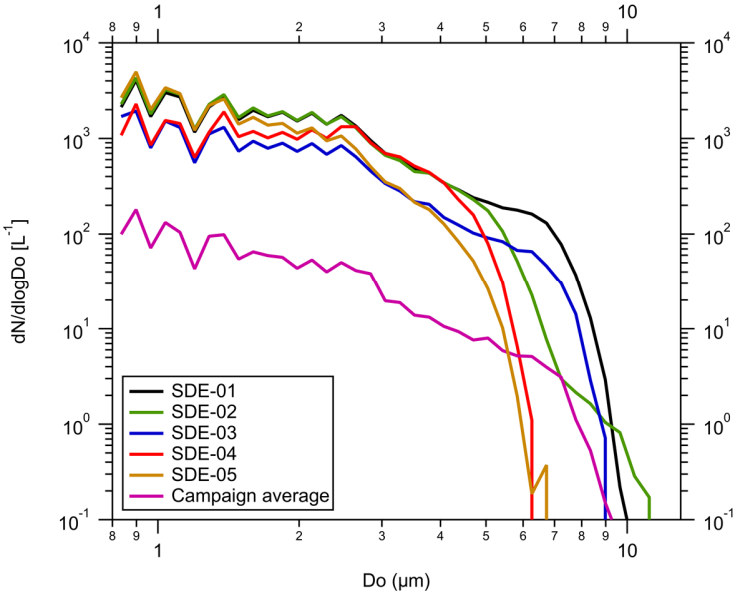


Figure 5.4: Total aerosol number size distribution of the total aerosol particles during Saharan dust events at JFJ.

Although it is rather speculative, presence of some viable bacterial aerosol may explain the high F2 and F3 signal for particles between 1.5 µm and 4 µm. In a recent study Gabey et al. (2013) reported the fluorescent aerosol at high altitude site in central France. They found the similar feature that the NADH-like particles are almost always greater than the Try-like particles and lack of correlation between two particle classes. They further concluded that the data were inconsistent with previous UV-LIF measurements, pointing out the fluorescence of non-urban aerosol may have included partially decomposed biological material, soil dust and/or plant debris. An interesting feature of soil dust aerosol is the weak fluorescence on channel F2 and channel F3 which is not common for the aerosol that was detected at JFJ site.

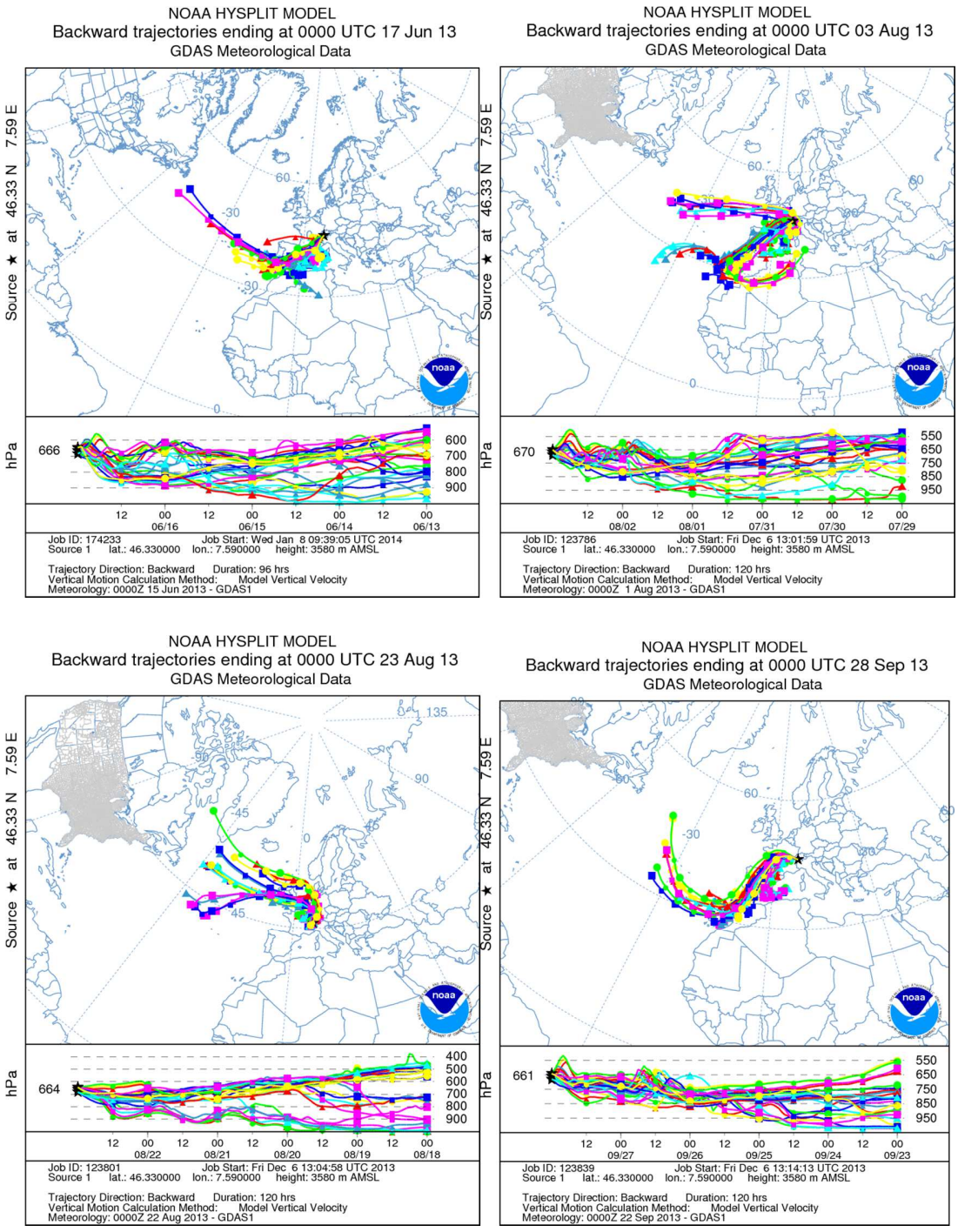


Figure 5.5: An ensemble HYSPLIT backtrajectory from JFJ station to show the origin of the transported air mass over the sampling site.

## 3.2. Saharan dust event 02

The second SDE was the strongest event that has been observed during the whole sampling period and lasted for almost five days. Similar to the first SDE, the total and the bioaeorosol number concentration increased from background concentrations to several hundreds. Figure 5.6 illustrates the WIBS fluorescence data together with corresponding Dream8b simulation. In contrary to SDE01, during SDE02 the $N_{F1}$ was larger and the size distribution of fluorescent biological aerosol was shifted to larger particles. Back trajectory analysis (Figure 5.5, upper panel right) points out that the air masses reach JFJ station on August 3 originated mostly from southwest (Sahara desert) and west (North Atlantic Ocean).

It can be seen from the Figure 5.6 that two different particles modes dominated the channel F3. First mode was observed at the beginning of the SDE and included particles between 3 and 6 µm, while the second mode which was first seen after 12 hours had a broader size distribution. The channel F2 on the other hand showed a broad spectrum covering particles between 0.8 and 6 µm during whole SDE. Apparently the $N_{F2}/N_{F3}$ ratio changed in the afternoon on August 03, suggesting a different type of bioaerosol source. The laboratory tests with different fungal spores (e.g., *alternia alternata, cladosporium cladosporioides, penicillium notatum*) showed that the $N_{F2}/N_{F3}$ has values around 1.1 which was almost constant for all fungal spores tested in the laboratory. Except the first 12 hours during the SDE02 $N_{F2}/N_{F3}$ was between 1 and 2. I suggest that the Saharan dust arrived to the JFJ station was mixed with fungal spores. $N_{F1}/N_{F3}$ and $N_{F1}/N_{F2}$ values are also consistent with laboratory tests. However the data for the first 12 hours of SDE02 cannot be explained by known fluorescence data of fungal spores.

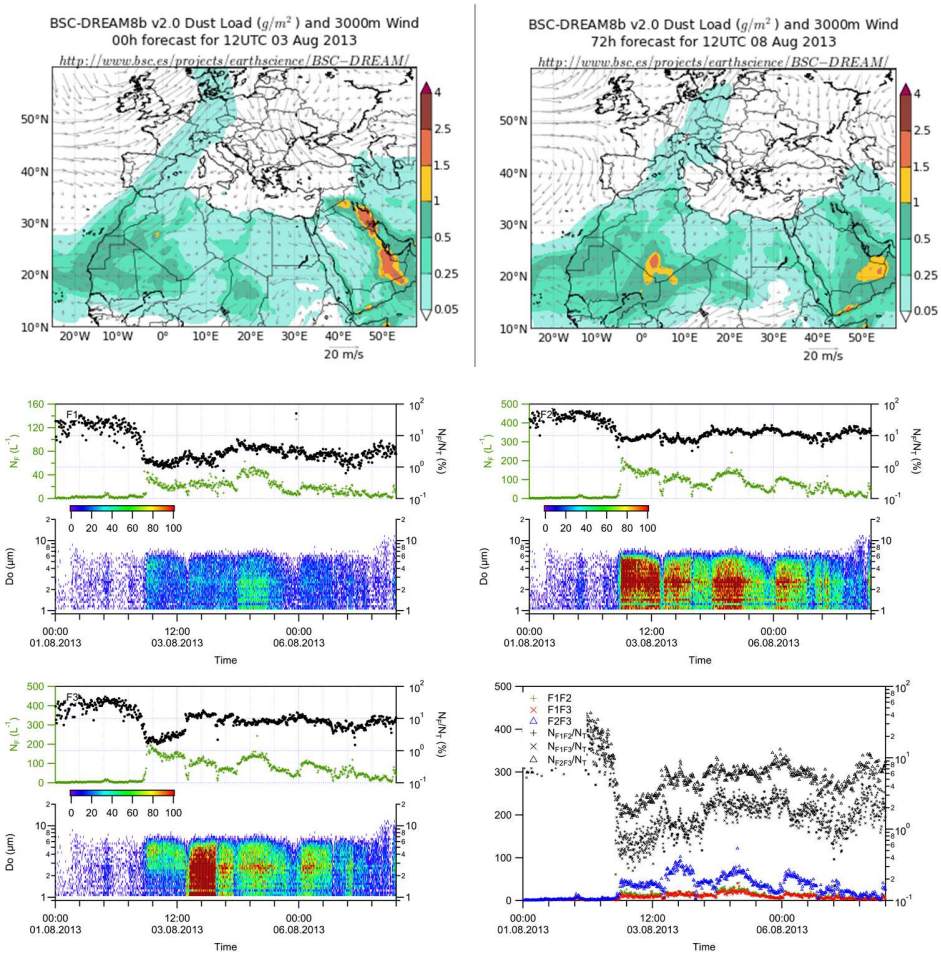


Figure 5.6: Time series of fluorescent biological aerosol particles for SDE02

## 3.3. Saharan dust event 03

The SDE03 is interesting from several ways. First of all, SDE03 cannot be seen neither on corresponding Dream8b simulation (Fig. 5.6 upper panel) nor suggests back trajectory analysis (Figure 5.5, lower panel left) air masses originating from Sahara region. However the requirements for a Saharan dust event have been fulfilled and a steep increase on total aerosol number concentration was observed. Although the $N_{FBAP}$ was not as high as the other two events, particles fluorescing mostly channel F2 and channel F3 were seen. Third event lasted only for 10h and therefore it can be regarded as a weak event. Different from the first event the number size distribution covered a narrower size band between 1 and 8

µm. $N_{F1}$ was measured around 20 $L^{-1}$, while the $N_{F2}$ and $N_{F3}$ were approximately 40 $L^{-1}$. These results are again in a very good agreement with the study published by Hallar et al. (2011).

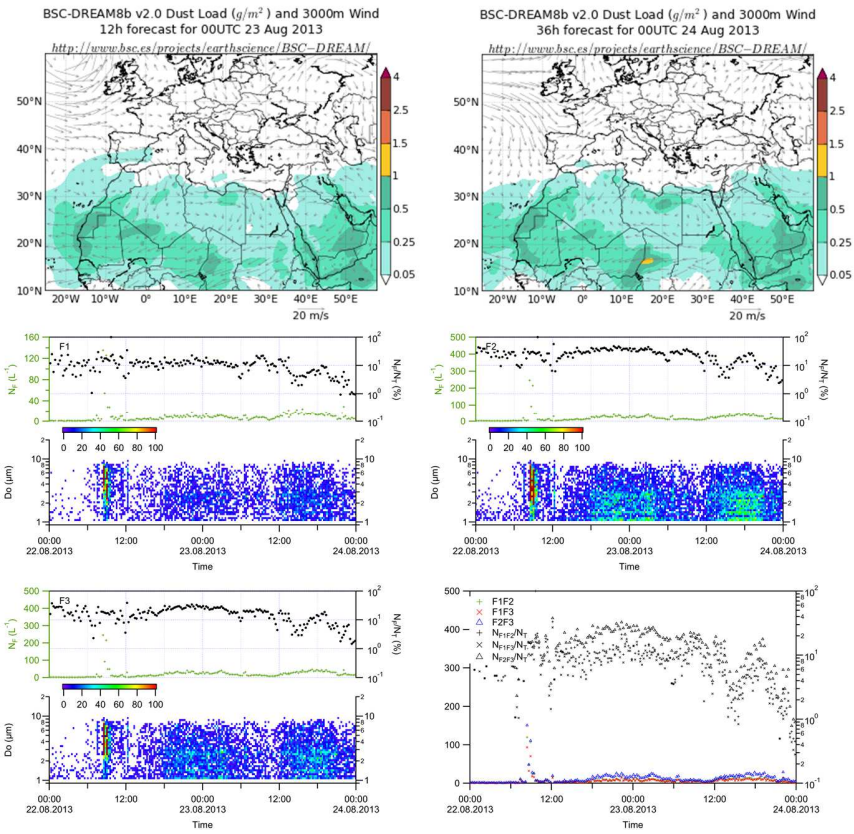


Figure 5.7: Time series of fluorescent biological aerosol particles for SDE03

They found the mean FBAP measured by UV-APS to be between 10 and 30 $L^{-1}$ for two consecutive dust events at Storm Peak Laboratory (SPL, 3210 m a.s.l.). When compared with the features observed from fungal spores that have been tested under controlled laboratory conditions, ratios of number of fluorescent particles on different detection bands of WIBS suggest that the aerosol detected during SDE03 is consistent with fungal spores. After analyzing three different fungal spores the following results were observed; $N_{F2}/N_{F3}$ appears between 1.1 and 1.2, $N_{F1}/N_{F3}$ falls within 0.5 and 1.0, and $N_{F1}/N_{F2}$ between 0.5 and 0.8 respectively.

## 3.4. Saharan dust event 04

The SDE04 showed different features than all other events. For the first time $N_{F2}/N_{F3}$ was measured as lower than unity (e.g., $N_{F2}/N_{F3}$=0.5; $N_{F1}/N_{F3}$=0.5; $N_{F1}/N_{F2}$=1). This difference may be explained with differences in chemical compositions of the aerosol detected during SDE04. In compared to the first two events this event can also be considered as a weak event since it lasted only for eleven hours. Corresponding Dream8b simulation together with fluorescence data was illustrated on Figure 5.8. Different from other events, size distribution of fluorescent particles was narrower. One mode around 3-4 µm dominated the bioaerosol size distribution. Calculated HYSPLIT ensemble (Figure 5.5, lower panel right) indicates that the air reached JFJ station on September 28 originated from North Atlantic Ocean and must have travelled over Sahara desert. Back trajectories also pointed out that the air was in contact with the surface before it reached the JFJ station.

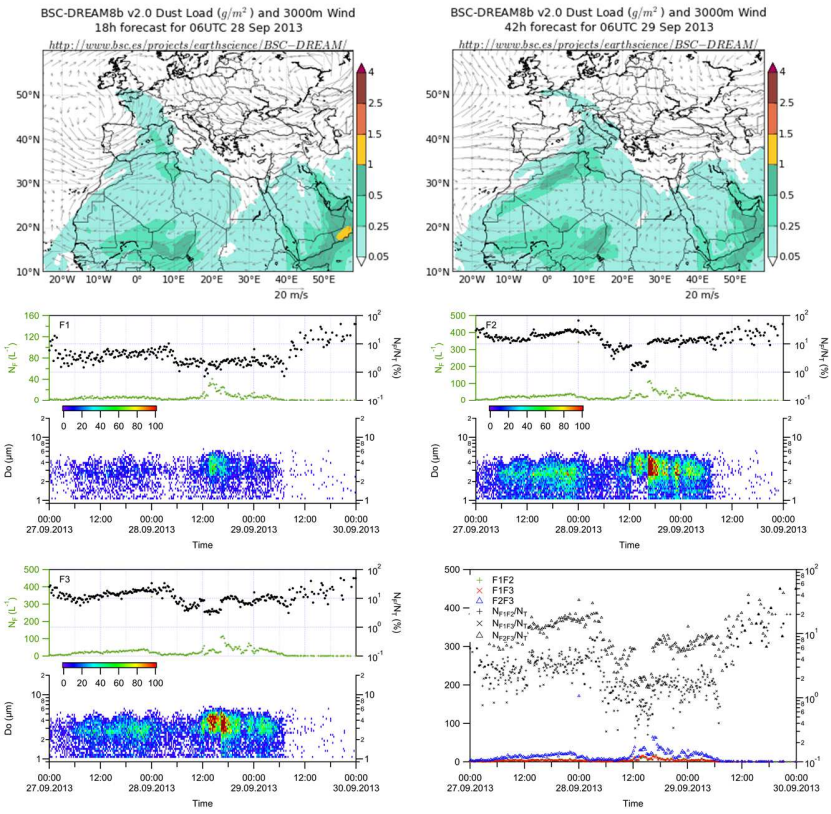


Figure 5.8: Time series of fluorescent biological aerosol particles for SDE04

## 3.5. Saharan dust event 05

Different from the other four Saharan dust events, during the SDE05 WIBS has been operated behind a special inlet called the new Ice Selective Inlet (ISI, designed and operated in cooperation with Karlsruhe Institute of Technology and Paul Scherer Institute). There is not yet any published study where the ISI was deployed. However Kupiszewski et al. (2014) published an abstract, which will be presented during the AMS Cloud Physics conference. The authors state that the design of the new ice selective inlet is inspired by the Ice-CVI inlet (Mertes et al., 2007), albeit with major differences.

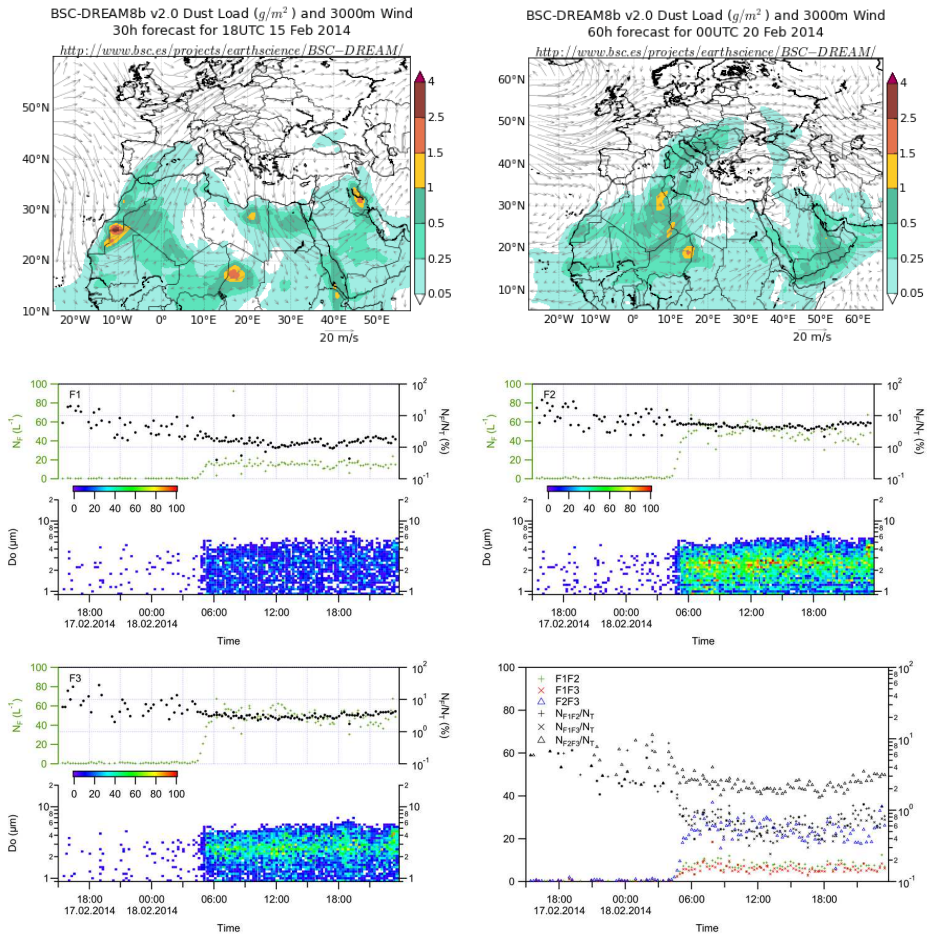


Figure 5.9: Time series of fluorescent biological aerosol particles for SDE05

In the ISI, droplets are evaporated during their presence in the droplet evaporation unit, which consists of ice coved inner walls, and ice crystals are transmitted. During the SDE05 autofluorescence of these ice crystals were analyzed by WIBS and are shown in Figure 5.9. The autofluorescence features were similar to the other four SDE, showing low F1 counts and comparably higher F2 and F3 counts. To find the evolution of biological particles in ice crystals WIBS was operated at the TSP inlet for several hours and then deployed behind the ISI for the rest of the dust event. Size segregated fluorescent particle ratios ($N_F/N_T$) are illustrated in Figure 5.10. An enrichment of the fluorescent biological aerosol has been observed in the ice phase, especially for the particles up to 2 µm.

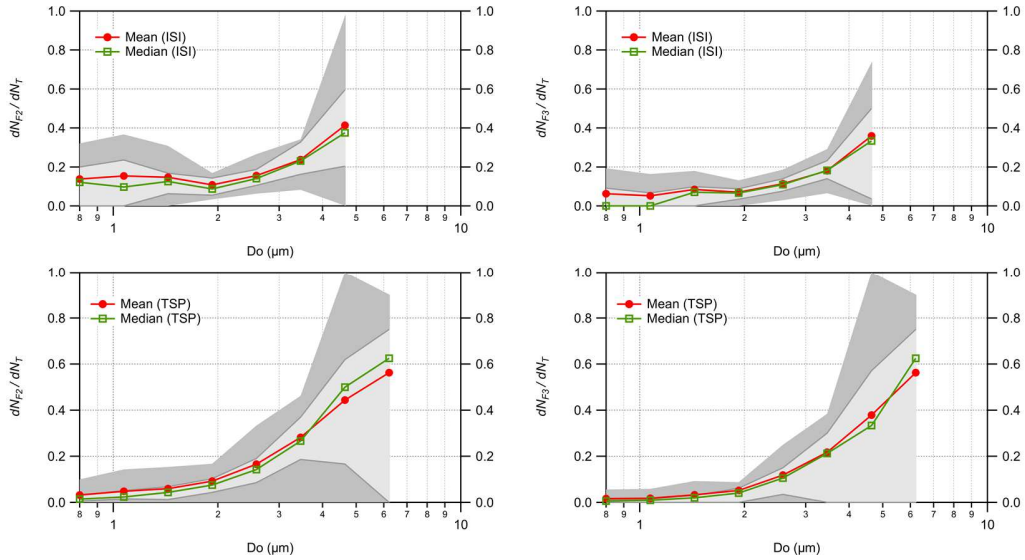


Figure 5.10: Enrichment of bio-particles in the ice phase during SDE05. TSP: total suspended particles, ISI: ice selective inlet. Panels left: Fluorescence data for channel F2; Panels right: Fluorescence data for channel F3.

## 4. Summary and conclusions

During the course of this thesis four extreme dust transportation events were observed and investigated by using the so called Dream8b dust model (Peres et al., 2006a, 2006b), single scattering albedo approach (Coen et al., 2004) and the latest version of WIBS instrument in real time. Back trajectory ensembles confirmed that in three of four dust events air was in

contact with Sahara desert before it arrives at JFJ station. The strongest event was observed on August 03 and lasted for almost five days. An OPC, which was operated parallel to the WIBS instrument, confirmed the arrival of dust at sampling station. However a minor difference on measured total aerosol numbers has been observed, especially during SDE events. Mainly, the four events showed similar features where the main bioaerosol mode was dominated by channel F2 and channel F3. In some cases temporary changes on ratios between fluorescence detection channels have also been observed. Except the SDE03 all events were reflected on corresponding Dream8b model simulations and HYSPLIT back trajectory ensembles. In case of SDE03 the air was originated from North Atlantic Ocean and was not in contact with Sahara desert. Dream8b simulation suggested no dust transportation on that day either. However the increased total and bioaerosol number concentrations and that the single scattered albedo coefficient was negative for at least four hours points out a Saharan dust event. This difference can only be explained by examining the filter samples that EMPA collected on that day. Though the aerosol number ratios were higher during non-SDE periods, the bioaerosol number concentrations were approximately five times higher during SDE events than they were during non-SDE days. The results were corrected by taking the cross-sensitivity of WIBS detection method to non-biological fluorescent aerosols into account and were presented in Table 5.1.

# Executive summary and outlook

Main objectives of this study can be given as the spatial and temporal investigation of the biological aerosols at central Europe, ice nucleation capability of pre-activated Saharan dust aerosol to enhance the biological activity, and the monitoring of ambient aerosol at the high altitude research station Jungfraujoch (JFJ) with the specific focus on relation between the increasing bioaerosol concentrations and extreme dust transportations over central Europe. For this purpose the latest version of the Wideband Integrated Bioaerosol Sensor (WIBS) has been operated under controlled laboratory conditions and later on during three consecutive long term field campaigns in Karlsruhe, at Zugspitze, and at Jungfraujoch. A data analysis tool (WDES) has been written and used to handle the huge data collected during three field campaigns and laboratory tests. This data analysis software will be used for future studies and is therefore suggested to be a valuable contribution to the scientific community. Laboratory tests have shown that WIBS is capable of distinguishing biological and non-biological aerosol. However, in some cases a minor cross-sensitivity to the non-biological fluorescent aerosol has also been found. To overcome this cross-sensitivity in the case of analysis of the Saharan dust aerosol samples a background correction was applied to all laboratory tests and to the Saharan dust events (SDE) presented in this study. Beside that in Karlsruhe a continuous release of wetly discharged fungal spores was found, especially in summer period. This diurnal change on bioaerosol number concentration was related to the relative humidity (RH) change which is a key parameter for the release of wetly discharged fungal spores. The current literature supported this idea and a new parameterization dealing with the release of fungal spores was developed by Hummel et al. (2014) and will be published soon. Monitoring of the bioaerosols at Zugspitze site has shown that the bioaerosols are transported over very long distances and therefore may affect the cloud formation and precipitation, not in globe scale but in some regions (Hoose et al., 2010). Moreover despite its high elevation Zugspitze is strongly affected by the planetary boundary layer which was reflected on diurnal changes of fluorescent biological aerosol particles. Jungfraujoch station was very important because it is most of the time in free troposphere and less affected by the vegetation around the mountain site. After WIBS

was tested and operated at two different locations (Karlsruhe and Zugspitze) some detection and activation experiments have been performed by using Saharan dust and the procedure described in section 2.4. WIBS was used to detect the number of bioaerosols in some soil dusts (Steinke et al., 2013) and for Saharan dust samples. Unfortunately the bioaeorosol concentrations in pre-activated and wet dispersed Saharan dust samples were not detectible, while soil dust contained significant amount of biological material. These samples were then tested for ice nucleation in so called AIDA chamber. It has been seen that the soil dust samples which has been suggested to contain significant amount of biological material (see Steinke et al., 2013) are better ice nuclei than the Saharan dust samples used in this study. A simple comparison between the pre-activated and the dry dispersed Saharan dust samples has shown that the dispersion method that has been used in this study was not suitable for wet dispersion. This was reflected on number and surface size distributions of wet and dry dispersed samples. So, the low ice nucleation activity of pre-activated, wet dispersed Saharan dust samples may be due to the dispersion method not the material itself. Pre-activation of Saharan dust samples may still cause an increase of biological material on the dust and may impact the ice formation but needs to be further investigated. As a final step bioaerosol concentrations at JFJ were monitored for 10 months. By using the Dream8b model and the single scattered albedo coefficient five case studies have been investigated. It has been found that bioaerosols are transported via Saharan dust events both directly from Sahara desert and also over North Atlantic Ocean. Which path the aerosols followed may have affected the amount and also the type of the aerosols detected at JFJ. Although the ratio of biological aerosol at JFJ is lower during SDE the absolute amount of bioaerosols are greater than the amounts at non-SDE days. By using the new ice selective inlet (ISI) designed by Paul Scherer Institute (PSI) and the Karlsruhe Institute of Technology (KIT) together, the biological aerosol inside the ice residuals (i.e, larger than approximately 20 µm ice particles were selected and evaporated in the ISI) have been investigated. For the first time a clear enrichment of the biological aerosol in the ice phase has been observed.

# Appendix A

List of frequently used acronyms

| Short name | Description |
|---|---|
| TAP | Total aerosol particle (all particles detected by WIBS; fluorescent and non-fluorescent including missed particle counts) |
| FBAP* | Fluorescent biological aerosol particle (any type of fluorescent particle) |
| NON | Non-fluorescent aerosol particle |
| $N_T$ | Number of all particles detected by WIBS (same as TAP but used on figures) |
| $N_{NON}$ | Number of non-fluorescent particles |
| $N_{F1}$ | Number of fluorescent particles in channel F1 |
| $N_{F2}$ | Number of fluorescent particles in channel F2 |
| $N_{F3}$ | Number of fluorescent particles in channel F3 |
| $N_{F1,F2}$ | Number of fluorescent particles in channel F1 and F2 |
| $N_{F1,F3}$ | Number of fluorescent particles in channel F1 and F3 |
| $N_{F2,F3}$ | Number of fluorescent particles in channel F2 and F3 |
| F1 | Particles fluoresce in channel F1 |
| F2 | Particles fluoresce in channel F2 |
| F3 | Particles fluoresce in channel F3 |
| $N_{Try}$ | Particles fluoresce only in F1 but not in F2 or F3 (only Try-like) |
| $N_{NADH}$ | Particles fluoresce only in F3 but not in F1 or F2 (only NADH-like) |
| F1&F2 | Particles fluoresce both in F1 and F2 at the same time |
| F1&F3 | Particles fluoresce both in F1 and F3 at the same time |
| F2&F3 | Particles fluoresce both in F2 and F3 at the same time |

# Appendix B

Seasonal comparison of coarse-mode median total aerosol particle ($N_{T,C}$), median fluorescent biological aerosol particle ($N_{F,C}$) and bioparticle ratio ($N_{F,C}/N_{T,C}$) trends at Eggenstein-Leopoldshafen (Karlsruhe, Germany), at Zugspitze, and at Jungfraujoch sites. Missed particle count correction has been applied only for $N_{T,C}$. For the calculation of bioparticle ratios only real events have been considered. Variability in each case listed as ± standard deviation. Following Trenberth (1983) seasons were defined meteorologically: Spring (1 March-31 May), Summer (1 June-31 August), Fall (1 September-30 November), and Winter (1 December-29 February).

**Leopoldshafen, Karlsruhe (112 m a.s.l.)**

| | | Spring | Summer | Fall | Winter |
|---|---|---|---|---|---|
| $N_T$ ($L^{-1}$) | 25$^{th}$ | 287 | 262 | 241 | 178 |
| | Median | 453 | 361 | 375 | 323 |
| | Mean | 798 | 442 | 427 | 390 |
| | 75$^{th}$ | 750 | 501 | 537 | 503 |
| $N_{F1}$ ($L^{-1}$) | 25$^{th}$ | 32 | 46 | 43 | 21 |
| | Median | 45 | 65 | 68 | 31 |
| | Mean | 59 | 95 | 92 | 41 |
| | 75$^{th}$ | 65 | 102 | 112 | 47 |
| $N_{F2}$ ($L^{-1}$) | 25$^{th}$ | 55 | 74 | 66 | 39 |
| | Median | 88 | 103 | 110 | 68 |
| | Mean | 175 | 131 | 1217 | 113 |
| | 75$^{th}$ | 142 | 153 | 165 | 133 |
| $N_{F3}$ ($L^{-1}$) | 25$^{th}$ | 38 | 55 | 45 | 25 |
| | Median | 54 | 78 | 76 | 42 |
| | Mean | 68 | 96 | 89 | 62 |
| | 75$^{th}$ | 81 | 115 | 113 | 76 |
| $N_{F1F3,C}$ ($L^{-1}$) | 25$^{th}$ | 19 | 33 | 28 | 11 |
| | Median | 28 | 48 | 43 | 17 |
| | Mean | 37 | 68 | 62 | 22 |
| | 75$^{th}$ | 41 | 76 | 76 | 27 |

| **Lepoldshafen, Karlsruhe (112 m a.s.l.)** | | | | | |
|---|---|---|---|---|---|
| | | Spring | Summer | Fall | Winter |
| $N_{F1}/N_T$ (%) | 25th | 5.5 | 12.8 | 13.0 | 6.7 |
| | Median | 10.1 | 20.9 | 21.0 | 10.6 |
| | Mean | 13.5 | 25.2 | 24.6 | 13.3 |
| | 75th | 17.7 | 33.4 | 32.9 | 15.7 |
| $N_{F2}/N_T$ (%) | 25th | 10.8 | 21.2 | 23.0 | 16.7 |
| | Median | 20.7 | 34.1 | 33.8 | 32.0 |
| | Mean | 32.3 | 35.2 | 34.3 | 30.0 |
| | 75th | 40.6 | 46.5 | 44.4 | 40.6 |
| $N_{F3}/N_T$ (%) | 25th | 6.8 | 15.8 | 15.2 | 10.9 |
| | Median | 13.1 | 25.1 | 22.5 | 18.0 |
| | Mean | 15.7 | 27.0 | 23.8 | 17.2 |
| | 75th | 21.6 | 35.2 | 30.4 | 22.8 |
| $N_{F1F3}/N_T$ (%) | 25th | 3.1 | 9.1 | 8.2 | 3.6 |
| | Median | 6.4 | 15.4 | 13.4 | 5.8 |
| | Mean | 9.3 | 19.1 | 16.4 | 7.0 |
| | 75th | 12.4 | 25.3 | 22.2 | 8.9 |

| **Zugspitze, Germany (2650 m a.s.l.)** | | | | | |
|---|---|---|---|---|---|
| | | Spring | Summer | Fall | Winter |
| $N_T$ ($L^{-1}$) | 25th | 21 | 32 | 16 | 7 |
| | Median | 84 | 99 | 30 | 16 |
| | Mean | 189 | 321 | 66 | 28 |
| | 75th | 183 | 269 | 65 | 36 |
| $N_{F1}$ ($L^{-1}$) | 25th | 1 | 4 | 1 | 1 |
| | Median | 3 | 11 | 3 | 1 |
| | Mean | 6 | 14 | 6 | 2 |
| | 75th | 8 | 19 | 7 | 3 |
| $N_{F2}$ ($L^{-1}$) | 25th | 3 | 8 | 3 | 2 |
| | Median | 9 | 22 | 7 | 3 |
| | Mean | 17 | 41 | 12 | 6 |
| | 75th | 20 | 53 | 15 | 7 |
| $N_{F3}$ ($L^{-1}$) | 25th | 2 | 6 | 2 | 1 |
| | Median | 6 | 16 | 4 | 2 |
| | Mean | 10 | 28 | 8 | 3 |
| | 75th | 13 | 37 | 10 | 4 |
| $N_{F1F3,C}$ ($L^{-1}$) | 25th | 1 | 3 | 1 | - |
| | Median | 2 | 8 | 2 | - |
| | Mean | 3 | 10 | 4 | - |
| | 75th | 5 | 14 | 4 | - |

| **Zugspitze, Germany (2650 m a.s.l.)** | | | | | |
|---|---|---|---|---|---|
| | | Spring | Summer | Fall | Winter |
| $N_{F1}/N_T$ (%) | 25$^{th}$ | 2.3 | 4.5 | 5.1 | 4.3 |
| | Median | 4.1 | 9.2 | 9.8 | 8.4 |
| | Mean | 8.5 | 11.7 | 11.9 | 13.1 |
| | 75$^{th}$ | 8.7 | 16.7 | 16.5 | 16.7 |
| $N_{F2}/N_T$ (%) | 25$^{th}$ | 7.4 | 13.7 | 14.5 | 14.3 |
| | Median | 11.9 | 20.7 | 23.9 | 24.1 |
| | Mean | 16.0 | 24.0 | 25.1 | 27.0 |
| | 75$^{th}$ | 19.2 | 32.0 | 33.3 | 35.1 |
| $N_{F3}/N_T$ (%) | 25$^{th}$ | 4.5 | 9.2 | 8.2 | 7.1 |
| | Median | 7.3 | 13.8 | 14.0 | 12.1 |
| | Mean | 9.6 | 17.0 | 15.5 | 15.5 |
| | 75$^{th}$ | 11.5 | 22.9 | 20.5 | 19.4 |
| $N_{F1F3}/N_T$ (%) | 25$^{th}$ | 1.1 | 3.1 | 2.9 | 2.2 |
| | Median | 2.3 | 6.7 | 5.9 | 4.4 |
| | Mean | 4.6 | 8.7 | 7.7 | 7.3 |
| | 75$^{th}$ | 5 | 12.5 | 10.7 | 9.1 |

| **Jungfraujoch, Switzerland (3580 m a.s.l.)** | | | | | |
|---|---|---|---|---|---|
| | | Spring | Summer | Fall | Winter |
| $N_T$ ($L^{-1}$) | 25$^{th}$ | 1 | 22 | 4 | 1 |
| | Median | 2 | 48 | 8 | 2 |
| | Mean | 6 | 98 | 21 | 4 |
| | 75$^{th}$ | 6 | 84 | 18 | 5 |
| $N_{F1}$ ($L^{-1}$) | 25$^{th}$ | 0.3 | 2 | - | - |
| | Median | 0.6 | 5 | 1 | - |
| | Mean | 0.7 | 10 | 2 | - |
| | 75$^{th}$ | 0.9 | 10 | 2 | - |
| $N_{F2}$ ($L^{-1}$) | 25$^{th}$ | 0.3 | 4 | 1 | - |
| | Median | 0.6 | 11 | 1 | - |
| | Mean | 1.1 | 23 | 4 | - |
| | 75$^{th}$ | 1.4 | 23 | 3 | - |
| $N_{F3}$ ($L^{-1}$) | 25$^{th}$ | 0.3 | 2 | - | - |
| | Median | 0.6 | 7 | 1 | - |
| | Mean | 0.8 | 13 | 3 | - |
| | 75$^{th}$ | 0.9 | 13 | 2 | - |
| $N_{F1F3,C}$ ($L^{-1}$) | 25$^{th}$ | - | 1 | - | - |
| | Median | - | 3 | 1 | - |
| | Mean | - | 6 | 2 | - |
| | 75$^{th}$ | - | 7 | 1 | - |

| **Jungfraujoch, Switzerland (3580 m a.s.l.)** | | | | | |
|---|---|---|---|---|---|
| | | Spring | Summer | Fall | Winter |
| $N_{F1}/N_T$ (%) | 25$^{th}$ | 5.7 | 6.5 | 4.2 | 5.9 |
| | Median | 10.0 | 11.4 | 8.3 | 10.0 |
| | Mean | 16.3 | 13.0 | 11.0 | 14.1 |
| | 75$^{th}$ | 18.8 | 16.9 | 14.3 | 16.7 |
| $N_{F2}/N_T$ (%) | 25$^{th}$ | 14.3 | 14.3 | 10.0 | 11.8 |
| | Median | 26.4 | 25.9 | 18.2 | 20.0 |
| | Mean | 42.3 | 29.2 | 21.0 | 30.2 |
| | 75$^{th}$ | 69.2 | 38.5 | 28.9 | 33.3 |
| $N_{F3}/N_T$ (%) | 25$^{th}$ | 7.7 | 7.7 | 6.3 | 7.0 |
| | Median | 14.0 | 14.7 | 11.5 | 12.5 |
| | Mean | 24.3 | 17.1 | 13.9 | 18.9 |
| | 75$^{th}$ | 28.6 | 23.6 | 19.0 | 22.2 |
| $N_{F1F3}/N_T$ (%) | 25$^{th}$ | 4.2 | 3.7 | 2.9 | 5.0 |
| | Median | 7.6 | 7.3 | 5.9 | 7.7 |
| | Mean | 13.7 | 8.3 | 7.7 | 11.8 |
| | 75$^{th}$ | 15.0 | 11.4 | 10.0 | 14.3 |

# List of figures

# List of tables

# References

ARCANGELI, C., ZUCCONI, L., ONOFRI, S., & CANNISTRARO, S. 1997 Fluorescence study on whole Antarctic fungal spores under enhanced UV irradiation, *Journal of Photochemistry and Photobiology B:Biology,* **39**, 258-264.

BROSSEAU, LISA, M., VESLEY, D., RICE, N., GOODELL, K., NELLIS, M., & HAIRSTON, P. 2000 Differences in Detected Fluorescence Among Several Bacterial Species Measured with a Direct-Reading Particle Sizer and Fluorescence Detector, *Aerosol Science and Technology*, **32**, 6, 545-558.

CALDERON, C., LACEY, J., MCCARTNEY, H.A., & ROSAS, I. 1995 Seasonal and Diurnal Variation of Airborne Basidiomycete Spore Concentrations in Mexico City, *Grana*, **34**, 4, 260-268.

COEN, C.M., WEINGARTNER, E., SCHAUB, D., HUEGLIN, C., CORRIGAN, C., HENNING, S., SCHWIKOWSKI, M., & BALTENSPERGER, U. 2004 Saharan dust events at the Jungfraujoch: detection by wavelength dependence of the single scattering albedo and first climatology analysis, *Atmospheric Chemistry and Physics*, **4**, 2465-2480, doi:10.5194/acp-4-2465-2004.

CHOU, C., STETZER, O., WEINGARTNER, E., JURÁNYI, Z., KANJI, Z. A., & LOHMANN, U. 2011 Ice nuclei properties within a Saharan dust event at the Jungfraujoch in the Swiss Alps, *Atmospheric Chemistry and Physics*, **11**, 4725-4738, doi:10.5194/acp-11-4725-2011.

DESPRES, V. R., HUFFMAN, J. A., BURROWS, S. M., HOOSE, C., SAFATOV, A. S., BURYAK, G., FRÖHLICH-NAWOISKY, J., ELBERT, W., ANDREAE, M. O., PÖSCHL, U., & JAENICKE, R. 2012 Primary Biological Aerosol Particles in the Atmosphere: A Review, *Tellus B*, 10.3402/tellusb.v64i0.15598.

ELBERT, W., TAYLOR, P. E., ANDREAE, M. O., & PÖSCHL, U. 2007 Contribution of fungi to primary biogenic aerosols in the atmosphere: wet and dry discharged spores,

carbohydrates, and inorganic ions, *Atmospheric Chemistry and* Physics, **7**, 4569-4588, 10.5194/acp-7-4569-2007.

EVERSOLE, J.D., HARDGROVE, J.J., CARY JR, W.K., CHOULAS, D.P., & SEAVER, M. 1999 Continuous, rapid biological aerosol detection with the use of UV fluorescence: Outdoor test results, *Field Analytical Chemistry and Technology*, **3**, 249–259.

FOOT, V. E., KAYE, P. H., STANLEY, W. R., BARRINGTON, S. J., GALLAGHER,M., & GABEY, A. 2008 Low-cost real-time multiparameter bio-aerosol sensors, *Optically Based Biological and Chemical Detection for Defence IV*, Cardiff, Wales, UK, 71160I–71112.

FORSTER, P., V. RAMASWAMY, P. ARTAXO, T. BERNTSEN, R. BETTS, D.W. FAHEY, J. HAYWOOD, J. LEAN, D.C. LOWE, G. MYHRE, J. NGANGA, R. PRINN, G. RAGA, M. SCHULZ & R. VAN DORLAND 2007 *Changes in Atmospheric Constituents and in Radiative Forcing. Climate Change 2007: The Physical Science Basis. Contribution of Working Group I to the Fourth Assessment Report of the Intergovernmental Panel on Climate Change*, [Solomon, S., D. Qin, M. Manning, Z. Chen, M. Marquis, K.B. Averyt, M.Tignor and H.L. Miller (eds.)]. Cambridge University Press, Cambridge, United Kingdom and New York, NY, USA.

GABEY, A.M., GALLAGHER, M.W., WHITEHEAD, J., DORSEY, J.R., KAYE, P.H., & STANLEY, W. R. 2010 Measurements and comparison of primary biological aerosol above and below a tropical forest canopy using a dual channel fluorescence spectrometer, *Atmospheric Chemistry and Physics*, **10**, 4453-4466, 10.5194/acp-10-4453-2010.

GABEY, A.M., STANLEY, W.R., GALLAGHER, M.W., & KAYE, P.H. 2011 The fluorescence properties of aerosol larger than 0.8 μm in urban and tropical rainforest locations, *Atmospheric Chemistry and Physics*, **11**, 5491-5504, 10.5194/acp-11-5491-2011.

GABEY, A.M., VAITILINGOM, M., FRENEY, E., BOULON, J., SELLEGRI, K., GALLAGHER, M.W., CRAWFORD, I.P., ROBINSON, N.H., STANLEY, W.R., & KAYE, P.H. 2013 Observations of fluorescent and biological aerosol at a high-altitude site in central

France, *Atmospheric Chemistry and Physics*, **13**, 7415-7428, doi:10.5194/acp-13-7415-2013.

HALLAR, A.G., CHIROKOVA, G., MCCUBBIN, I., PAINTER, T.H., WIEDINMYER, C., DODSON, C. 2011 Atmospheric bioaerosols transported via dust storms in the western United States, *Geophysical Research Letters*, **38**, L17801.

HEALY, D.A., O'CONNOR, D.J., SODEAU, J.R. 2012a Measurement of the particle counting efficiency of the "Waveband Integrated Bioaerosol Sensor" model number 4 (WIBS-4), *Journal of Aerosol Science*, **47**, 94-99, doi: 10.1016/j.jaerosci.2012.01.003.

HEALY, D.A., O'CONNOR, D.J., MURKE, A.M., & SODEAU, J.R. 2012b A laboratory assessment of theWaveband Integrated Bioaerosol Sensor (WIBS-4) using individual samples of pollen and fungal spore material, *Atmospheric Environment*, **60**, 534-543.

HEALY, D.A., HUFFMAN, J.A., O'CONNOR, D. J., PÖHLKER, C., PÖSCHL, U., & SODEAU, J.R. 2014 Ambient measurements of biological aerosol particles near Killarney, Ireland: a comparison between real-time fluorescence and microscopy techniques, Atmos. Chem. Phys. Discuss., 14, 3875-3915, doi:10.5194/acpd-14-3875-2014.

HILL, S.C., PINNICK, R.G., NILES, S., PAN, Y.-L., HOLLER, S., CHANG, R.K., BOTTIGER, J., CHEN, B.T., ORR, C.-S., & FEATHER, G. 1999 Realtime measurement of fluorescence spectra from single airborne biological particles, *Field Analytical Chemistry and Technology*, **3**, 221–239.

HILL, S.C., PINNICK, R.G., NILES, S., FELL, N.F., PAN, Y.-L., BOTTIGER, J., BRONK, B.V., HOLLER, S., & CHANG, R.K. 2001 Fluorescence from Airborne Microparticles: Dependence on Size, Concentration of Fluorophores, and Illumination Intensity, *Applied Optics*, **40**, 3005–3013.

HILL, S.C., MAYO, M.W., & CHANG, R.K. 2009 Fluorescence of Bacteria, Pollens, and Naturally Occurring Airborne Particles: Excitation/Emission Spectra, *Army Research Laboratory*.

HIRST, J.M. 1953 Changes in atmospheric spore content: Diurnal periodicity and the effects of weather, Trans. Brit. Mycol. Soc., 36, 375-393.

HIRST, E., KAYE, P.H., GREENAWAY, R.S., FIELD, P., & JOHNSON, D.W. 2001 Discrimination of micrometre-sized ice and super-cooled droplets in mixed-phase cloud, *Atmospheric Environ*ment, **35**, 33-47.

HOOSE, C., KRISTJÁNSSON, J.E., & BURROWS, S.M. 2010 How important is biological ice nucleation in clouds on a global scale?, *Environmental Research Letters*, **5**, 024009, doi:10.1088/1748-9326/5/2/024009.

HOOSE, C. & MÖHLER, O. 2012 Heterogeneous ice nucleation on atmospheric aerosols: a review of results from laboratory experiments, *Atmospheric Chemistry and Physics*, **12**, 9817-9854, doi:10.5194/acp-12-9817-2012.

HUFFMAN, J.A., TREUTLEIN, B., & PÖSCHL, U. 2010 Fluoroscent biological aerosol particle concentrations and size distributions measured with an Ultraviolet Aerodynamic Particle Sizer (UV-APS) in Central Europe, *Atmospheric Chemistry and Physics*, **10**, 3215-3233.

HUFFMAN, J.A., SINHA, B., GARLAND, R.M., SNEE-POLLMANN, A., GUNTHE, S.S., ARTAXO, P., MARTIN, S.T., ANDREAE, M.O., & PÖSCHL, U. 2012 Size distributions and temporal variations of biological aerosol particles in the Amazon rainforest characterized by microscopy and real-time UV-APS fluorescence techniques during AMAZE-08, *Atmospheric Chemistry and Physics*, **12**, 11997-12019, doi:10.5194/acp-12-11997-2012.

HUFFMAN, J.A., PRENNI, A.J., DEMOTT, P.J., PÖHLKER, C., MASON, R.H., ROBINSON, N.H., FRÖHLICH-NOWOISKY, J., TOBO, Y., DESPRÉS, V.R., GARCIA, E., GOCHIS, D.J., HARRIS, E., MÜLLER-GERMANN, I., RUZENE, C., SCHMER, B., SINHA, B., DAY, D.A., ANDREAE, M.O., JIMENEZ, J.L., GALLAGHER, M., KREIDENWEIS, S.M., BERTRAM, A.K., & PÖSCHL, U. 2013 High concentrations of biological aerosol particles and ice nuclei during and after rain, *Atmospheric Chemistry and Physics*, **13**, 6151-6164, doi:10.5194/acp-13-6151-2013.

HUMMEL, M., HOOSE, C., GALLAGHER, M., HEALY, D. A., HUFFMAN, J. A., O'CONNOR, D., PÖSCHL, U., PÖHLKER, C., ROBINSON, N. H., SCHNAITER, M., SODEAU, J. R., TOPRAK, E., & VOGEL, H. 2014 Regional-scale simulations of fungal spore aerosols using an emission parameterization adapted to local measurements of fluorescent biological aerosol particles, *Atmospheric Chemistry and Physics Discussions*, **14**, 9903-9950, doi:10.5194/acpd-14-9903-2014.

HURST, CHRISTON, J. 2007 Manual of environmental microbiology, *Washington, DC : ASM Press*, 3. Ed.

JAENICKE, R. & MATTHIAS-MASER, S. 1993 The Direct Contribution of the Biosphere to the Atmopspheric Aerosol, *Journal of Aerosol Science*, **24**, 537-538.

JAENICKE, R. 2005 Abundance of cellular material and proteins in the atmosphere, *Science*, **308**, 73, doi:10.1126/science.1106335.

KAYE, P.H., STANLEY, W.R., HIRST, E., FOOT, E.V., BAXTER, K.L., & BARRINGTON, S. J. 2005 Single particle multichannel bio-aerosol fluorescence sensor, *Optics Express*, **13**, 3583-3593.

KAYE, P.H., APTOWICZ, K., CHANG, R.K., FOOT, V., & VIDEEN, G. 2007 Angularly resolved elastic scattering from airborne particles - Potential for characterizing, classifying, and identifying individual aerosol particles, *Optics of Biological Particles*, **238**, 31-61.

KULKARNI, P., BARON, P.A., & WILLEKE, K. 2011 Aerosol Measurement: Principles, Techniques, and Applications, 3rd Edition, *A John Wiley & Sons. Inc. Publication*.

LI, J., & HUMPHREY, E.A. 1991 Use of Fluorometry for Monitoring and Control of a Bioreactor, *Biology and Bioengineering*, **37**, 1043-1049.

LIGHTHART, B. & SHAFFER, B. T. 1995 Airborne Bacteria in the Atmospheric Surface Layer: Temporal Distribution above a Grass Seed Field, *Applied Environmental Microbiology*, **61**, 4, 1492-1496.

LIGHTHART BRUCE 1997 The ecology of bacteria in the alfresco atmosphere, *FEMS Microbiology Ecology*, **23**, 263-274.

MANCINELLI, ROCCO L. & SHULLS, WELLS A. 1978 Airborne Bacteria in an Urban Environment, *Applied and Environmental Microbiology*, **35**, 6, 1095-1101.

MERTES, S., VERHEGGEN, B., WALTER,S., CONNOLLY, P., EBERT, M., SCHNEIDER, J., BOWER, K.N., COZIC, J., WEINBRUCH, S., BALTENSPERGER, U. & WEINGARTNER, E. 2007 Aerosol Science Technology, **41**, 848–864.

MONKS, P.S., GRANIER, C., FUZZI, S., STOHL, A., WILLIAMS, M.L., AKIMOTO, H., AMANN, M., BAKLANOV, A., BALTENSPERGER, U., BEY, I., BLAKE, N., BLAKE, R.S., CARSLAW, K., COOPER, O. R., DENTENER, F., FOWLER, D., FRAGKOU, E., FROST, G.J., GENEROSO, S., GINOUX, P., GREWE, V., GUENTHER, A., HANSSON, H. C., HENNE, S., HJORTH, J., HOFZUMAHAUS, A., HUNTRIESER, H., ISAKSEN, I.S.A., JENKIN, M.E., KAISER, J., KANAKIDOU, M., KLIMONT, Z., KULMALA, M., LAJ, P., LAWRENCE, M.G., LEE, J.D., LIOUSSE, C., MAIONE, M., MCFIGGANS, G., METZGER, A., MIEVILLE, A., MOUSSIOPOULOS, N., ORLANDO, J.J., O'DOWD, C.D., PALMER, P.I., PARRISH, D.D., PETZOLD, A., PLATT, U., PÖSCHL, U., PRÉVÔT, A.S.H., REEVES, C.E., REIMANN, S., RUDICH, Y., SELLEGRI, K., STEINBRECHER, R., SIMPSON, D., TEN BRINK, H., THELOKE, J., VAN DER WERF, G.R., VAUTARD, R., VESTRENG, V., VLACHOKOSTAS, C., & VON GLASOW, R. 2009 Atmospheric composition change – global and regional air quality, *Atmospheric Environment*, **43**, 5268-5350, 10.1016/j.atmosenv.2009.08.021.

MÖHLER, O., FIELD, P.R., CONNOLLY, P., BENZ, S., SAATHOFF, H., SCHNAITER, M., WAGNER, R., COTTON, R., KRAMER, M., MANGOLD, A., & HEYMSFIELD, A.J. 2006 Efficiency of the deposition mode ice nucleation on mineral dust particles, *Atmospheric Chemistry and Physics*, **6**, 3007-3021.

MÖHLER, O., GEORGAKOPOULOS, D.G., MORRIS, C.E., BENZ, S., EBERT, V., HUNSMANN, S., SAATHOFF, H., SCHNAITER, M., & WAGNER, R. 2008 Heterogeneous ice nucleation

activity of bacteria: new laboratory experiments at simulated cloud conditions, *Biogeosciences*, **5**, 1425-1435, doi:10.5194/bg-5-1425-2008.

NIEMAND, MONIKA 2012 A Particle–Surface–Area–Based Formulation of Heterogeneous Ice Nucleation by Mineral Dust Aerosols, PhD thesis, University of Karlsruhe.

NICKOVIC, S., PAPADOPOULOS, A., KAKALIAGOU, O. & KALLOS, G. 2001 Model for prediciton of desert dust cycle in the atmosphere. Journal of Geophysical Research, **106**, 18113-18129.

PADY, S.M. & KRAMER, C.L. 1967 Diurnal periodicity in airborne fungi in an orchard, *Mycologia*, **39**, 5, 302-310.

PAN, Y.-L., PINNICK, R.G., HILL, S.C., ROSEN, J.M., & CHANG, R.K. 2007 Single-particle laser-induced-fluorescence spectra of biological and other organic-carbon aerosols in the atmosphere: Measurements at New Haven, Connecticut, and Las Cruces, New Mexico, *Journal of Geophysical Research*, **112**, 10.1029/2007jd008741.

PAULITZ, T.C. 1996 Diurnal release of ascospores by Gibberella zeae in inoculated wheat plots, *Plant Disease*, **80**, 674–678.

PENNER, J. E., ANDREAE, M., ANNEGARN, H., BARRIE, L., FEICHTER, J., HEGG, D., JAYARAMAN, A., LEAITCH, R., MURPHY, D., NGANGA, J., & PITARI, G. 2001 Aerosols, their Direct and Indirect Effects, in: Climate Change 2001: The Scientific Basis, edited by: Houghton, J. T., Ding, Y., Griggs, D. J., Noguer, M., Van der Linden, P. J., Dai, X., Maskell, K., and Johnson, C. A., *Report to Intergovernmental Panel on Climate Change from the Scientific Assessment Working Group (WGI), Cambridge University Press*, 289–416.

PEREZ, C., NICKOVIC, S., BALDASANO, J.M., SICARD, M., ROCADENBOSCH, F., & CACHORRO, V.E. 2006a, A long Saharan dust event over the western Mediterranean: Lidar, Sun photometer observations, and regional dust modeling, *Journal of Geophysical Research*, 111, D15214, doi:10.1029/2005JD006579.

PEREZ, C., NICKOVIC, S., PEJANOVIC, G., BALDASANO, J.M., & OZSOY, E. 2006b, Interactive dust-radiation modeling: A step to improve weather forecasts, *Journal of Geophysical Research*, 111, D16206, doi:10.1029/2005JD006717.

PINNICK, R.G., HILL, S.C., NACHMAN, P., PENDLETON, J.D., FERNANDEZ, G.L., MAYO, M.W., & BRUNO, J.G. 1995 Fluorescence Particle Counter for Detecting Airborne Bacteria and Other Biological Particles, *Aerosol Science and Technology*, **23**, 653-664.

PÖHLKER, C., HUFFMAN, J.A., & PÖSCHL, U. 2012 Autofluorescence of atmospheric bioaerosols – fluorescent biomolecules and potential interferences, *Atmospheric Measurement Techniques*, **5**, 37-71, 10.5194/amt-5-37-2012.

PÖSCHL, U. 2005 Atmospheric aerosols: composition, transformation, climate and health effects, *Angewandte Chemie International Edition*, **44**, 7520-7540, doi:10.1002/anie.200501122.

PRATT, K.A., DEMOTT, P.J., FRENCH, J.R., WANG, Z., WESTPHAL, D.L., HEYMSFIELD, A.J., TWOHY, C.H., PRENNI, A.J., & PRATHER, K.A. 2009 In situ detection of biological particles in cloud ice-crystals, Nature Geoscience, 2, 397–400, doi:10.1038/ngeo521.

PROSPERO, J.M., GINOUX, P., TORRES, O., NICHOLSON, S.E., GILL, T.E. 2002 Environmental characterization of global sources of atmospheric soil dust identified with the Nimbus 7 Total Ozone Mapping Spectrometer (TOMS) absorbing aerosol product, *Reviews of Geophysics*, **40**, 1002, doi:10.1029/2000RG000095.

ROSENFELD, D., LOHMANN, U., RAGA, G.B., O'DOWD, C.D., KULMALA, M., FUZZI, S., REISSELL, A., & ANDREAE, M.O. 2008 Flood or drought: how do aerosols affect precipitation?, *Science*, **321**, 1309-1313, 10.1126/science.1160606.

SAYDAM, A.C., & SENYUVA, H.Z. 2002 Deserts: Can they be the potential suppliers of bioavailable iron?, *Geophysical Research Letters*, **29**, 11, 1524, doi:10.1029/2001GL013562.

SCHNAITER, M., GIMMLER, M., LLAMAS, I., LINKE, C., JAGER, C., MUTSCHKE, H. 2006 Strong spectral dependence of light absorption by organic carbon particles formed by propane combustion, *Atmospheric Chemistry and Physics*, **6**, 2981-2990.

SCHUMACHER, C.J., PÖHLKER, C., AALTO, P., HILTUNEN, V., PETÄJÄ, T., KULMALA, M., PÖSCHL, U., & HUFFMAN, J.A. 2013 Seasonal cycles of fluorescent biological aerosol particles in boreal and semi-arid forests of Finland and Colorado, *Atmospheric Chemistry and Physics*, **13**, 11987-12001, doi:10.5194/acp-13-11987-2013.

SKROTZKI, J., 2012 High-accuracy multiphase humidity measurements using TDLAS: application to the investigation of ice growth in simulated cirrus clouds, PhD thesis, Ruperto–Carola–University of Heidelberg.

SMITH, D.J., GRIFFIN, D.W., & JAFFE, D.A. 2011 The High Life: Transport of Microbes in the Atmosphere, EOS, Transactions, American Geophysical Union, 92, 249-256.

STEINKE, I. 2013 Ice nucleation properties of mineral dusts, PhD Thesis, http://www.ub.uni-heidelberg.de/archiv/15967.

TEXTOR, C., SCHULZ, M., GUIBERT, S., KINNE, S., BALKANSKI, Y., BAUER, S., BERNTSEN, T., BERGLEN, T., BOUCHER, O., CHIN, M., DENTENER, F., DIEHL, T., EASTER, R., FEICHTER, H., FILLMORE, D., GHAN, S., GINOUX, P., GONG, S., GRINI, A., HENDRICKS, J., HOROWITZ, L., HUANG, P., ISAKSEN, I., IVERSEN, I., KLOSTER, S., KOCH, D., KIRKEVÅG, A., KRISTJANSSON, J. E., KROL, M., LAUER, A., LAMARQUE, J. F., LIU, X., MONTANARO, V., MYHRE, G., PENNER, J., PITARI, G., REDDY, S., SELAND, Ø., STIER, P., TAKEMURA, T., & TIE, X. 2006 Analysis and quantification of the diversities of aerosol life cycles within AeroCom, *Atmospheric Chemistry and Physics*, **6**, 1777-1813, doi:10.5194/acp-6-1777-2006.

TONG YONGYI & LIGHTHART BRUCE 1999 Diurnal Distribution of Total and Culturable Atmospheric Bacteria at a Rural Site, *Aerosol Science and Technology*, **30**, 2, 246-254.

TOPRAK, E. & SCHNAITER, M. 2013 Fluorescent biological aerosol particles measured with the Waveband Integrated Bioaerosol Sensor WIBS-4: laboratory tests combined with a one year field study, *Atmospheric Chemistry and Physics*, **13**, 225-243, doi:10.5194/acp-13-225-2013.

TRENBERTH, K.E. 1983 What are the seasons?, *Department of Atmospheric Sciences, University of Illinois at Urbana-Champaign, Urbana*, 7 pp.

UNO, I., EGUCHI, K., YUMIMOTO, K., TAKEMURA, T., SHIMIZU, A., UEMATSU, M., LIU, Z., WANG, Z., HARA, Y., SUGIMOTO, N. 2009 Asian dust transported one full circuit around the globe, *Nature Geoscience*, **2**, 557.

WU, H., CATHY, & WARREN, H.L. 1984 Autofluorescence in Fungi, and Its Correlation with Viability, *Mycologia*, **76**, 6, 1049-1058.